RADC-TDR-64-150

2 of 3

A THEORETICAL ANALYSIS AND EXPERIMENTAL RESULTS OF A FREQUENCY STEPPING METHOD FOR RADAR SCATTERING MEASUREMENTS

118 P

4.00

TECHNICAL DOCUMENTARY REPORT NO. RADC-TDR-64-150
March 1964

Space Defense Systems Laboratory
Rome Air Development Center
Research and Technology Division
Air Force Systems Command
Griffiss Air Force Base, New York

Project No. 6503

(Prepared by General Dynamics/Fort Worth,
A Division of General Dynamics Corporation
under Contract No. AF30(602)-2831)

NOTICES

Copies available at Office of Technical Services.

Qualified requesters may obtain copies from Defense Documentation Center (TISIA-2), Cameron Station, Alexandria, V., 22313. Orders will be expedited if placed through the librarian or other person designated to request documents from DDC.

When US Government drawings, specifications, or other data are used for any purpose other than a definitely related government procurement operation, the government thereby incurs no responsibility nor any obligation whatsoever, and the fact that the government may have formulated, furnished, or in any way supplied the said drawings, specifications, or other data is not to be regarded by implication or otherwise, as in any manner licensing the holder or any other person or corporation, or conveying any rights or permission to manufacture, use, or sell any patented invention that may in any way be related thereto.

Do not return this copy. Retain or destroy.

FOREWORD

This Technical Documentary Report, RADC-TDR-64-150, is the RAT SCAT Research and Development Report No. 3 and has been assigned the report number FZE-222-3 by General Dynamics/Fort Worth. The contents of this report and the abstract are unclassified. This report was prepared by J. W. Tucker, J. W. Jones, C. H. Fletcher, and W. P. Cahill.

ABSTRACT

When a large, complex target is rotated to obtain a radar cross section (RCS) pattern, the observed RCS typically exhibits violent oscillations. These oscillations are characteristic of the changing relative phase between reflections from individual scatterers as the target rotates. Significant RCS data may be obscured by the oscillations. These oscillations may be smoothed through the use of a frequency-stepping technique in which the radar frequency is shifted from pulse to pulse. The result is an RCS pattern in which the characteristics of individual scatterers are emphasized rather than the interactions between the scatterers.

An ancillary result of the frequency-stepping technique is that it may be used to obtain greatly improved range resolution. This capability arises as a direct consequence of the wide bandwidth of the frequency stepping waveform. Instrumentation requirements include a stairstep voltage waveform generator, a voltage-tuned oscillator, a narrow-band filter, and a moving corner reflector.

The results of frequency stepping measurements on a two-element interferometer, a target with theoretically predictable back scattering characteristics, correspond closely to predicted results. Predictable features appear on frequency-stepping measurements of a vehicle mock-up. No theoretically significant changes in the experimental frequency-stepping system are required to implement an operational system.

PUBLICATION REVIEW

This report has been reviewed and is approved. For further technical information on this project, contact

Approved: DONALD M. MONTANA
Program Directors' Office
Space Surveillance and Instrumentation Branch

Approved: JOSEPH FALLIK
Chief, Space Surveillance and
Instrumentation Branch
Surveillance and Control Division

TABLE OF CONTENTS

LIST OF FIGURES

LIST OF TABLES

SECTION 1

INTRODUCTION

This report contains a description of the frequency stepping techniques and instrumentation provided at the RAT SCAT Site under Contract AF30(602)-2831, RADC Project 6503. The theoretical material discussed herein is based on a summary of techniques and theoretical aspects of frequency stepping presented to participants in the RAT SCAT Technical Direction Meeting held at General Dynamics/Fort Worth on 28-29 November 1962 by Dr. Franklin A. Rodgers, Jr. A frequency stepping theoretical analysis, contained in Reference 1, by J. W. Tucker, J. W. Jones, and C. H. Fletcher is also reproduced herein in revised form. The measurement data are the results of an experiment performed at the RAT SCAT Site in September, 1963.

The general problem of smoothing radar cross section data is considered, and the concept of phase averaging is defined in Section 2. A detailed mathematical development of frequency stepping is presented in Section 3, and supporting material is provided in the appendices. The character of the averaging process is analyzed, and the resolution enhancement technique is demonstrated through spectral analysis. A description of the instrumentation is given in Section 4. In Section 5 the results of a series of frequency stepping measurements are presented and compared with theoretically predicted results. Recommendations for an operational frequency stepping system are made in Section 6.

SECTION 2

FREQUENCY STEPPING FUNDAMENTALS

Radar Cross Section (RCS) data are commonly presented in the form of polar or rectilinear graphs of RCS (expressed in decibels as $10 \log_{10} RCS/\sigma_o$, where σ_o is an arbitrary reference level, typically 1 square meter) as a function of aspect angle θ. For small bodies, the curves are characterized by relatively wide and infrequent lobes. However, large complex bodies exhibit violent oscillations of RCS because of the angular dependence of the phase relations between individual scatterers. These violent oscillations sometimes obscure useful information, and it is commonly accepted practice to perform some sort of smoothing of the data.

The most commonly used smoothing technique for RCS data is angular smoothing over a small angular interval. However, since the violent oscillations for which smoothing is desired arise from the angular dependence of phase relations between individual scatterers, a more useful averaging is phase averaging. When this is used, the oscillations arising from the changing phase relations between individual scatterers are de-emphasized, and the effects of individual scatterers and closely spaced groups of scatters are more easily studied.

A simple example of phase averaging is obtained by considering two scatterers which are separated a distance ΔX and are observed by a radar signal, in which the angular frequency is ω_o, directed in the X direction. If σ_1 and σ_2 are the respective RCS's of the scatterers, the observed RCS is

$$\sigma_o = \left| \sqrt{\sigma_1} + \sqrt{\sigma_2}\ e^{-i2\Delta X\omega/c} \right|^2$$

$$= \sigma_1 + \sigma_2 + 2\sqrt{\sigma_1\sigma_2}\cos 2\Delta X\omega/c \qquad (2\text{-}1)$$

If the frequency is varied so that the relative phase angle $2\Delta X\omega/c$ is uniformly distributed over $0, 2\pi$, the average of the cosine term will be zero, and the observed average RCS will be

$$\overline{\sigma}_o = \sigma_1 + \sigma_2 \qquad (2\text{-}2)$$

A more detailed analysis is presented in Section 3.

The indicated phase averaging is easily implemented through the use of a radar which is capable of frequency-stepped transmission. In this system, a uniform, pulse-to-pulse frequency increment is used to provide a sufficient number of pulses to cover a bandwidth B. The frequency stairstep is then repeated.

At times it is desirable to be able to accurately locate the position in range of flare spots on a complex target. These spots can be located by using the range resolution capability inherent in the wideband waveform which is characteristic of frequency stepping. A detailed discussion of a suitable technique is presented in the following sections.

SECTION 3

TECHNICAL DISCUSSION

Cross Section Averaging

As stated in Section 2, a phase averaging process is easily implemented through the use of variable frequency transmission. In particular. a frequency-stepped transmission will be considered. The two-scatterer case will be analyzed first, and the results will then be extended to the N-scatterer (complex) target.

In the frequency-stepped radar, the transmitted frequency is changed in uniform frequency steps from pulse to pulse through a set frequency interval. Each shift in frequency is accomplished during an interpulse period. The staircase variation of frequency with time is shown in Figure 3-1, in which T_c is the staircase repetition period and T_p is the interpulse period.

As shown in Figure 3-2 a radar at K is used to observe a target composed of scatterers 1 and 2. The distance from radar K to scatterer 1 is d_1, and the distance to scatterer 2 is d_2. The difference between d_1 and d_2 is Δd. The radar frequency is $\omega = 2\pi f$. The total signal voltage, V_s, received by the radar at K is

$$V_s = \sqrt{2}\, a_1 \cos\left(\omega t - \frac{4\pi d_1}{\lambda} - \phi_1\right) + \sqrt{2}\, a_2 \cos\left(\omega t - \frac{4\pi d_2}{\lambda} - \phi_2\right) \tag{3-1}$$

For a pulsed transmission, a square law detector provides an output that consists of a sequence of positive voltage pulses in which the amplitude is proportional to

$$P(\omega) = \overline{V_s^2} \tag{3-2}$$

where the bar indicates a time average over one pulse.

By multiplying and using the identity $2\cos A \cos B = \cos(A-B) + \cos(A+B)$,

$$P(\omega) = 2a_1^2\overline{\cos^2\left(\omega t - \frac{4\pi d_1}{\lambda} - \phi_1\right)} + 2a_2^2\overline{\cos^2\left(\omega t - \frac{4\pi d_2}{\lambda} - \phi_2\right)}$$

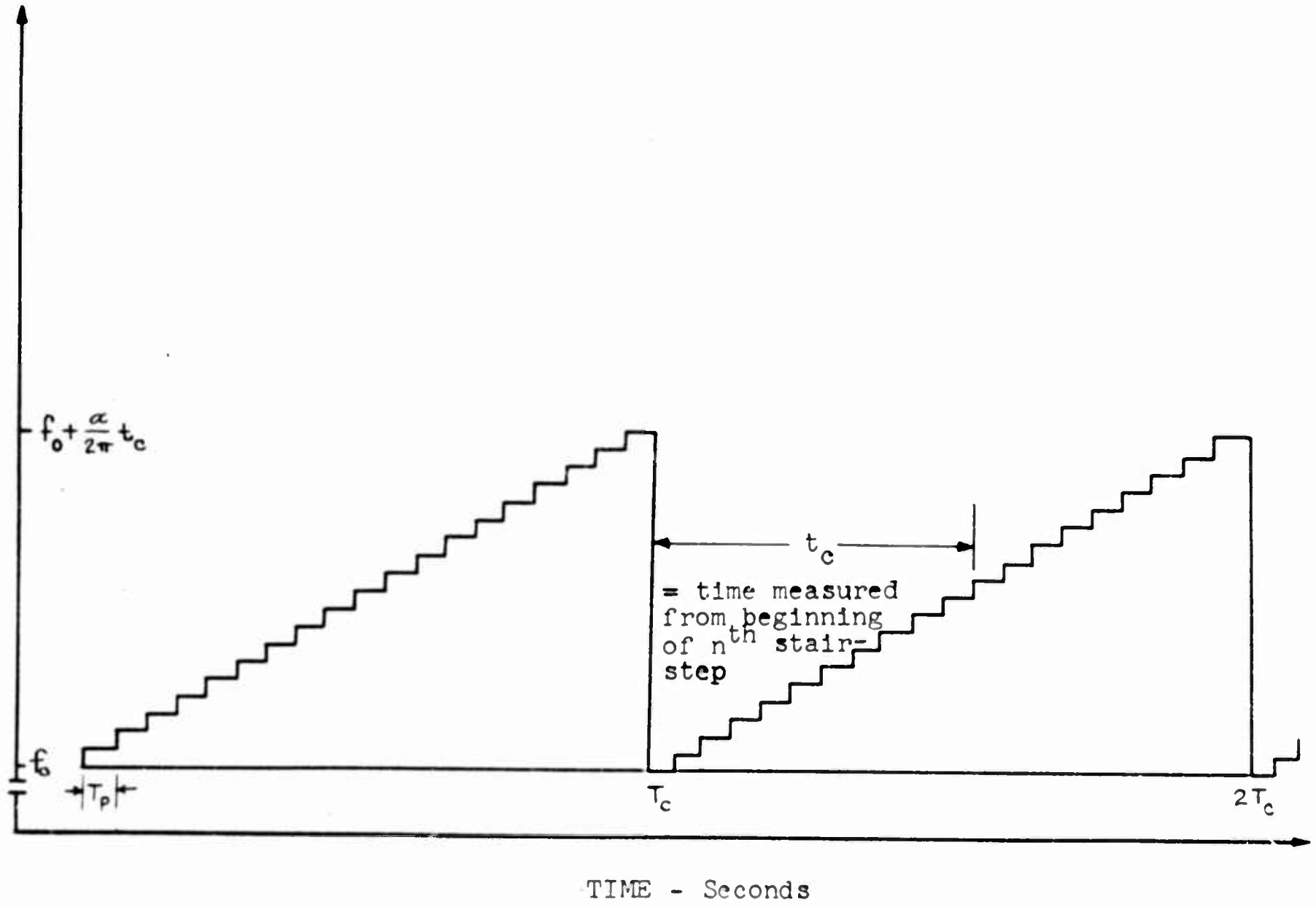

Fig. 3-1 FREQUENCY STEPPING WAVE FORM

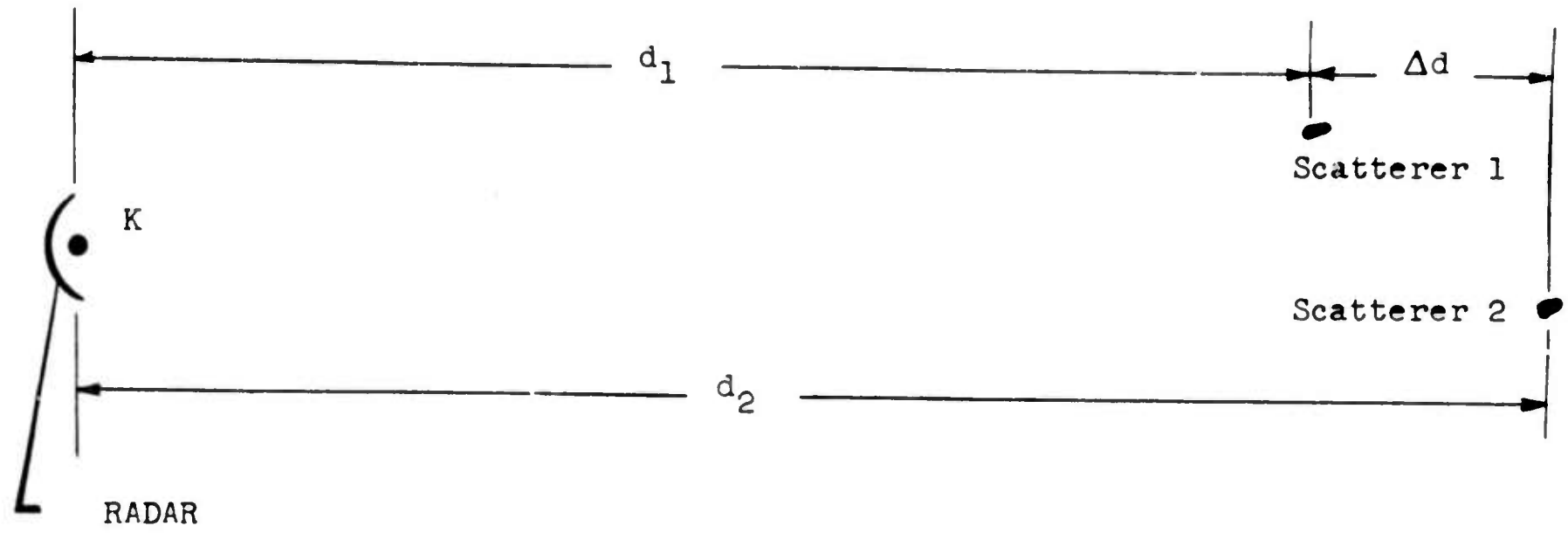

Fig. 3-2 TWO SCATTERER TARGET

$$+2a_1a_2\overline{\left[\cos\left(\frac{4\pi\Delta d}{\lambda}+\Delta\phi\right)+\cos\left(2\omega t-\frac{4\pi(d_1+d_2)}{\lambda}-\phi_1-\phi_2\right)\right]} \tag{3-3}$$

and since $\overline{\cos^2(\omega t-\alpha)} = 1/2$ and $\overline{\cos(2\omega t-\beta)} = 0$,

$$P(\omega) = a_1^2 + a_2^2 + 2a_1a_2\cos\left[\frac{4\pi\Delta d}{\lambda}+\Delta\phi\right] \tag{3-4}$$

or, by writing $\frac{2\pi}{\lambda} = \frac{\omega}{c}$

$$P(\omega) = a_1^2 + a_2^2 + 2a_1a_2\cos\left[\frac{2\Delta d}{c}\omega+\Delta\phi\right] \tag{3-5}$$

If the frequency is stepped along a uniform staircase, as described above and shown in Figure 3-1, the envelope of the pulse amplitudes is a function of time as shown in Figure 3-3. The envelope function P(t) for the linear frequency staircase, shown in Figure 3-1, is obtained from $P(\omega)$ by substituting $\omega=\omega_o+\alpha t_c$ in equation 3-5 to obtain

$$P(t) = a_1^2 + a_2^2 + 2a_1a_2\cos\left[\frac{2\Delta d\omega_o}{c}+\Delta\phi+\frac{2\Delta d\alpha}{c}t_c\right] \tag{3-6}$$

where t_c goes from zero to T_c and then repeats, as shown in Figure 3-1. The resemblance between this equation and equation 2-1 is apparent. However, the phase angle is not necessarily uniform over an integral number of 2π radians. The actual average observed can be found by averaging P(t) with respect to time over the observation interval T_c:

$$\bar{P} = \frac{1}{T_c}\int_0^{T_c} P(t)\,dt$$

$$= a_1^2 + a_2^2 + 2a_1a_2\cos\left(\frac{2\Delta d\omega_o}{c}+\Delta\phi+\frac{\Delta d\alpha}{c}T_c\right)\frac{\sin\frac{\Delta d\alpha T_c}{c}}{\frac{\Delta d\alpha T_c}{c}}$$

Finally, by substituting (1) $\alpha T_c = 2\pi B$, where B is the total bandwidth in cycles per second, and (2) $\omega_o/c = 2\pi/\lambda_o$,

$$\bar{P} = a_1^2 + a_2^2 + 2a_1a_2\cos\left(\frac{4\pi\Delta d}{\lambda_o}+\Delta\phi+\frac{2\pi\Delta d B}{c}\right)\frac{\sin\frac{2\pi\Delta d B}{c}}{\frac{2\pi\Delta d B}{c}} \tag{3-7}$$

Thus $\bar{P}$ is seen to consist of two parts:

1. The incoherent scattering

$$a_1^2 + a_2^2$$

2. The coherent scattering

$$2\, a_1 a_2 \cos\left(\frac{4\pi\Delta d}{\lambda_o} + \Delta\phi + \frac{2\pi\Delta d\, B}{c}\right) \frac{\sin\frac{2\pi\Delta d\, B}{c}}{\frac{2\pi\Delta d\, B}{c}}$$

The precise manner in which the averaging process suppresses the coherent scattering term (and it is this term that gives rise to the violent oscillation of RCS) can now be seen from the $(\sin x)/x$ factor in the coherent scattering term. If the argument x is greater than approximately $\pi/1.23$, then $-10 \log_{10} (\sin x)/x$ is always greater than 6.7 db. In other words, the coherent scattering term is suppressed more than 6.7 db when

$$x = \frac{2\pi\Delta d\, B}{c} \geq \frac{\pi}{1.23}$$

This result will be obtained whenever the scatterer separation is

$$\Delta d \geq \frac{c}{2.46\, B}$$

By way of example, if the bandwidth is 1 kilomegacycle (10 per cent at X-band), then $c/(2.46B) = 0.4$ feet or 4.8 inches. Hence, in the case of scatterers farther apart than 4.8 inches, this coherent scattering interaction will be suppressed by at least 6.7 db. The actual averaging process is most directly accomplished by a low-pass filter.

It is of interest to examine the frequency spectrum of the envelope function shown in Figure 3-3. The spectrum of one period is given by the Fourier transform of equation 3-6.

$$F(\omega) = \int_{-T/2}^{T/2} \cos(\omega'_o t + \psi)\, e^{-i\omega t}\, dt \qquad (3\text{-}8)$$

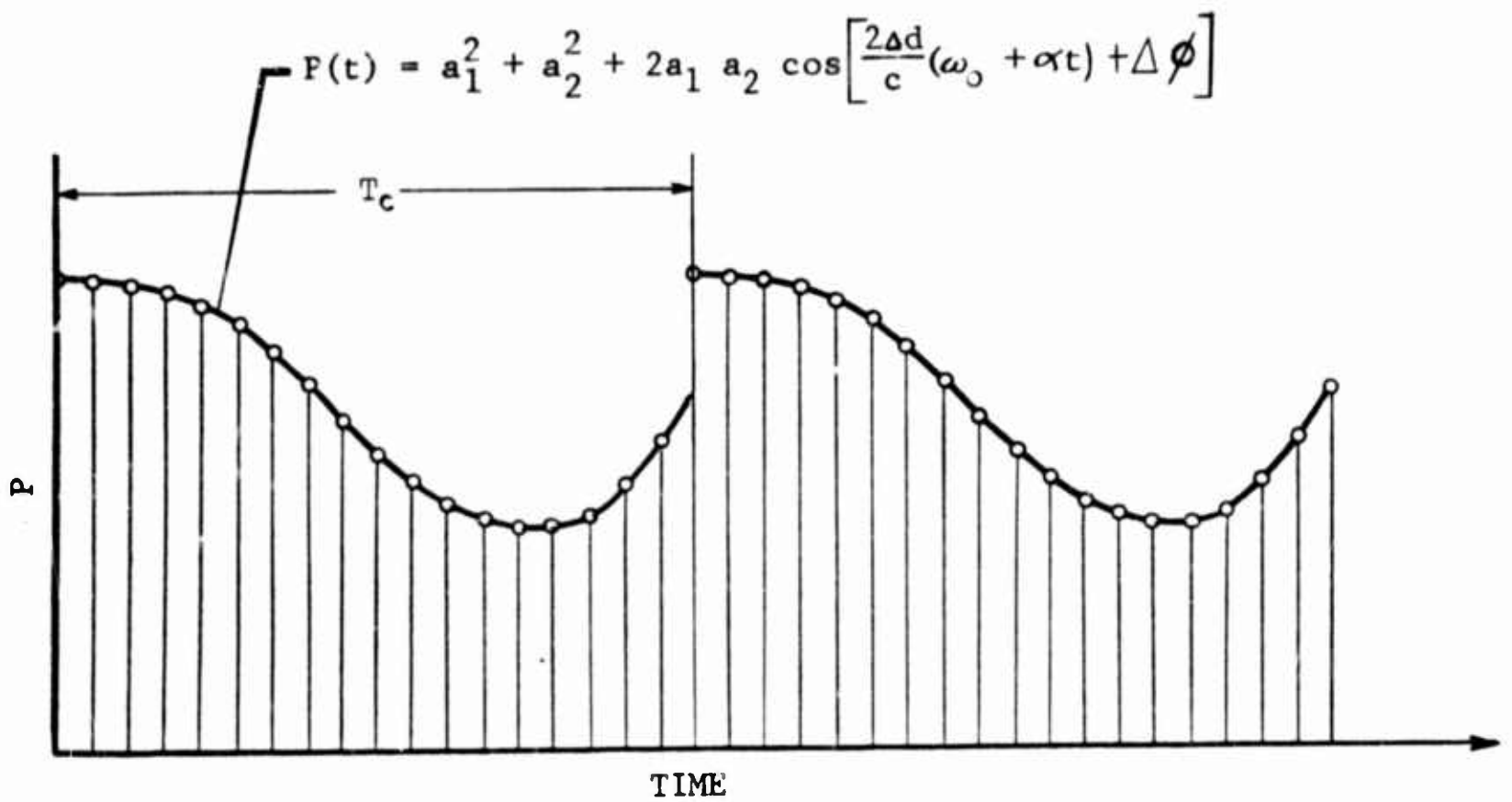

Fig. 3-3 DETECTOR OUTPUT

where

$$\omega_o' t + \psi = \frac{2\Delta d \omega_o}{c} + \Delta\phi + \frac{2\Delta d \alpha}{c} t_c$$

The power spectral density is

$$\left|F(\omega)\right|^2 = \left[\frac{\sin(\omega-\omega_o')\frac{T}{2}}{(\omega-\omega_o')\frac{T}{2}}\right]^2 + \left[\frac{\sin(\omega+\omega_o')\frac{T}{2}}{(\omega+\omega_o')\frac{T}{2}}\right]^2$$

$$+ \frac{\cos\omega_o' T - \cos\omega T}{\omega^2 - \omega_o'^2} \cos 2\psi \qquad (3\text{-}9)$$

The spectrum consists of two continuous (sin x)/x spectra centered at ω_o' and $-\omega_o'$. If this wave form is considered to be a strictly periodic function (i.e., over $-\infty$, $+\infty$), the continuous spectrum will be replaced by a discrete spectrum with lines centered at multiples of $2\pi/T_c$ and (sin x)/x envelopes centered at ω_o' and $-\omega_o'$, as shown in Figure 3-4. The spectrum which results from an intermediate observation interval is similar to that shown by the dotted lines in Figure 3-4. The lines which occur at multiples of $2\pi/T_c$ have now become continuous spectra centered around the multiples of $2\pi/T_c$.

The geometry of the situation in which a radar is used to observe a multi-source target is shown in Figure 3-5. The radar is located at K. The target is composed of N scatterers, and the distance from radar K to scatterer i is d_i. The total signal voltage V_s received by the radar K is

$$V_s = \sqrt{2}\sum_{i=1}^{N} a_i \cos\left(\omega t - \frac{4\pi d_i}{\lambda} - \phi_i\right) \qquad (3\text{-}10)$$

where a_i is the amplitude of return from scatterer i.

The square law detector produces an output that consists of a sequence of positive voltage pulses in which the amplitude is proportional to

$$P(\omega) = \overline{V_s^2} \qquad (3\text{-}11)$$

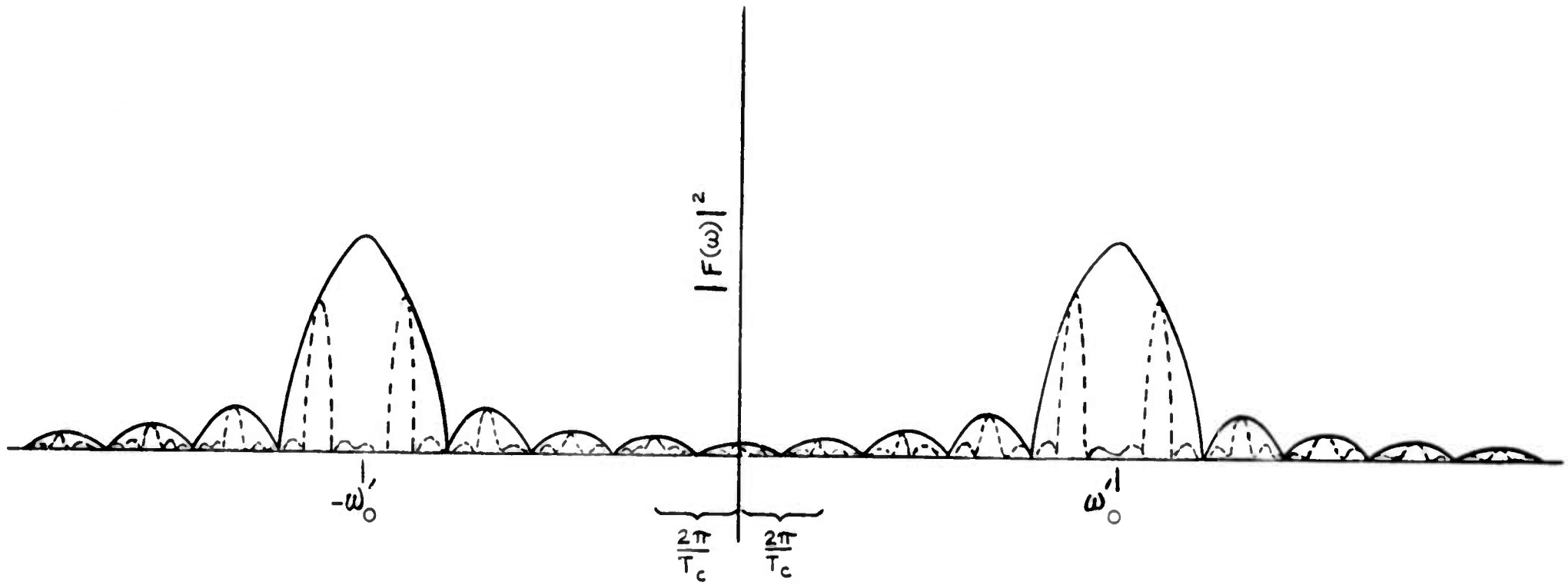

Fig. 3-4 FREQUENCY SPECTRUM OF P(t)

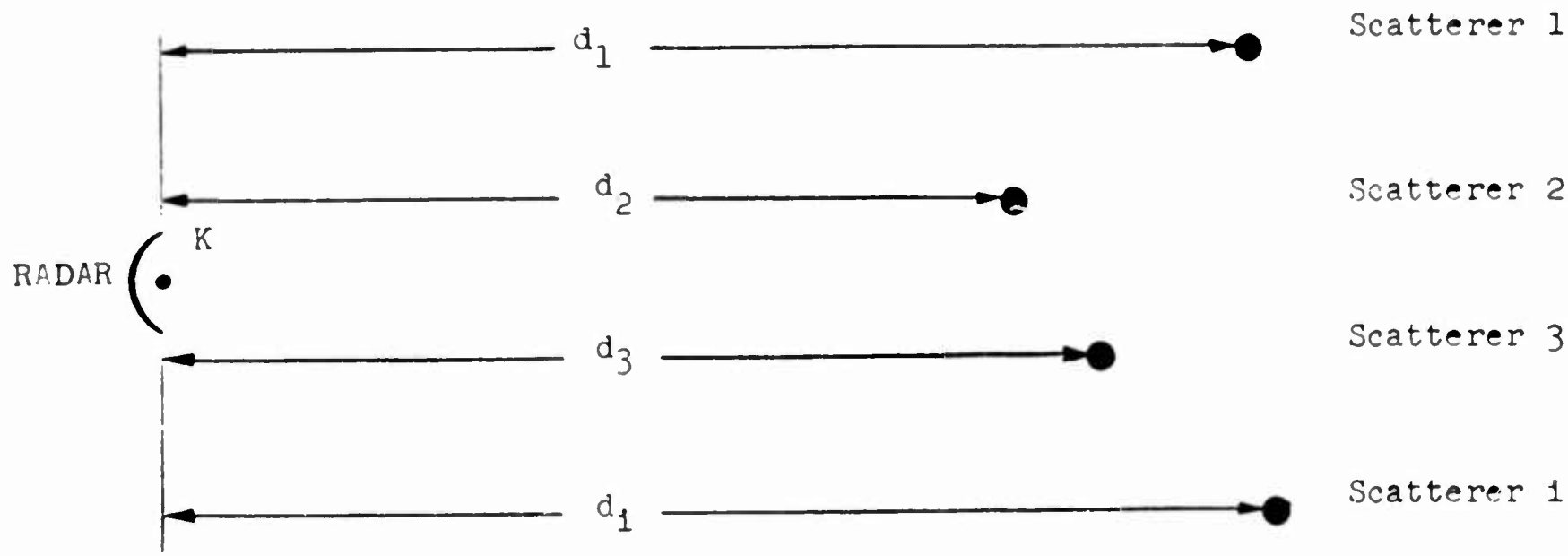

Fig. 3-5 MULTI-SCATTERER TARGET

By substituting equation 3-10 into equation 3-11 and performing the indicated operations,

$$P(\omega) = 2\sum\sum a_i a_q \overline{\cos\left[\omega t - \frac{4\pi d_i}{\lambda} - \phi_i\right] \cos\left[\omega t - \frac{4\pi d_q}{\lambda} - \phi_q\right]}$$

By using the identity, $2\cos B\cos A = \cos(B-A)+\cos(B+A)$, $P(\omega)$ may be written as

$$P(\omega) = \sum\sum a_i a_q \left(\overline{\cos\left[\left(\frac{4\pi d_q}{\lambda} - \frac{4\pi d_i}{\lambda}\right) + (\phi_q - \phi_i)\right]} + \overline{\cos\left[2\omega t - \frac{4\pi}{\lambda}(d_i + d_q) - (\phi_i + \phi_q)\right]} \right) \quad (3\text{-}12)$$

And, since $\overline{\cos(2\omega t - \beta)} = 0$,

$$P(\omega) = \sum\sum a_i a_q \cos\left[\frac{4\pi \Delta d_{q,i}}{\lambda} + \Delta\phi_{q,i}\right] \quad (3\text{-}13)$$

If $2\pi/\lambda$ is now replaced by its equivalent ω/c, equation 3-13 may be written as

$$P(\omega) = \sum_{i=1}^{N}\sum_{q=1}^{N} a_i a_q \cos\left[\frac{2\omega \Delta d_{q,i}}{c} + \Delta\phi_{q,i}\right] \quad (3\text{-}14)$$

By considering two separate cases, namely, $a_i = a_q$ and $a_i \neq a_q$, equation 3-14 may be expanded into

$$P(\omega) = \sum_{i=1}^{N} a_i^2 + \sum_{i=1}^{N}\sum_{\substack{q=1 \\ i\neq q}}^{N} a_i a_q \cos\left[2\omega\frac{\Delta d_{q,i}}{c} + \Delta\phi_{q,i}\right] \quad (3\text{-}15)$$

If the frequency is now stepped along a uniform staircase, as previously described, the envelopes of the pulse amplitudes are a function of time. For the linear frequency staircase the envelope function, $P(t)$, is obtained from $P(\omega)$ by substituting $\omega = \omega_o + \alpha t_c$ in equation 3-15 to obtain

$$P(t) = \sum_{i=1}^{N} a_i^2 + \sum_{i=1}^{N}\sum_{\substack{q=1 \\ i\neq q}}^{N} a_i a_q \cos\left[\frac{2\Delta d_{q,i}\omega_o}{c} + \Delta\phi_{q,i} + \frac{2\Delta d_{q,i}\alpha}{c} t_c\right] \quad (3\text{-}16)$$

where t_c goes from zero to T_c and then repeats. The first term of equation 3-16 may be called "incoherent scattering," and the second term may be called "coherent scattering."

By taking the time average of equation 3-16 over a period,

$$\bar{P} = \sum_{i=1}^{N} a_i^2 + \sum_{\substack{i=1 \\ i \neq q}}^{N} \sum_{q=1}^{N} a_i a_q \frac{\sin \frac{2\pi \Delta d\, B}{c}}{\frac{2\pi \Delta d\, B}{c}} \cos\left(\frac{4\pi \Delta d_{q,i}}{\lambda_o} + \Delta\phi_{q,i} + \frac{2\pi \Delta d\, B}{c}\right) \tag{3-17}$$

The averaging process is the same as that described previously for equation 3-7.

The coherent scattering is the dc component,

$$P = \sum_{i=1}^{N} a_1^2$$

The phase averaging thus results in the smoothing of the violent oscillations which are characteristic of the RCS patterns of complex targets.

Range Resolution

The most important result of the use of a frequency-stepping radar in RCS measurement lies in the phase averaging process previously described. In addition, a fine range resolution capability can also be realized by virtue of the wide bandwidth of the frequency-stepped transmission. In the system to be described, a coherent reference is used in the form of an auxiliary reflector in the neighborhood of the target. In addition, to overcome the effects of spectral spreading, this auxiliary reflector is moved at a constant speed past the target toward the radar (Spectral spreading is caused by (1) the cyclic nature of the frequency sweep, which gives rise to an output envelope that consists of pieces of a sinusoidal function, as shown in Figure 3-3, and (2) non-linearities in the frequency-time characteristic of the frequency sweep).

A multitarget geometry, similar to that shown in Figure 3-5, is again used; A_r is the reference reflector, the pulsed radar used to observe the complex is located at K. The total

signal voltage V_s received by the radar at K is

$$V_s = \sqrt{2}\left[\sum_{i=1}^{N} a_i \cos\left(\omega t - \frac{4\pi d_i}{\lambda} - \phi_i\right) + A_r \cos\left(\omega t - \frac{4\pi d_r}{\lambda} - \phi_r\right)\right] \tag{3-18}$$

When this signal is fed through a square law detector, the output, $P(\omega)$, is proportional to the original voltage and may be written as

$$P(\omega) = \overline{V_s^2} \tag{3-19}$$

When equation 3-18 is substituted into equation 3-19, the right hand side of equation 3-19 will have the same form as that of equation 3-3. Since these expressions have the same form, the evaluation of equation 3-19 may now be written as

$$P(\omega) = A_r^2 + \sum_{i=1}^{N}\sum_{q=1}^{N} a_1 a_q \cos\left[\frac{4\pi \Delta d_{q,i}}{\lambda} + \Delta\phi_{q,i}\right]$$

$$+ \sum_{i=1}^{N} 2a_i A_r \cos\left[\frac{4\pi \Delta d_{i,r}}{\lambda} + \Delta\phi_{i,r}\right] \tag{3-20}$$

Equation 3-20 may then be expanded to

$$P(\omega) = A_r^2 + \sum_{i=1}^{N} a_i^2 + \sum_{\substack{i=1 \\ i\neq q}}^{N}\sum_{q=1}^{N} a_i a_q \cos\left[\frac{4\pi \Delta d_{q,i}}{\lambda} + \Delta\phi_{q,i}\right]$$

$$+ \sum_{i=1}^{N} 2a_i A_r \cos\left[\frac{4\pi \Delta d_{i,r}}{\lambda} + \Delta\phi_{i,r}\right] \tag{3-21}$$

Equation 3-21 contains three characteristically different groups of terms:

1. The dc terms

$$\sum_{i=1}^{N} a_i^2 + A_r^2$$

2. The terms arising from the interaction of individual scatters within the target

$$\sum_{\substack{i=1 \\ i\neq q}}^{N} \sum_{q=1}^{N} a_i a_q \cos\left[\frac{4\pi\Delta d_{q,i}}{\lambda} + \Delta\phi_{q,i}\right]$$

3. The terms arising from interaction of the corner reflector with individual scatterers within the target

$$2 \sum_{i=1}^{N} a_i A_r \cos\left[\frac{4\pi\Delta d_{i,r}}{\lambda} + \Delta\phi_{i,r}\right]$$

In the static situation described by equation 3-21, these three types of terms are superposed. However, these terms can be separated by using the frequency stepping mode described earlier and shown in Figure 3-1. The result is a saw tooth variation of frequency with time which is sampled at the PRF of the radar. Appendix I contains a detailed calculation of the frequency components present in the radar output. The general characteristics of the spectrum can be discussed without investigating all of the details.

When the radar frequency is varied, the dc terms of equation 3-21 are unchanged and the effect of this variation on the other terms is qualitatively the same. A typical term may be written as

$$P(t) = \cos\left[\frac{2\Delta d}{c}\ (\omega_o + \alpha t_c)\right]$$

$$0 \leq t_c < T_c$$

$$t_c = t - n\ T_c \qquad (3\text{-}22)$$

This form shows explicity that P(t) is periodic with period T_c and that the behavior within the period is a cosinusoid with a frequency

$$f = \frac{1}{2\pi}\ \frac{2\Delta d}{c}\alpha \qquad (3\text{-}23)$$

that depends on (1) the rate $\alpha/2\pi$ at which the radar frequency is changed and (2) the distance, Δd, between two scatterers. The actual output is a sampling of this wave at the PRF, as shown in Figure 3-3, but this sampling need not be considered

in this qualitative description. The spectrum of the voltage envelope of the output, equation 3-22, is a set of lines at the harmonics of the frequency $1/T_c$. The harmonics which exhibit maximum amplitude are those falling nearest f and its harmonics. Thus, if the spectrum of the radar output is analyzed, the distances, $\Delta d_{q,i}$ and $\Delta d_{i,r}$, in equation 3-21 can be determined.

If the corner reflector is far enough behind the target, all of the distances, $\Delta d_{i,r}$, will be larger than any of the $\Delta d_{q,i}$, and a spectrum analysis will enable the determination of each distance. In practice, however, jitter and nonlinearities in the frequency sweep of the radar make it difficult to resolve these frequencies.

The technique of moving the corner reflector at constant velocity towards the radar provides a means for overcoming the effects of jitter and nonlinearity. It also provides a means for separating the interactions between the scatters from interaction between the reflector and its scatterers by frequency discrimination. This possibility arises because (1) a Doppler shift of $2v\ f_o/c$ is impressed on the lines involved in the interaction of the reflector with the target, (2) low frequency spectral components may now be used in the distance determination, and (3) these low frequency components are less affected by the jitter and nonlinearity previously mentioned. Since f_o is the radar frequency, significant Doppler frequencies can be obtained with modest velocities. Use of the moving reflector also permits discrimination between the interactions with scatterers that are equidistant from the reflector, one in front and the other behind.

The following qualitative description is based on the analysis in Appendix I. In the mathematical sense, the spectrum consists of two sets of lines. One set contains harmonics of the fundamental frequency $1/T_c$, and the amplitudes of this set depend on interactions between scatterers of the target. The other set is displaced from the $1/T_c$ lines by the Doppler shift, and the amplitudes depend on interactions between the moving reflector and the target. The interaction between the reflector and each scatterer furnishes a varying amplitude to these lines. Within the set of Doppler lines are two sets of lines which are shifted in opposite directions from the $1/T_c$ lines. The shifted lines showing the greatest amplitude occur at a frequency of large numerical value when the reflector is behind the scatterer; as the reflector moves toward the radar, lines nearer zero frequency have the greatest amplitude.

As far as any measuring equipment is concerned, the negative frequencies are measured as if they were positive. However, the Doppler shift for one set of lines increases the positive frequencies, and decreases the numerical value of the negative frequencies, and the converse is the case for the other set of Doppler-shifted lines. Consequently, for a set of doppler shifted lines, the fold-over that occurs in the representation of the information obtained from measuring equipment does not result in superposing the negative frequency lines on those of positive frequency unless the Doppler shift is related to the line spacing by $(n + 1/2)T_c$ where n is an integer.

The doppler frequency is chosen so that the shifted lines fall one-third or two-thirds of the way between the unshifted lines. Consequently, the folded-over lines of a set of Doppler shifted lines fall two-thirds or one-third of the way between the $1/T_c$ lines, and the result is three sets of equidistant lines (The folded lines at one set of Doppler shifted lines will always coincide with the real lines of the other set). When this choice is made, the possibility of interference between the returns from scatterers behind the reflector and those in front is minimized.

This choice of Doppler frequency provides optimum discrimination between scatterers in front of and behind the corner reflector as well as discrimination against spectral components which arise from interactions between the fixed scatterers. Mathematically, the optimum Doppler frequency is defined by

$$f_D = \frac{n}{3T_c} \qquad n \equiv 1,2 \text{ (modulo 3)}$$

$$\text{(i.e., } n = 1,2,4,5,7,8,10\ldots) \qquad (3\text{-}24)$$

where T_c is the period of the stairstep, as shown in Figure 3-1, and the symbol $\equiv$ means "congruent to."

When such a Doppler frequency is chosen, the 2 sets of lines represented by groups 2 and 3 will become three sets:

Set 1: Lines at $n(\frac{1}{T_c})$, no relative motion

Set 2: Lines at $(n+\frac{1}{3})\ \frac{1}{T_c}$, relative motion in one sense

Set 3: Lines at $(n-\frac{1}{3})\ \frac{1}{T_c}$, relative motion in the opposite sense.

As previously mentioned, a narrow band filter is provided to accept one of the Doppler components. This filter will respond to the $(\sin^2 x)/x^2$ type of envelope associated with a given source, as the separation, $\Delta d_{i,r}$, varies through the appropriate range. Fmphasis is placed on the fact that it is the envelope, and not the lines in the spectrum, that moves with variation in $\Delta d_{i,r}$. Thus all ambiguities which result from the sawtooth shown in Figure 3-2 can be removed.

The minimum distance, Δd, which will provide a full cosine cycle of P (equation 3-22) during one cycle period, T_c, can be found by equating the right hand side of equation 3-23 to $1/T_c$:

$$\frac{1}{2\pi} \frac{2\Delta d_{i,r} \alpha}{c} = \frac{1}{T_c}$$

$$\Delta d_{i,r} = \frac{c}{2T_c} \frac{2}{\alpha} = \frac{c}{2B} \qquad (3\text{-}25)$$

where $B = \alpha T_c/2$ is the bandwidth from the beginning to the end of one stairstep cycle. Appendix I contains a derivation of resolution based on spectral analysis while Appendix II contains a derivation based on computation of the autocorrelation function of the transmitted wave form.

SECTION 4

RAT SCAT

INSTRUMENTATION

In the preceding sections, consideration has been given to the basic principles of frequency stepping and the application of this technique to radar cross section measurement. This section contains a description of the instrumentation that has been incorporated in the RAT SCAT equipment to enable measurement based on the principles previously discussed. The three main groups of radar equipment will be discussed: the transmitter, the receiver, and the sigma servo. A more detailed description of this instrumentation will be found in References 2 and 3. The experimental moving corner reflector configuration is also discussed in this section.

Radar Equipment

Figure 4-1 is a block diagram of the transmitter, which incorporates a frequency stepping unit. This transmitter has been designed to operate in Band 7 (8 to 11.5 kilomegacycles). It consists of a master oscillator (backward wave oscillator), a driver amplifier (TWT), and a power amplifier (TWT), together with associated control and monitoring equipment. As shown, both of the TWT's are pulsed to produce a good on/off ratio and a good pulse wave form. The peak output power is 1 kilowatt. Other characteristics include the following:

1.	Pulse width:	0.1 microsecond to 1.0 microsecond, variable
2.	Pulse Power:	1.0 kilowatt
3.	Repetition rate:	500-5000 cps
4.	Stepped Frequency:	32,64,128,256 steps per cycle
5.	Stepped frequency mode, frequency range per sweep cycle:	0 to 1.5 kilomegacycles, adjustable
6.	Transmitter on/off ratio:	greater than 100 db

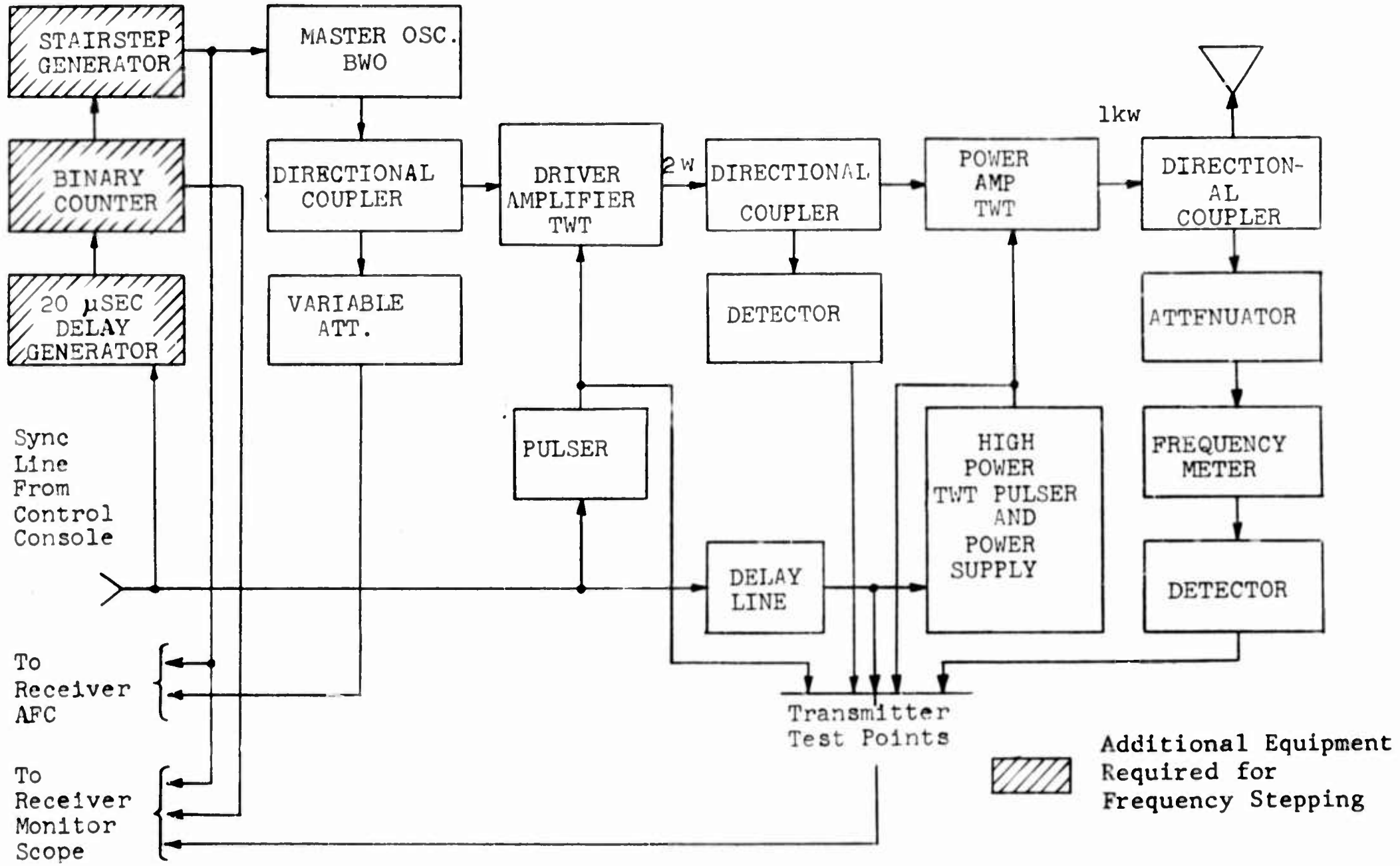

Fig. 4-1 TRANSMITTER BLOCK DIAGRAM

Frequency stepping is accomplished by applying a stairstep voltage to the voltage-tuned master oscillator. The stairstep generator produces a voltage of the desired stairstep form with a high degree of linearity and accuracy. The generator is controlled by a binary counter, which is triggered through a 20-microsecond-delay generator by the system synchronization pulse. One step of the stairstep voltage is produced for each synchronization pulse. A total of 32, 64, 128, or 256 steps is produced for each frequency sweep cycle; the number of steps is controlled by the setting on the operation control on the binary counter.

A block diagram of the receiving system is shown in Figure 4-2. The receiver receives a CW signal directly from the transmitter local oscillator. This signal is attenuated to approximately -50 dbm to reduce interference. The attenuated signal is mixed into the AFC IF amplifier and discriminator. The discriminator produces a dc error voltage which is proportional to the frequency error of the local oscillator. This error voltage is summed with the output of the transmitter frequency stepping unit and fed into the helix of the receiver BWO to control its frequency. The receiver BWO is identical to the one used for the transmitter master oscillator; the AFC will compensate for small frequency differences. Thus, the receiver's local oscillator is stepped in frequency and synchronized with the transmitter master oscillator to maintain a constant intermediate frequency.

The local oscillator provides 10 milliwatts of RF power. This power is divided, part being used to drive the signal channel mixer and part to drive the AFC mixer. Two ferrite isolators are incorporated in the line between the power splitter and the AFC mixer. These isolators are used to prevent the transmitter master oscillator signal from feeding through the AFC mixer, through the power splitter, and into the signal channel mixer. Since the frequency of this signal is the same as that of the transmitter, it tends to mask out low-level target echos.

The problem of converting the target echo signal to a proper form for recording is solved by comparing the signal with a standard reference oscillator signal and driving a servo with the resulting error signal. The complete servo loop, as shown in Figure 4-3, consists of the IF amplifier, gate circuits, boxcar circuit, error detector, amplifier, motor, 60-megacycle oscillator, attenuator, and amplifier.

For single frequency operation or for frequency stepping operation, when it is desirable to record average signal return, the equipment is operated in the following manner. Echo signals

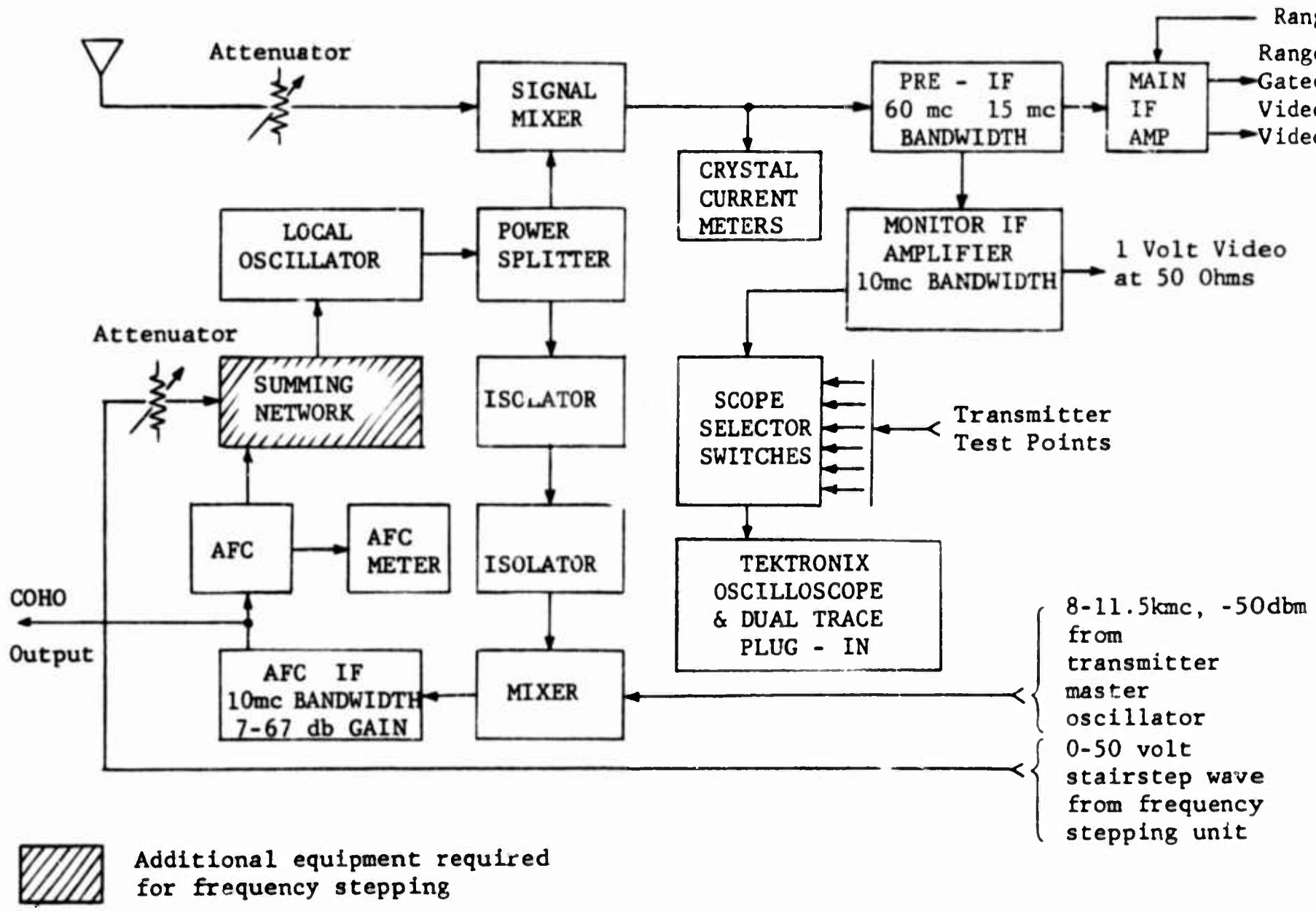

Fig. 4-2 RECEIVER BLOCK DIAGRAM

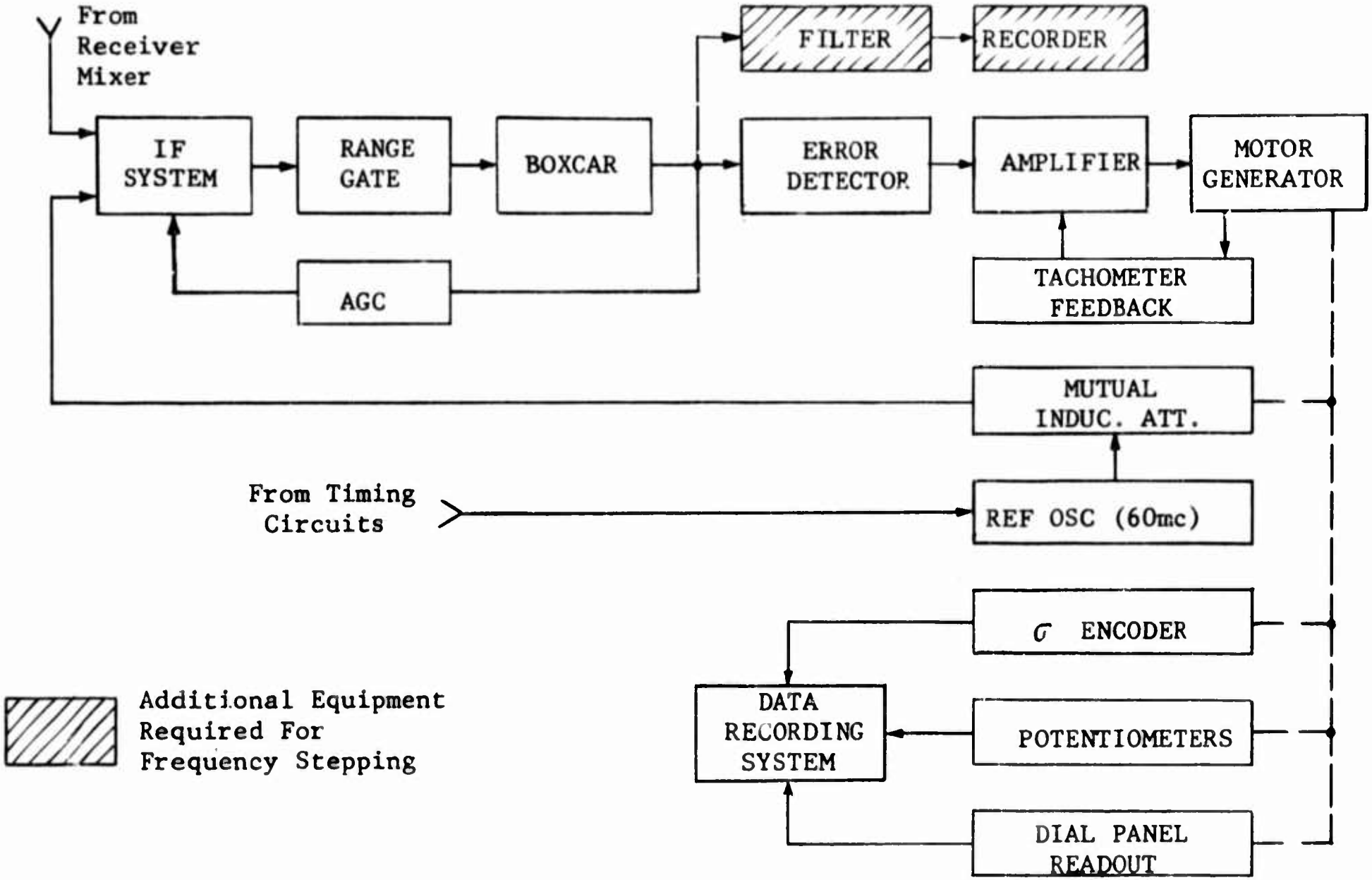

Fig. 4.3 IF AMPLIFIER AND SIGMA SERVO BLOCK DIAGRAM

are fed to the IF amplifier, along with a pulse from the reference oscillator. The gate circuits then allow the return pulse and reference pulse to be routed to the boxcar circuit. The boxcar stretches the pulses and relays them to the Error Detector. The error detector transforms the difference in pulse height between echo and reference signal into a 400-cps voltage to drive the servo. The servo drives in such a direction that the amplitude of the attenuated 60-megacycle reference oscillator pulse is matched to the amplitude of the echo signal. At this point, shaft position represents the intensity of the received signal or echo. For the case of frequency stepping the sigma servo acts as a low-pass filter and drives to a position that corresponds to the average echo return from the target.

An encoder on the sigma shaft permits a direct digital readout of cross section. Two potentiometers on the sigma shaft are used to control the pens on two recorders to yield polar or rectilinear plots of cross section, at the discretion of the operator.

To use the equipment for flare spot location, a high selectivity filter is connected to the boxcar output, and the filter output is recorded as a function of time. In this case, the sigma servo is rendered inoperative. The previously discussed instrumentation is shown in Figure 4-4, plus the additional instrumentation needed to obtain flare spot isolation. This additional instrumentation consists of a movable corner reflector and a set of railroad type tracks on which to move the reflector.

Experimental Moving Corner Reflector Equipment

A self-contained cart with a mast-mounted corner reflector, a track, and the necessary instrumentation were provided for the range resolution portion of the frequency stepping experiment. A photograph of the initial equipment configuration is shown in Figure 4-5. The cart platform is about 33 inches wide by 48 inches long; the top surface, exclusive of the protruding batteries, is about 6 inches above the track. The cart con ains a dc shunt-wound motor, batteries, and the necessary control circuits. The cart weighs approximately 200 pounds. Sealed bearings and compartments were used to avoid excessive deposition of dust or sand in the cart components. A shield, which extended to a height of 14 inches above the track, was placed on the front of the cart in an effort to reduce the radar cross section of the cart configuration.

The track for the cart was constructed of parallel 2.5-inch pipes, 3 feet apart on centers, in two 20-foot sections. Two

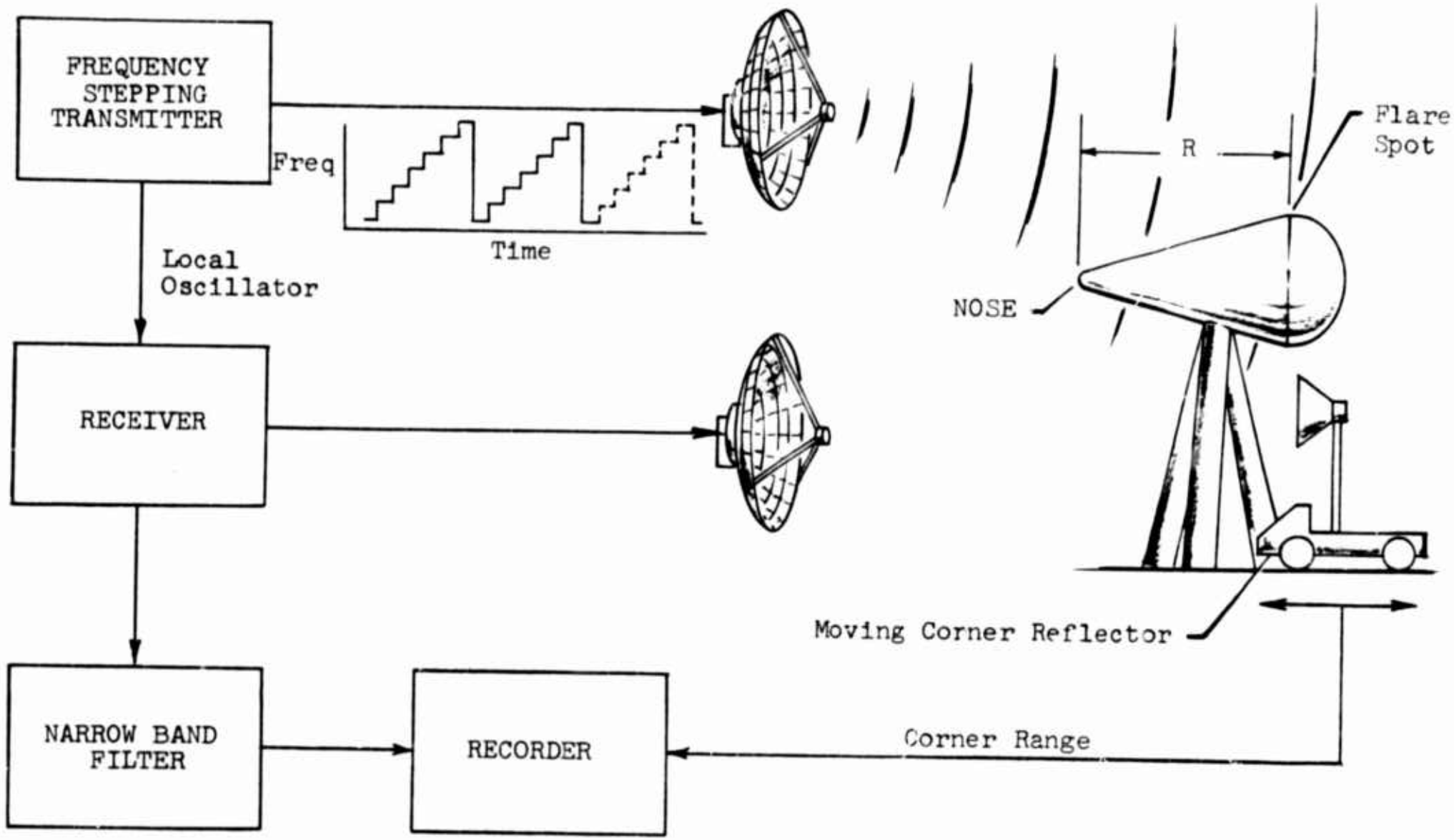

Fig. 4-4 SPECIAL FREQUENCY STEPPING EQUIPMENT

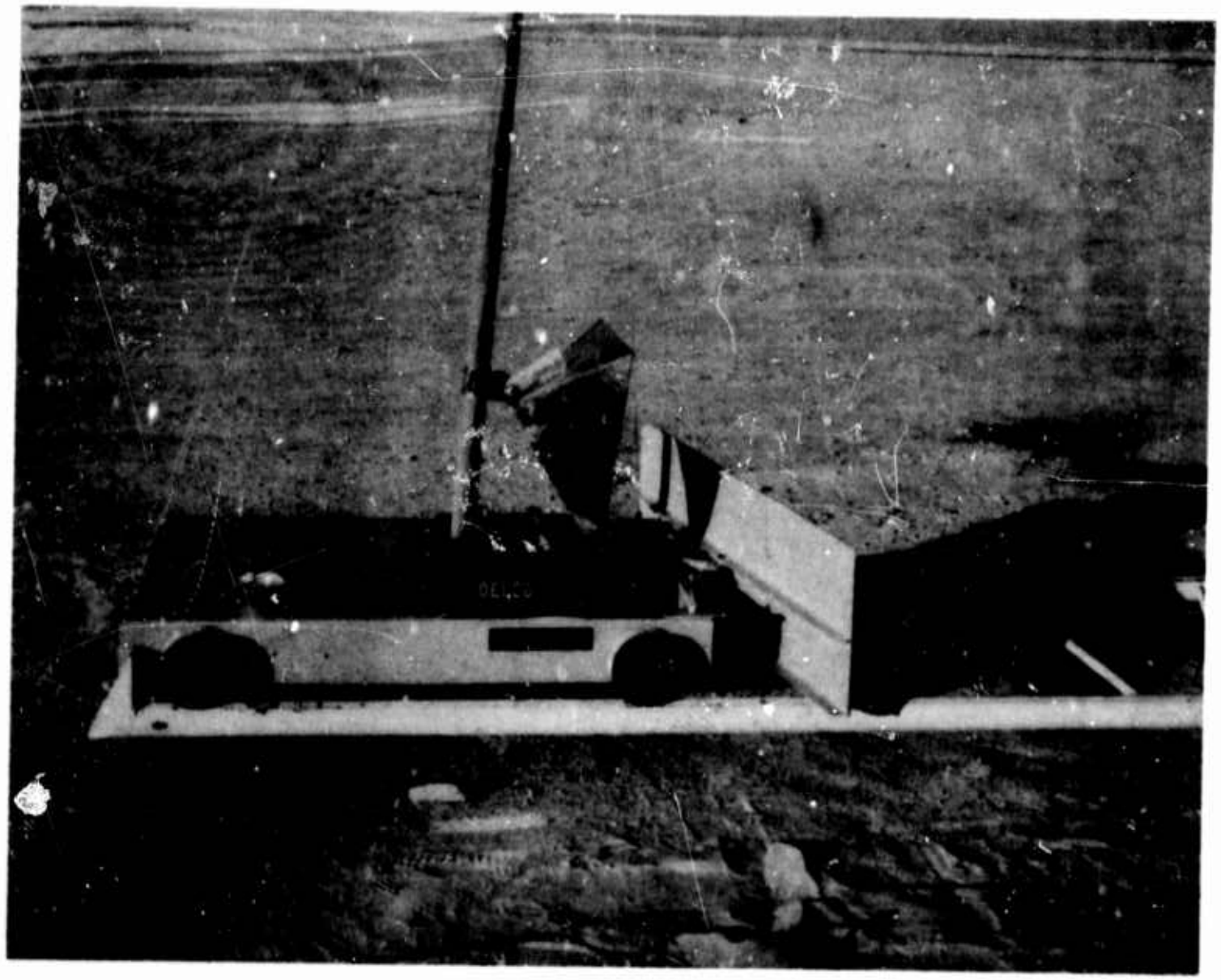

Fig. 4-5 INITIAL FREQUENCY STEPPING CART CONFIGURATION

men can position a section of track. A transit was used to establish the level of the track.

For operation of the frequency stepping system for range resolution measurement, the cart motion was started from the operations building with the cart at the far end of the track. The cart traveled to the near end of the track, automatically reversed direction, and moved to the far end of the track where it stopped automatically.

Five cart-operated switches were placed along the track at 5.0-foot intervals to provide signals for use in determining cart position and velocity; the timing signals and radar signals were simultaneously recorded on separate tracks of a multi-track, strip chart recorder. The experimental cart was designed to travel at a velocity variable from about 1.3 to 3 feet per second through the use of an electrical control and three different gear ratios. The cart was actually somewhat overpowered, and the velocity was higher than predicted and was not constant. Weights were added to the cart to provide a more constant velocity. Typical velocity measurement data obtained on different days is shown in Table 4-1. The effect of velocity variations is discussed in Section 5.

An examination of the preliminary data led to efforts to reduce the radar cross section of the cart configuration to insure that only one scatterer of significant cross section was present. The shield was replaced by a block of RAM, and the wooden mast by a thin Styrofoam column.

The preliminary data runs were made by using a 19-inch corner because the 4-inch corner specified for the experiment was lost in shipment. The final data runs were made with a 9-inch corner, which somewhat improved operation over the 4-inch. The 19-inch corner proved to be too large and was placed low on the mast, as shown in Figure 4-5.

Table 4-1 TYPICAL MOVING CORNER REFLECTOR VELOCITY MEASUREMENTS

Range Marker*	Velocity Toward Radar (fps)	Velocity Away From Radar (fps)
1-2	1.41	1.41
2-3	1.41	1.41
3-4	1.44	1.41
4-5	1.42	1.42
1-2	1.33	1.33
2-3	1.33	1.33
3-4	1.4	1.4
4-5	1.36	1.36

*Range marker 1 is at maximum range.

SECTION 5

FREQUENCY STEPPING MEASUREMENT DATA

Measurements were made at the RAT SCAT site with the equipment previously discussed. Special targets were used to provide a theoretical basis for analyzing measurement results. These targets and the results of these measurements are discussed in this section. Some interesting results associated with the ducting of RF energy by Styrofoam and frequency stepping range ambiguity are also discussed. A brief discussion of frequency-stepping measurements on a Mark 11 mock-up is included in this section. The majority of the data runs were made using the following radar parameters.

1.	Frequency:	9.3 kilomegacycles
2.	Bandwidth:	1 kilomegacycle
3.	PRF:	2560 $second^{-1}$
4.	Pulsewidth:	0.175 second
5.	Polarization:	horizontal
6.	Number of steps:	64
7.	Doppler Shift:	≈27 cps
8.	Moving Reflector Speed:	≈1.4 fps
9.	Filter Center Frequency:	≈53 cps
10.	Filter Bandwidth:	7 cps
11.	Theoretical Resolution:	0.5 feet

Variations from these parameters (except for the filter center frequency which was not accurately determined) are shown in the appropriate figures; both radar cross section and range resolution measurements were made on the experimental targets. Radar cross section results consisted of single-frequency measurements at 9.3 kilomegacycles and frequency-stepping measurements from 8.8 to 9.8 kilomegacycles; targets were rotated in both instances. The range resolution measurements were made by using

the moving corner reflector with the target fixed at known azimuth angles.

Experiment Targets

Targets with a theoretically predictable radar cross section pattern for some aspect angles were selected for the frequency stepping experiment. The initial target consisted of two 6.0-inch diameter spheres embedded in a shaped Styrofoam billet in dumb bell fashion and supported by a tapered Styrofoam column. A photograph of this target is shown in Figure 5-1. Single-frequency measurements were made on this target to provide data for comparison with the frequency-stepping measurements. Some aspects of the single-frequency measurements are discussed in this subsection.

The model chosen to represent the frequency-stepping target is that of two uncoupled point scatterers, as shown in Figure 5-2. The radar cross section of the model, consisting of two unit radar cross section point scatterers, can be defined as

$$\sigma = \left| 1 + e^{-i2kD \sin\beta} \right|^2 \qquad (5\text{-}1)$$

After simple manipulation, this equation becomes

$$\sigma = 4 \cos^2(2kD \sin\beta) \qquad (5\text{-}2)$$

Near broadside, the radar cross section can be defined as

$$\sigma = 4 \cos^2(2kD\beta) \qquad (5\text{-}3)$$

and the angle between the peaks of the pattern is

$$\Delta\beta = \frac{\pi}{kD} \qquad (5\text{-}4)$$

For the target configuration and frequency used, D = 3 feet and f = 9.3 kilomegacycles, $\Delta\beta$ = 1.0 degree. This broadside feature can be seen in the single-frequency measurements data for this target.

An examination of the preliminary data run shown in Figure 5-3, will reveal the presence of periodic variations in the maximum values of the trace near broadside. The variations are shown in the sketch in Figure 5-4. It can be seen that the

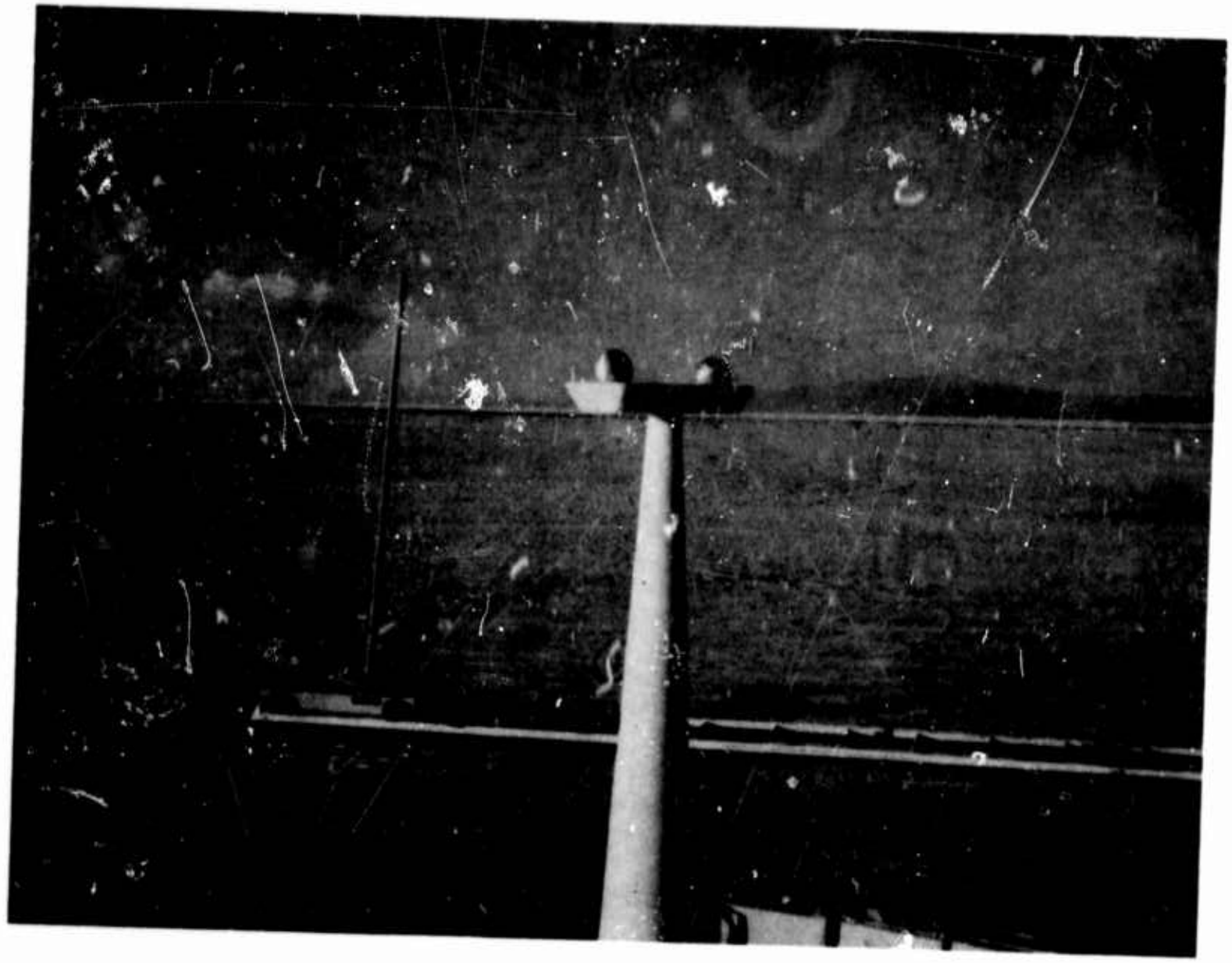

Fig. 5-1 INITIAL FREQUENCY STEPPING TARGET

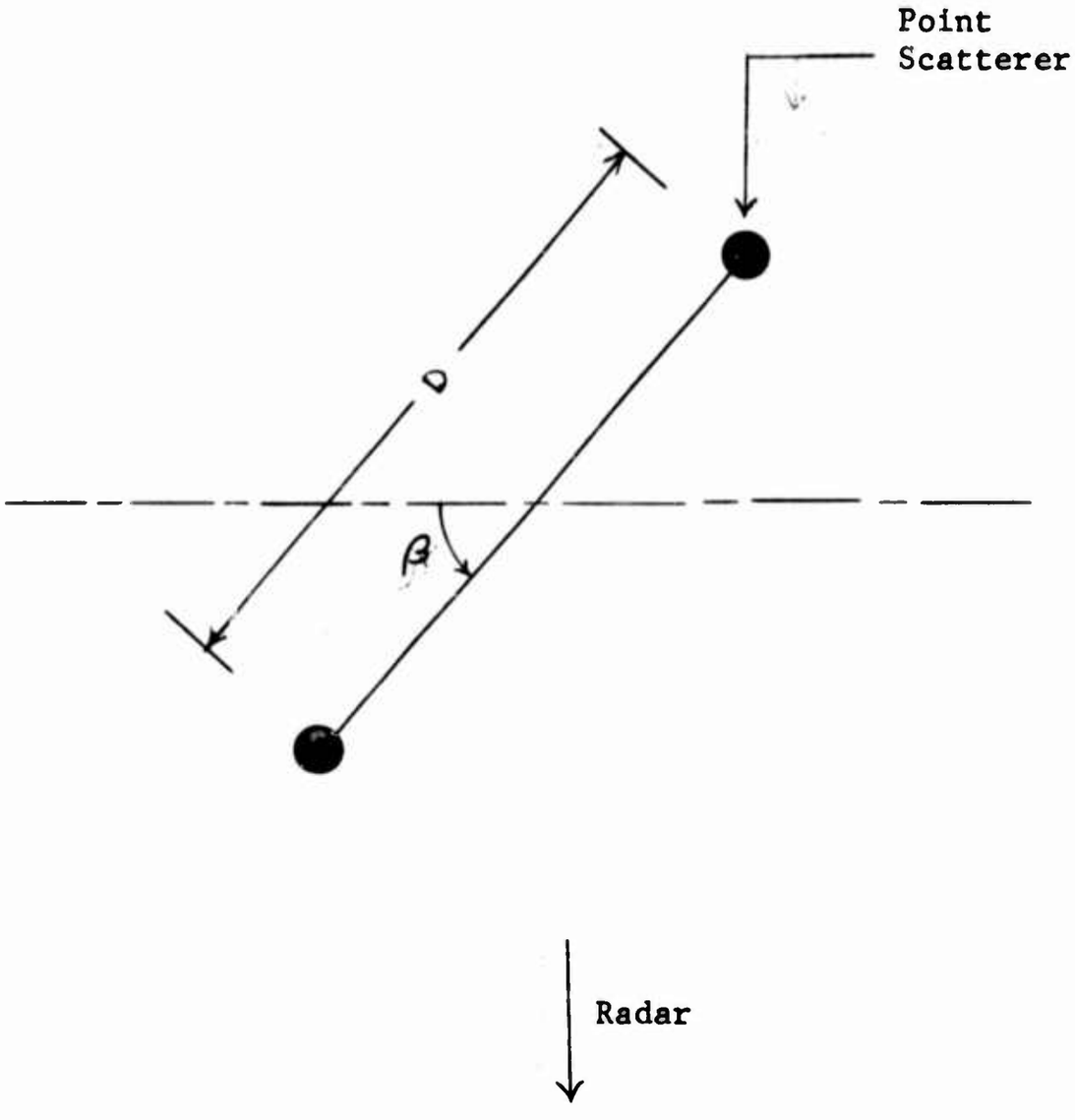

Fig. 5-2 TWO-ELEMENT INTERFEROMETER TARGET MODEL

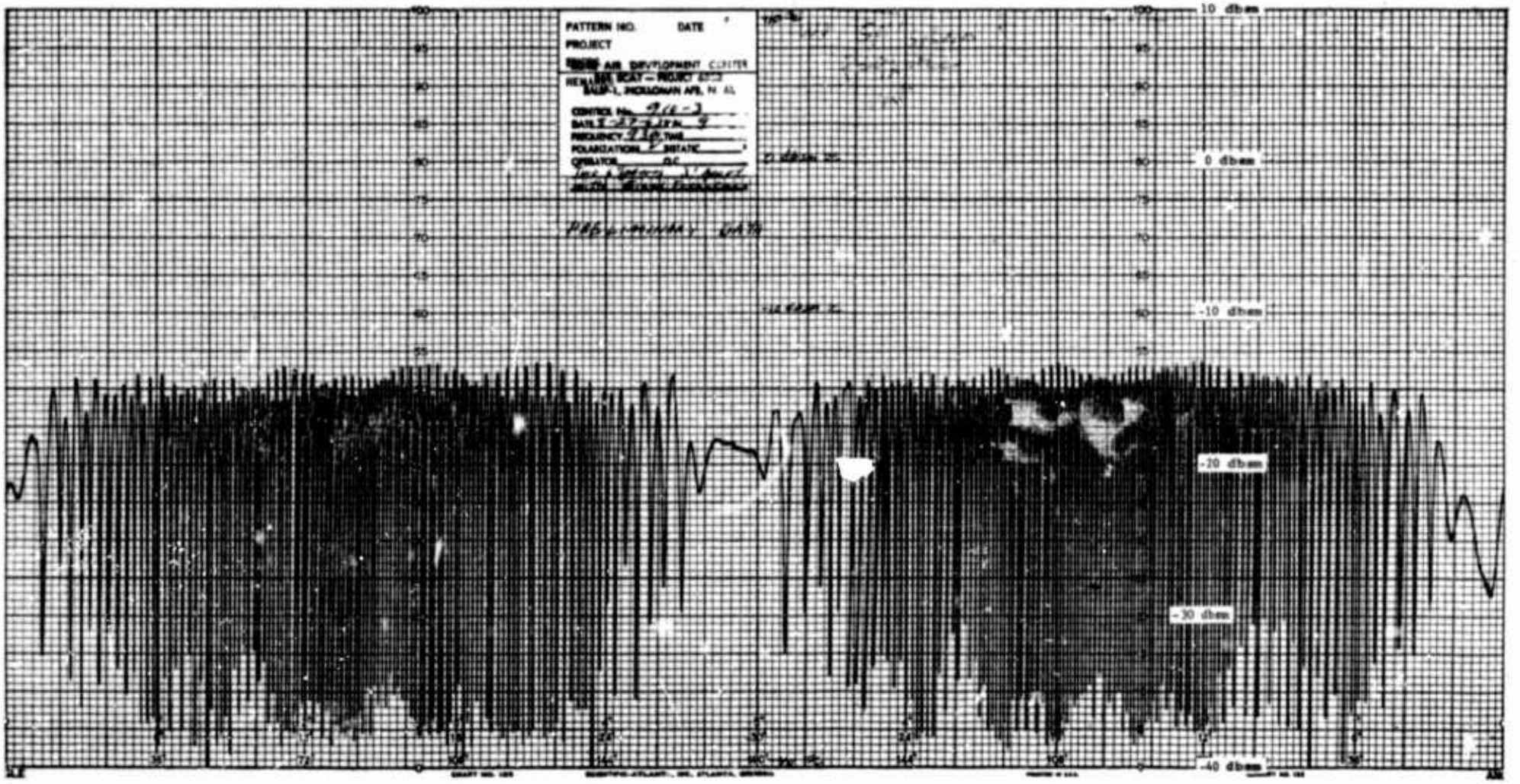

Fig. 5-3 RECTILINEAR SCATTERING DIAGRAM
(9300 mc, target A)

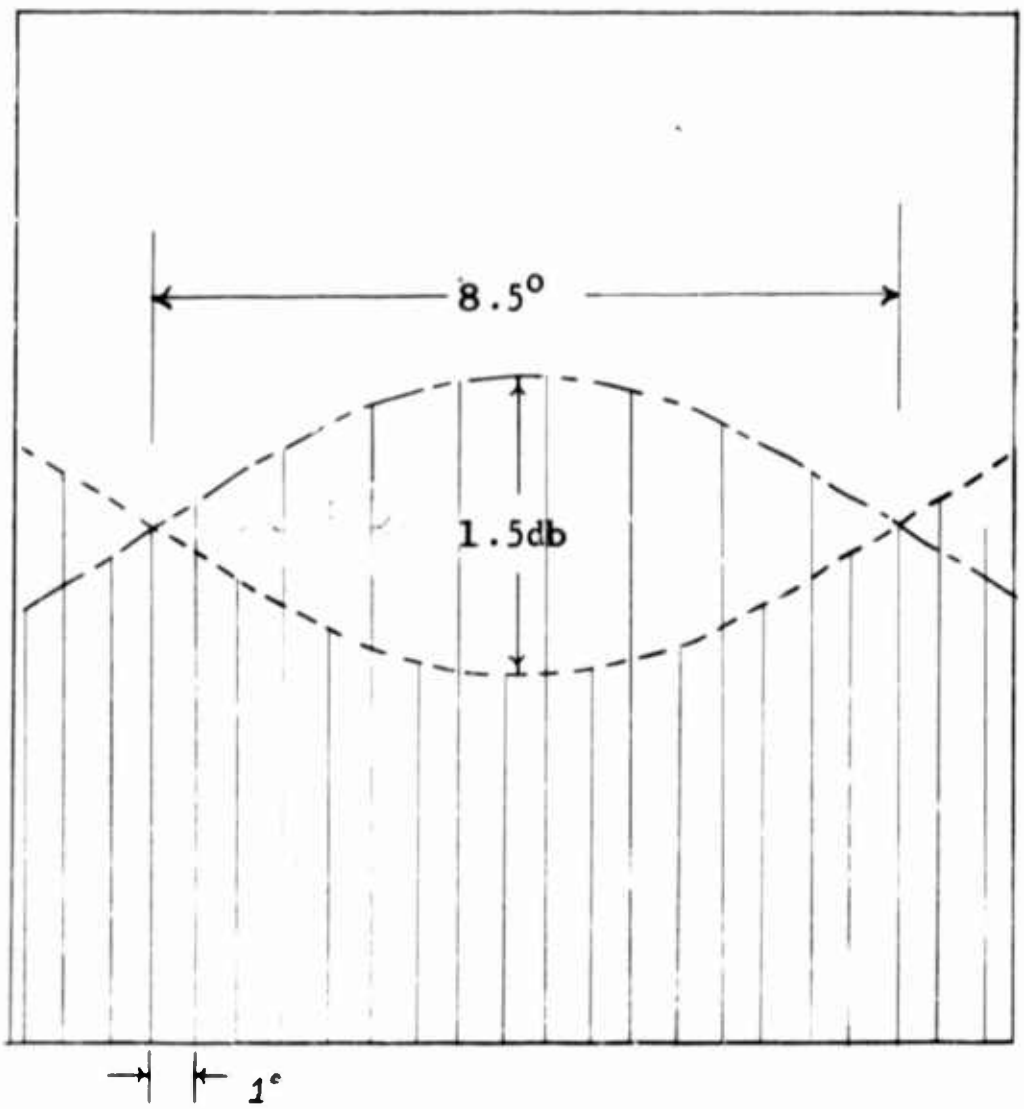

Fig. 5-4 EXAMPLE INTERFEROMETER PATTERN VARIATIONS

pattern maxima are alternately high and low rather than the same value (a periodic variation in the nulls is suggested but will not be considered further). As shown in the following analysis a phenomenon of this type could arise from the presence of a fixed scatterer.

If it is assumed that the target consists of the 2-element interferometer and a fixed scatterer, as shown in Figure 5-5, and that no interaction occurs, the back-scattering cross section can be found in the following straightforward manner:

$$\begin{aligned} d_1 &= y\cos\theta + (L/2 + x)\sin\theta \\ d_2 &= y\cos\theta + (L/2 - x)\sin\theta \\ d_3 &= \text{fixed} \end{aligned} \qquad (5\text{-}5)$$

The radar cross section, relative to the cross section of a single scatterer of the interferometer, can be defined as

$$\sigma(\theta) = \left| e^{i2kd_1} + e^{-i2kd_2} + a\, e^{-i2kd_3} \right|^2 \qquad (5\text{-}6)$$

where $k = 2\pi/\lambda$. After straightforward manipulation, this equation becomes

$$\begin{aligned} \sigma(\theta) = {} & a^2 + 4\cos^2(kL\sin\theta) \\ & + 4a\cos\left[2kd_3 + 2k(y\cos\theta + x\sin\theta)\right] \\ & \cdot\cos(kL\sin\theta) \end{aligned} \qquad (5\text{-}7)$$

In the vicinity of broadside, θ is small and

$$\begin{aligned} \sigma(\theta) = {} & a^2 + 4\cos^2(kL\theta) + 4a\cos\left[2kd_3 + 2ky + 2kx\theta)\right] \\ & \cdot\cos(kL\theta) \end{aligned} \qquad (5\text{-}8)$$

An examination of equation 5-8 will reveal the presence of (1) the interferometer periodicity; the $\cos^2(kL\theta)$ term, which has peaks for values of $\theta = \theta_p = n\pi/kL$; (2) a rapid periodicity introduced by the fixed scatterer, the cos $(kL\theta)$ term, which has maxima at $\theta = \theta_m = 2n\pi/kL$; and (3) a slower periodicity introduced by the fixed scatterer, the cos $(2kd_3 + 2ky + 2k\theta x)$ term,

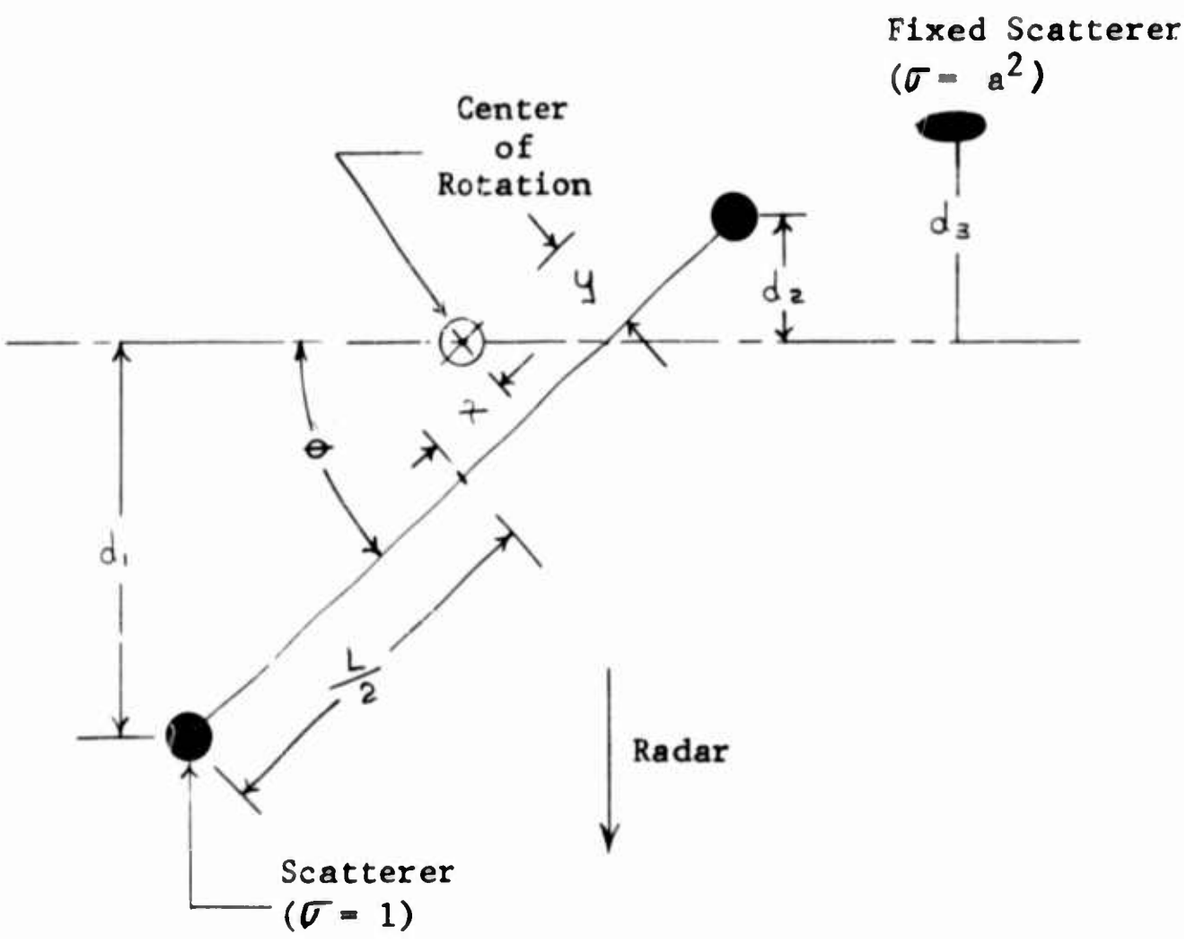

Fig. 5-5 INTERFEROMETER TARGET AND FIXED SCATTER MODEL

which has a period defined by $\Delta\theta = \pi/kx$. For the parameters used, L=3 feet and frequency = 9.3 kilomegacycles, the interferometer period is 1.0 degree, as previously shown, and the period of the fixed scatterer associated effects are 2.0 degrees and 28.6 λ/x degrees. An examination of the data shown in Figure 5-3 will verify the presence of the 1.0- and 2.0- degree periodicities; the slower variation would be caused if x = 2.1 inches, where $\Delta\theta$ is estimated to be 17 degrees.

The relative radar cross section of the fixed scatterer can be estimated by finding the ratio of the maximum and minimum value of the peaks. From equation 5-8, the maximum peak will be $(a + 2)^2$, and the minimum peak will be $(a - 2)^2$. Near broadside, the maximum difference in the peaks is approximately 1.5 db so that the ratio is 1.41 or $a^2 = 0.03$; this value corresponds to a relative level of -15.2 db. Since the radar cross section of the 6.0-inch diameter sphere is about -17.4 dbsm (geometrical optics approximation), the radar cross section of the fixed scatter is approximately -32.6 dbsm.

The model considered above provides a satisfactory explanation for some aspects of the data in the vicinity of broadside. In the vicinity of end-on, where the target interaction occurs, the model is no longer appropriate; some interesting end-on effects for this target are discussed later in this section. An apparent shielding of the sphere farthest from the radar by the Styrofoam billet resulted in a change in the target configuration. A sketch of the three basic target configurations is shown in Figure 5-6.

In subsequent data runs, the variations considered above are not as apparent for two possible reasons. First, an effort was made to reduce the background level; second, most measurements were made on Targets B and C and wind effects caused a variation in the observed cross section even when the target was not rotating. System stability was verified by monitoring the return from the more rigid transfer standard. The sensitivity of the cross section measurement to relative sphere position changes can readily be seen by considering the radial displacement required for one of the spheres to reduce the peak radar cross section value by a given amount. The expression $2\sigma + 2\sigma\cos(4\pi\Delta r/\lambda)$, where σ is the radar cross section of one sphere, can be used to illustrate this effect. When Δr is zero, the theoretical peak value of 4σ is realized, but the radar cross section measurement will be down more than 1 db when Δr is 0.12 inch. A similar but more pronounced effect can occur at the nulls of the pattern.

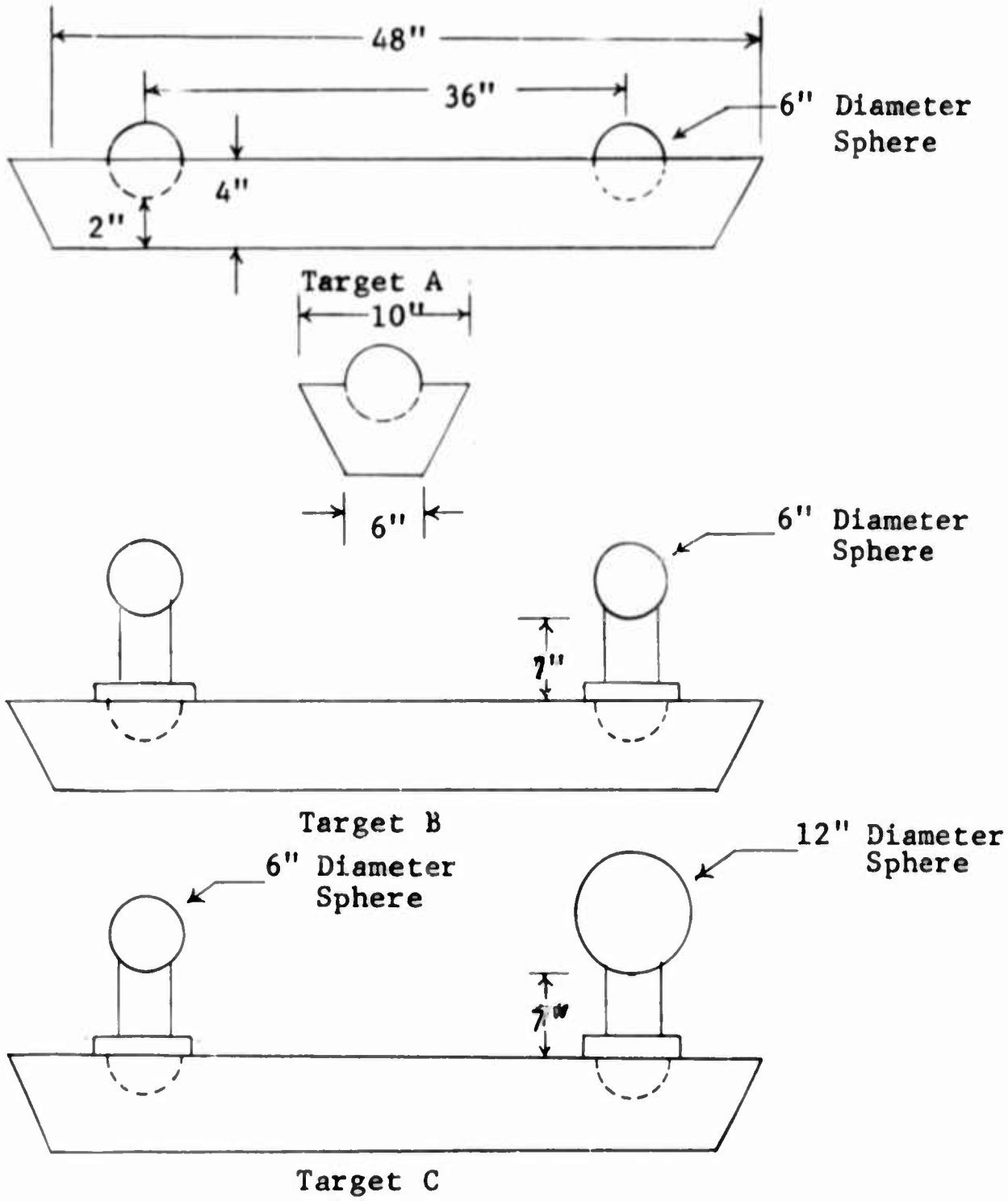

Fig. 5-6 FREQUENCY STEPPING EXPERIMENT TARGET CONFIGURATIONS

Cross Section Averaging

Polar and rectilinear scattering diagrams of the frequency-stepping targets with and without frequency stepping are shown in Figures 5-9 through 5-18. All scattering diagrams were made with the moving corner cart in place. The predicted near-broadside (90- or 270-degree azimuth) period of 1.0 degree is present in the pattern with and without frequency stepping. The predicted (sin x)/x envelope can be seen in the frequency-stepping data. The effect of some type of interaction, such as shielding and/or shadowing, can be seen near the end-on aspect (0 or 180 degrees of azimuth).

The theoretical frequency-stepping cross section pattern of the target with no coupling can be discussed by using the appropriate equation in Section 3.

$$\overline{P} = a_1^2 + a_2^2 + 2a_1 a_2 \cos\left[\frac{4\pi\,\Delta d}{\lambda_o} + \Delta\phi + \frac{2\pi\,\Delta dB}{c}\right] \quad \frac{\sin \frac{2\pi\,\Delta dB}{c}}{\frac{2\pi\,\Delta dB}{c}} \qquad (3\text{-}7)$$

The 1.0-degree-period observed arises from the $4\pi\Delta d/\lambda_o$ and the $2\pi\Delta dB/c$ terms which combine to give exactly the same theoretical period as that obtained in the single frequency case. The predicted (sin x)/x type of envelope appears on the pattern near broadside. A comparison of the measured and theoretical envelopes is shown in Figures 5-7 and 5-8; the theoretical values in these figures were calculated by using the expression

$$10\log_{10}\left[1 + \frac{\sin \frac{2\pi\,\Delta dB}{c}}{\frac{2\pi\,\Delta dB}{c}}\right] \qquad (5\text{-}9)$$

and the appropriate radar and target parameters. A plot of the measured peaks was made from the data in Figure 5-9 and fitted to the theoretical curve. The absolute amplitude of the measured data is not significant in itself in this case, especially in view of the wind effects previously discussed.

Interesting results were obtained when measurements were made with and without frequency stepping, on a target consisting of a 6- and a 12-inch diameter sphere. These data are shown in Figure 5-15 through 5-18. A pattern asymmetry can be clearly

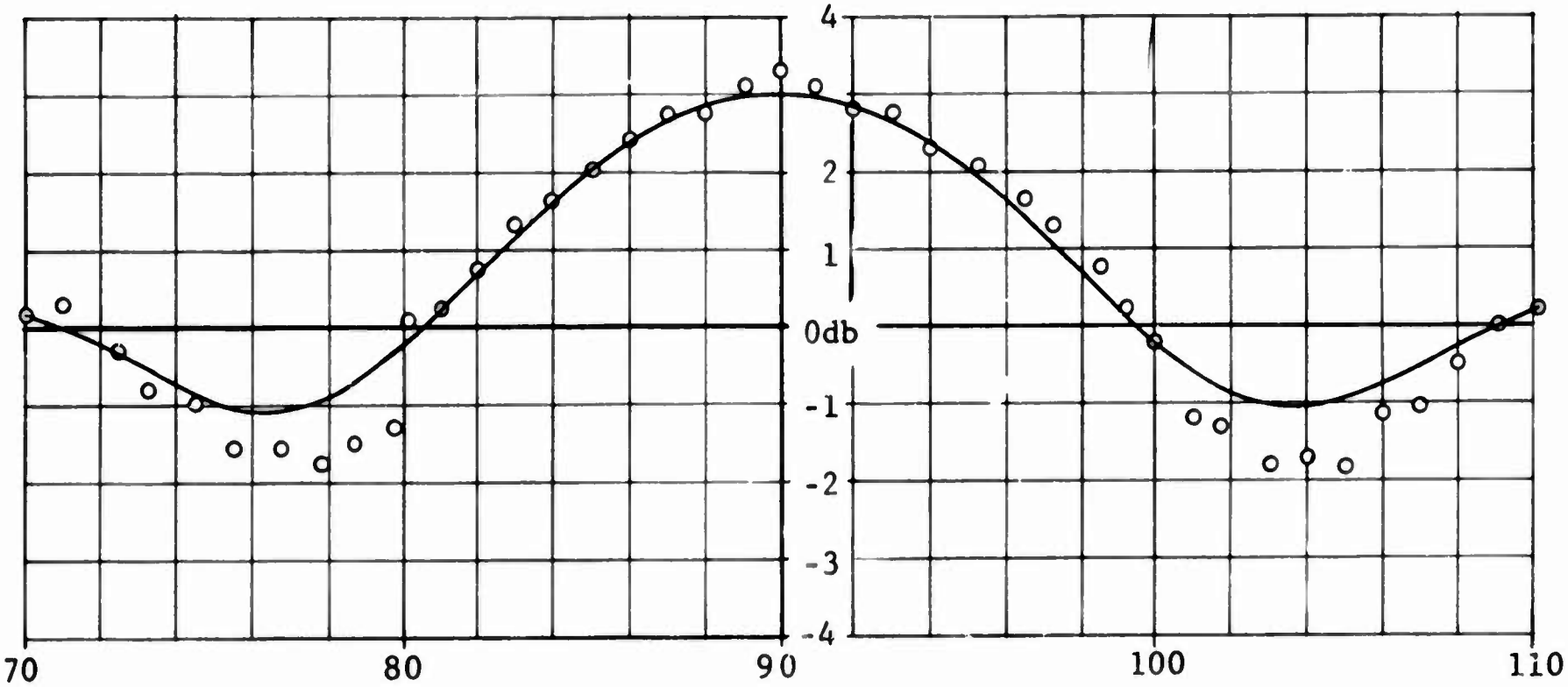

Fig. 5-7 MEASURED AND THEORETICAL FREQUENCY STEPPING PATTERN ENVELOPE

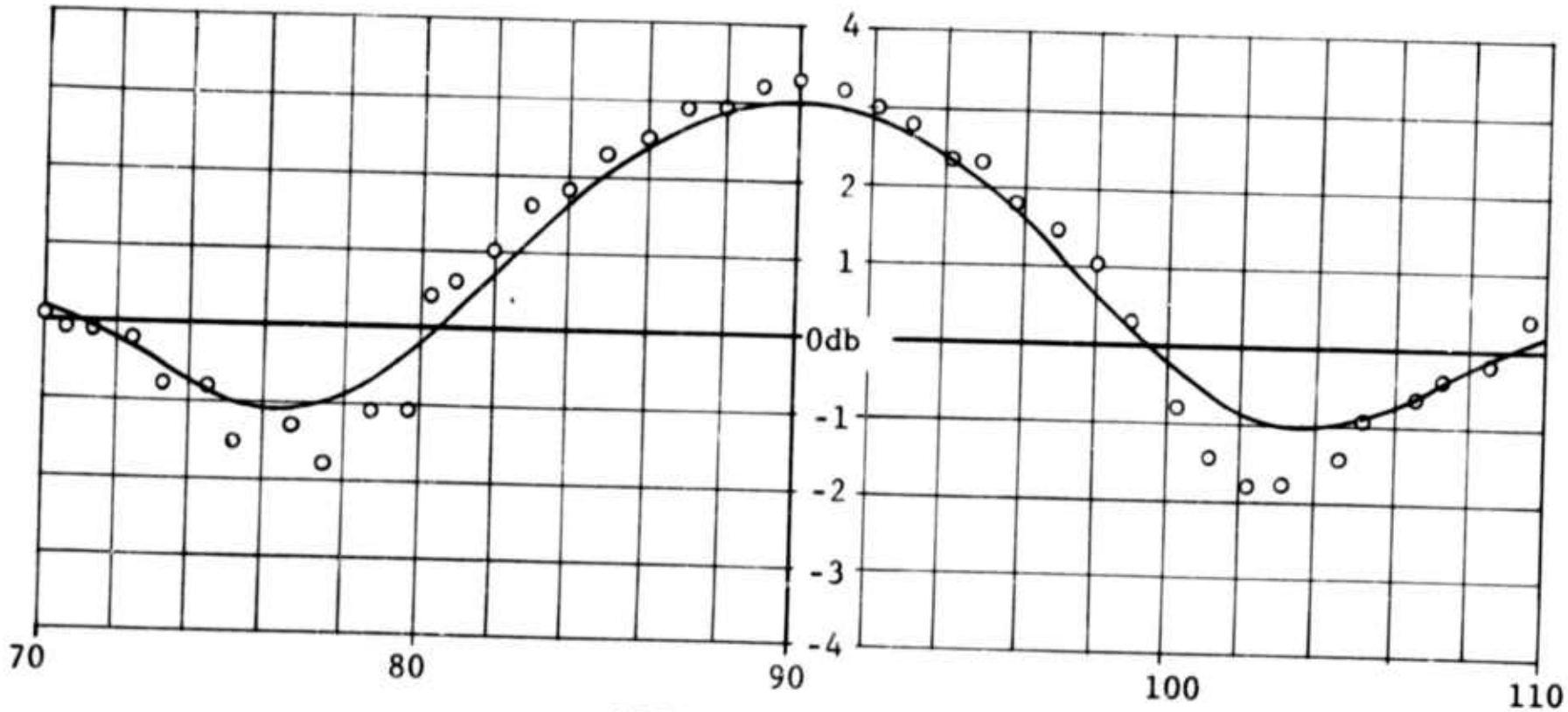

Fig. 5-8 MEASURED AND THEORETICAL FREQUENCY STEPPING PATTERN ENVELOPES

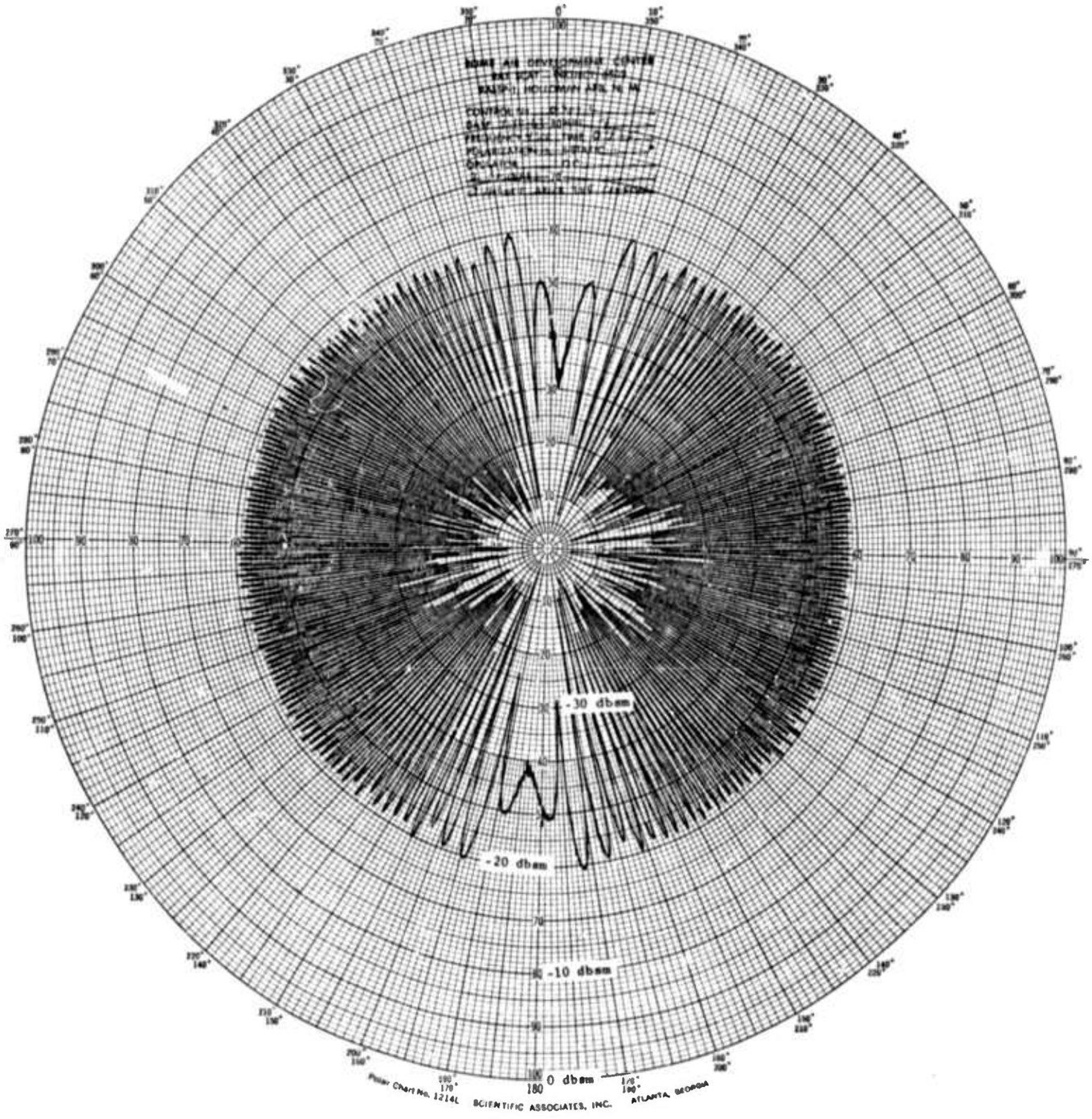

Fig. 5-9 POLAR SCATTERING DIAGRAM
(9300 mc, target B)

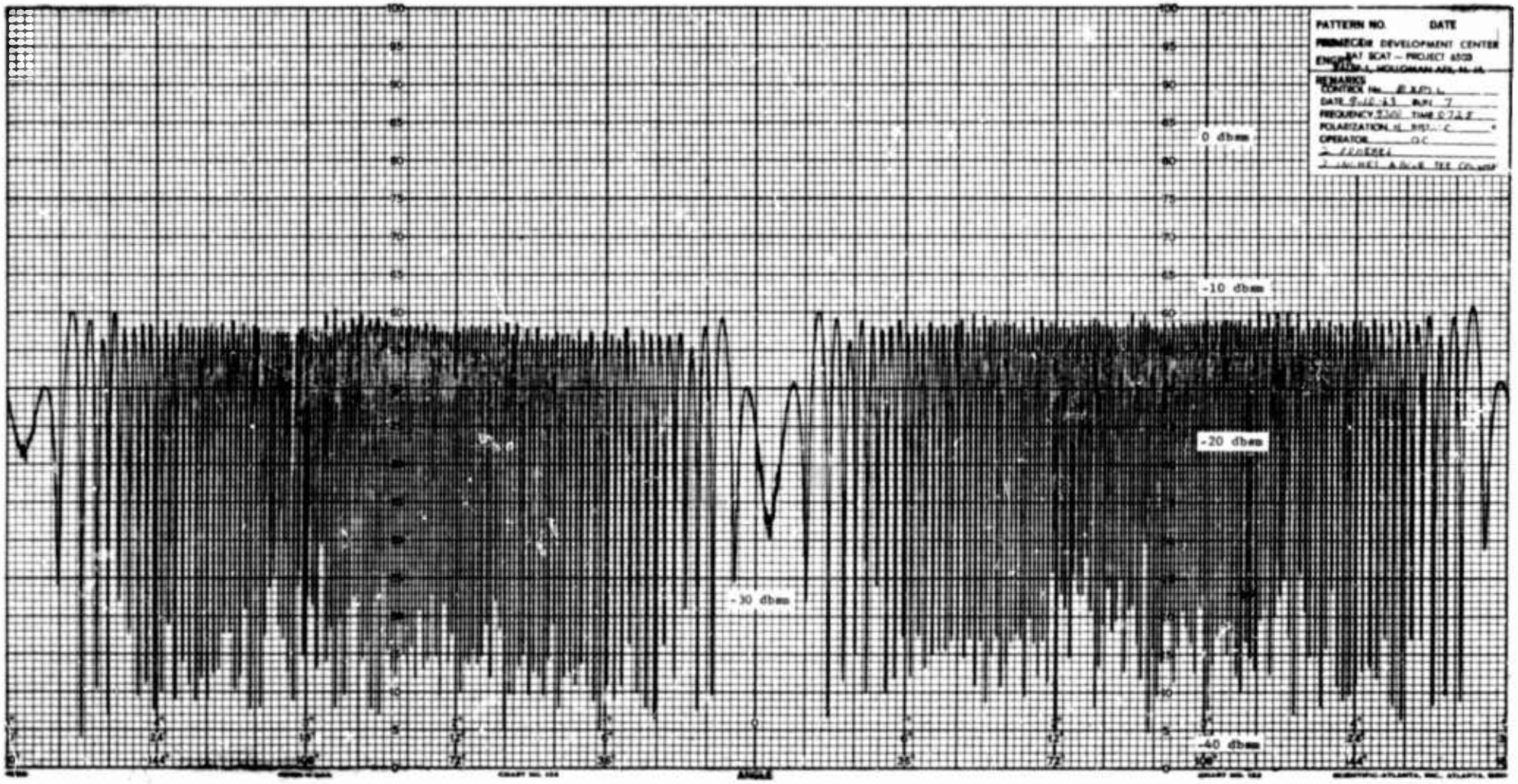

Fig. 5-10 RECTILINEAR SCATTERING DIAGRAM
(9300 mc, target B)

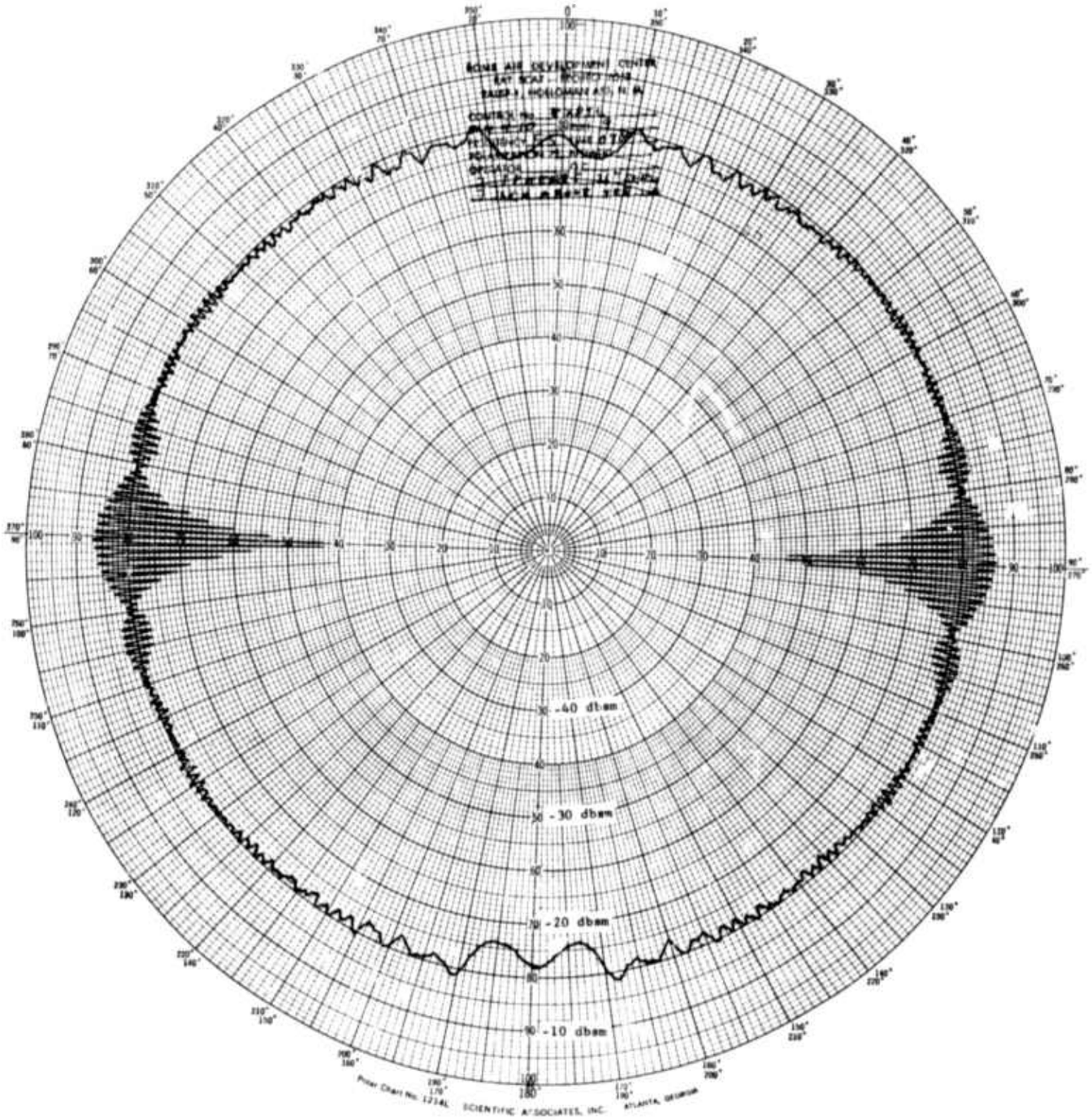

Fig. 5-11 POLAR SCATTERING DIAGRAM
(8800-9800 mc, 64 steps, target B)

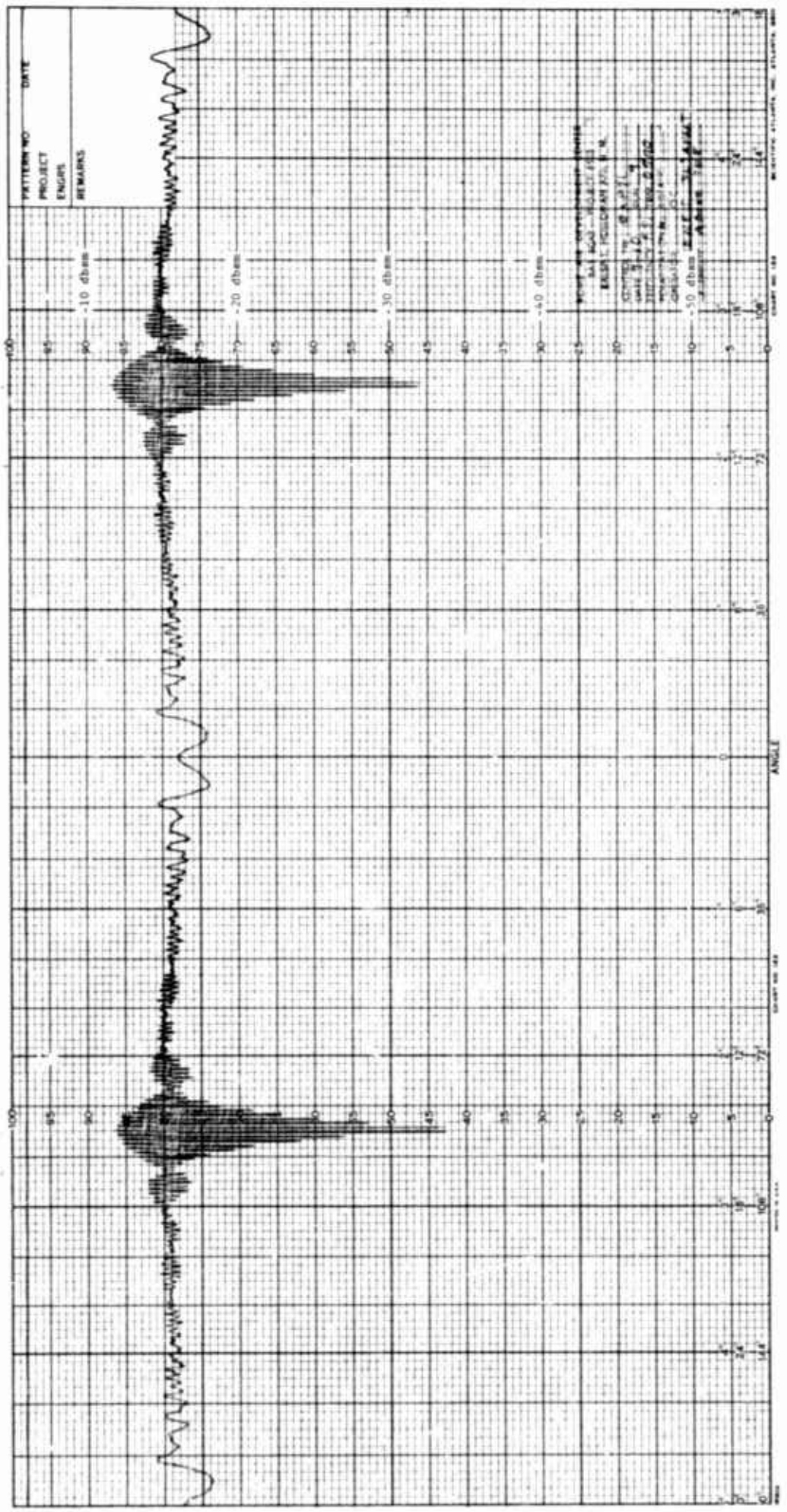

Fig. 5-12 RECTILINEAR SCATTERING DIAGRAM
(8800-9800 mc, 64 steps, target B)

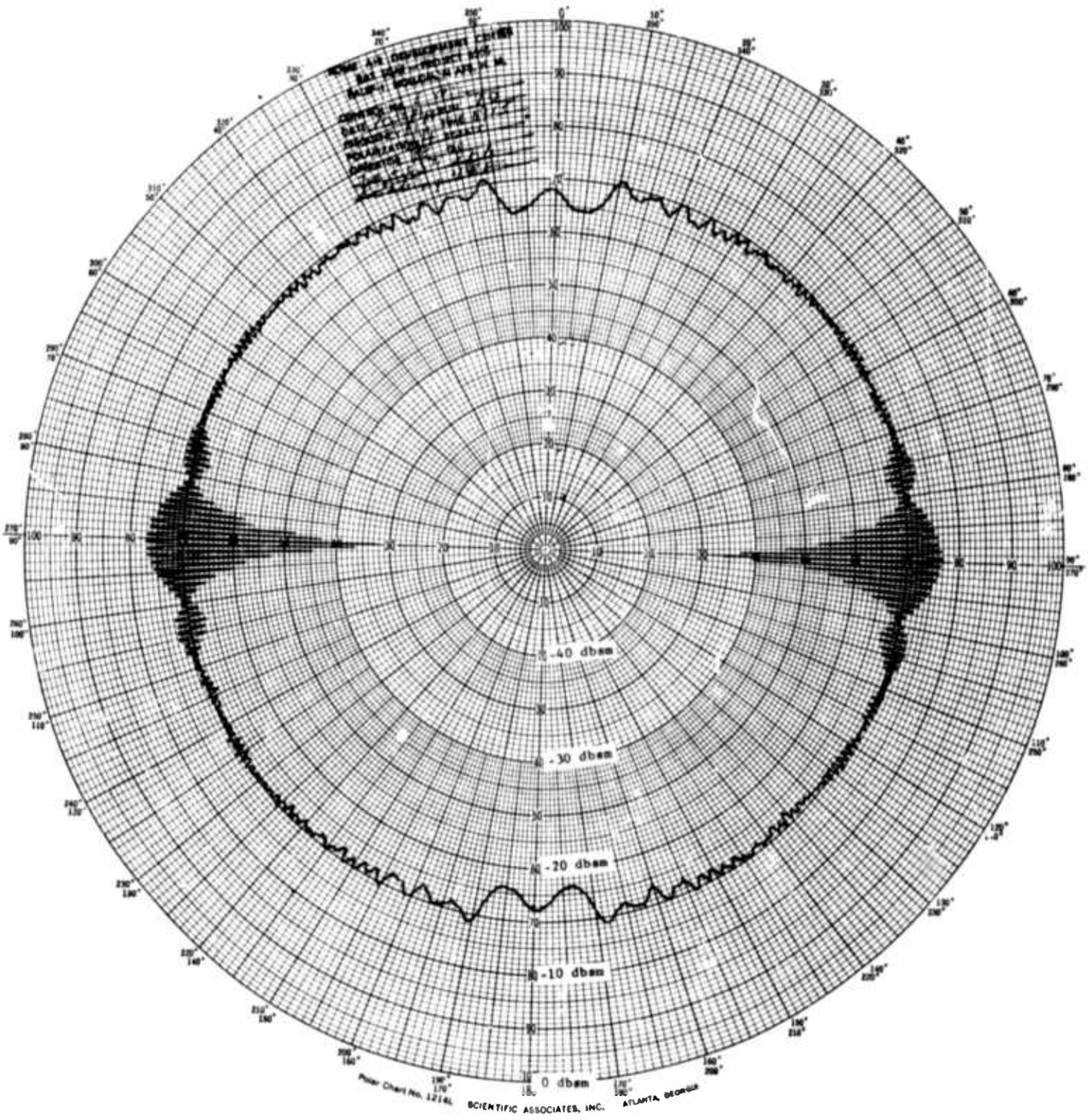

Fig. 5-13 POLAR SCATTERING DIAGRAM
(8800-9800 mc, 64 steps, target B)

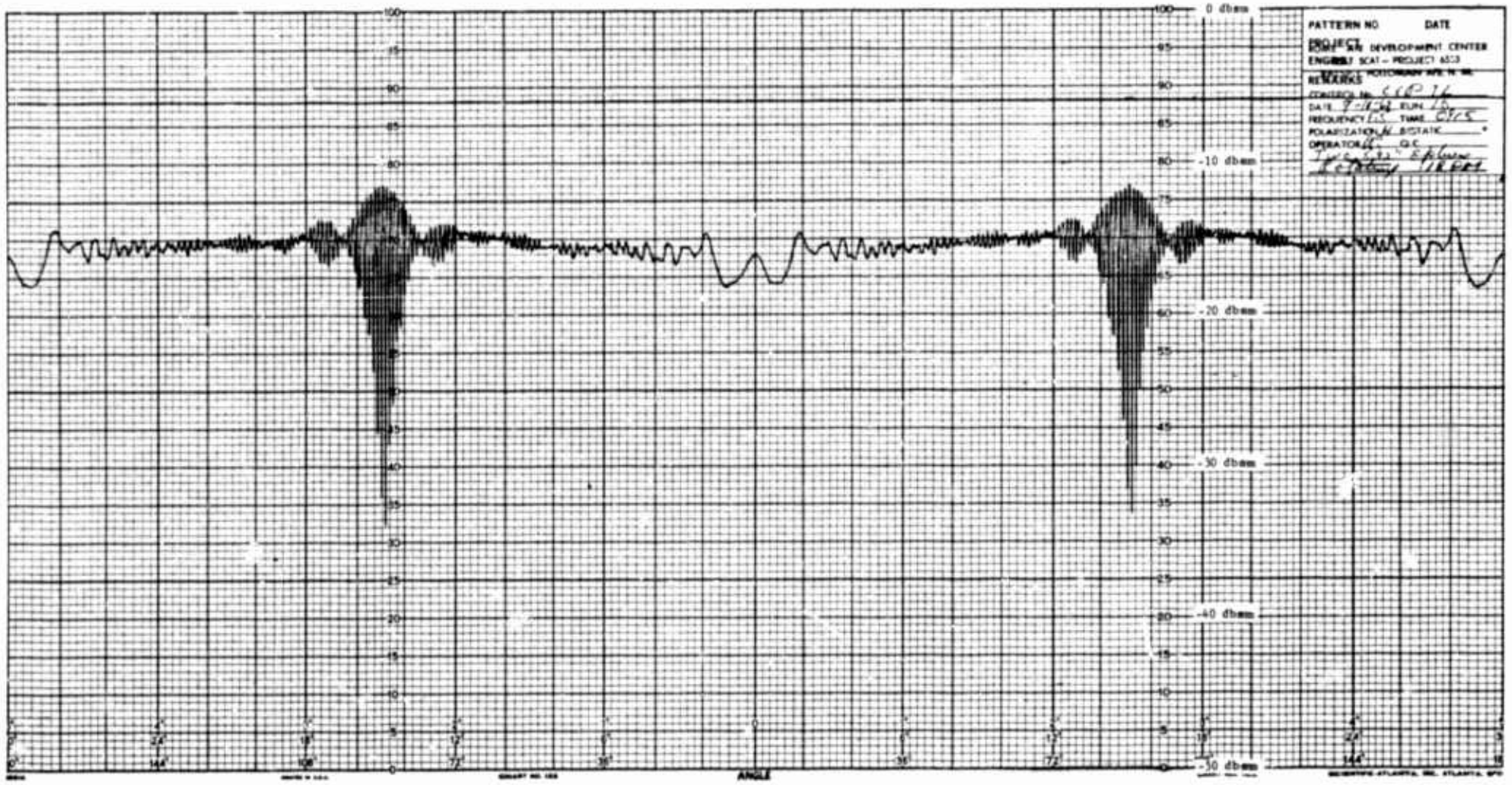

Fig. 5-14 RECTILINEAR SCATTERING DIAGRAM
(8800-9800 mc, 64 steps, target B)

seen in the frequency-stepping run. This effect is easily explained by the fact that the leading edges of the spheres are not at the same range at the 90- or 270-degree azimuth angle and the fact that, in the high frequency region, the phase center of the backscatter from a sphere is near the leading edge. The angular distance between the peaks, ≈171.2 degrees, can be very favorably compared with the calculated angle of 170.4 degrees (a setup error can also be seen in Figure 5-15 and 5-16).

An effect of using spheres of different diameters can be seen in the peak-to-peak variation in the patterns. If it is assumed that the cross section can be defined by the use of geometric optics, the theoretical variation for single-frequency operation is the ratio of the maximum value cross section $(\sqrt{4\sigma} + \sqrt{\sigma})^2$ to the minimum value $(\sqrt{4\sigma} - \sqrt{\sigma})^2$ where σ is the radar cross section of the smaller sphere. This ratio corresponds to 9.54 db; on the data trace, the average peak-to-peak level is close to the theoretical value. The theoretical variation of the frequency stepping trace from the peak to the average value can be readily determined by using equation 3-7. The peak value can be written $(5\sigma + 4\sigma)$; the average value is then 5σ, and the theoretical variation is 2.56 db for this case. For the equal diameter sphere case, the theoretical variation is 3 db.

All scattering diagram data runs were made with the cart in place and only the corner reflector was removed. Background (including the Styrofoam sphere support) scattering diagrams are shown in Figures 5-19 through 5-22. The average frequency stepping background is about 5 db above the 9.3-kilomegacycle level; the peak level is very nearly equal in both cases. Consideration of the theory of frequency stepping averaging leads to the implications that (1) the background could be lower if the background scattering were largely coherent and (2) the effects of relatively large, discrete background sources on target measurements would be reduced. In practice, the frequency stepping background level was greater, probably because of noise introduced through beam position and pattern and VSWR changes over the bandwidth. In spite of the greater frequency-stepping background level, the frequency stepping data is relatively clean, especially in the vicinity of the $(\sin x)/x$ envelope.

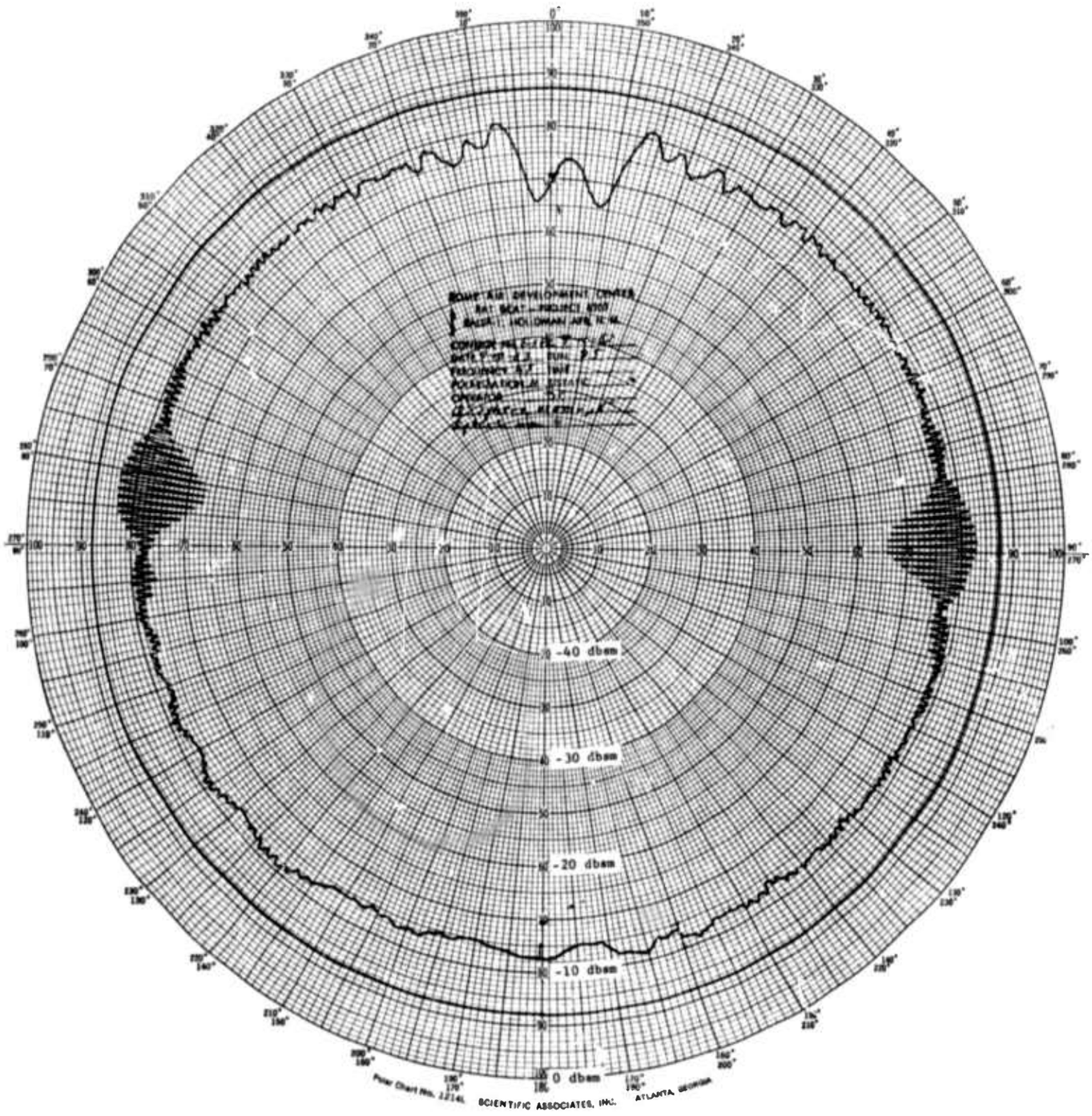

Fig. 5-15 POLAR SCATTERING DIAGRAM
(8800-9800 mc, 64 steps, target C)

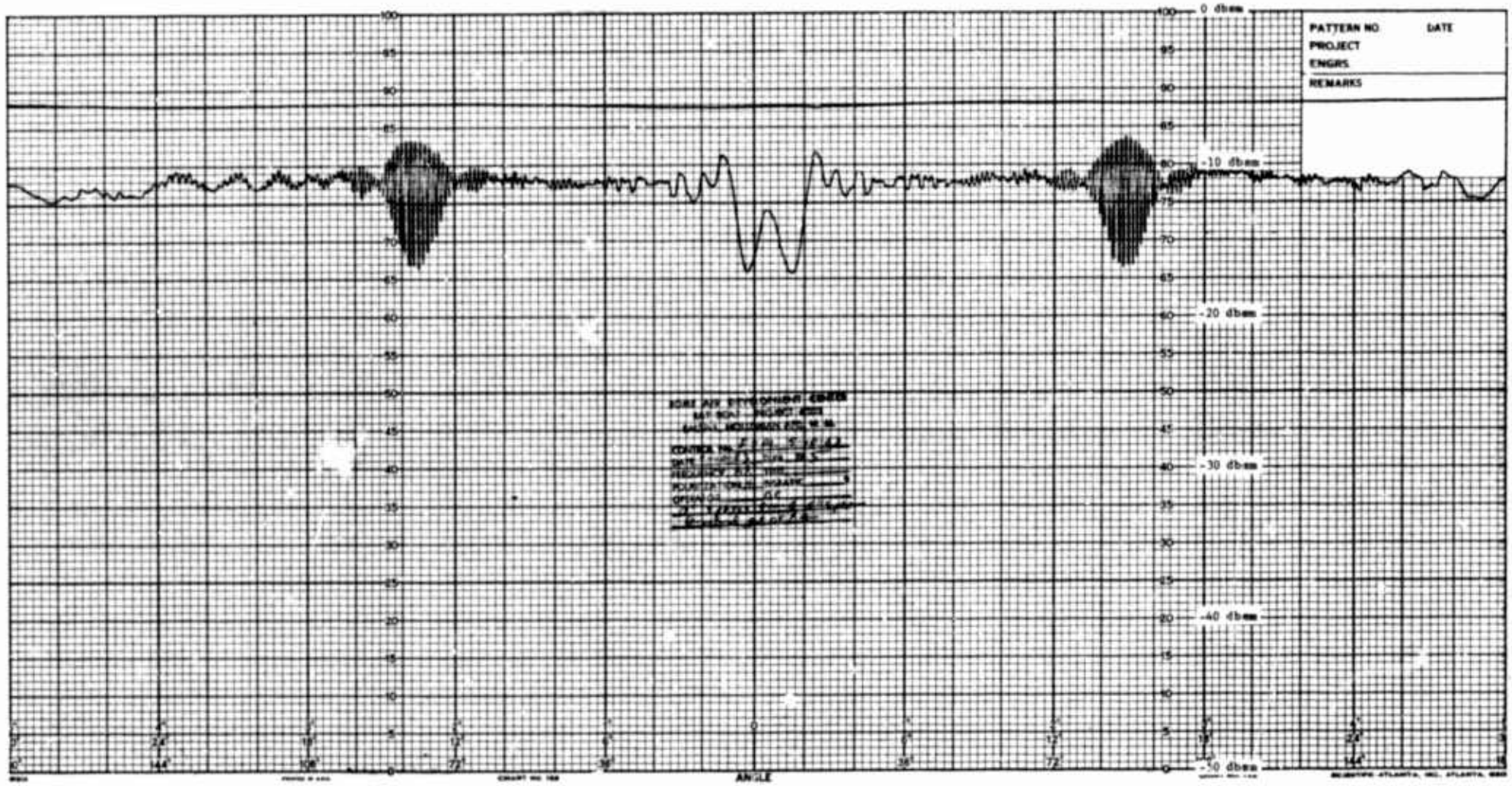

Fig. 5-16 RECTILINEAR SCATTERING DIAGRAM
(8800-9800 mc, 64 steps, target C)

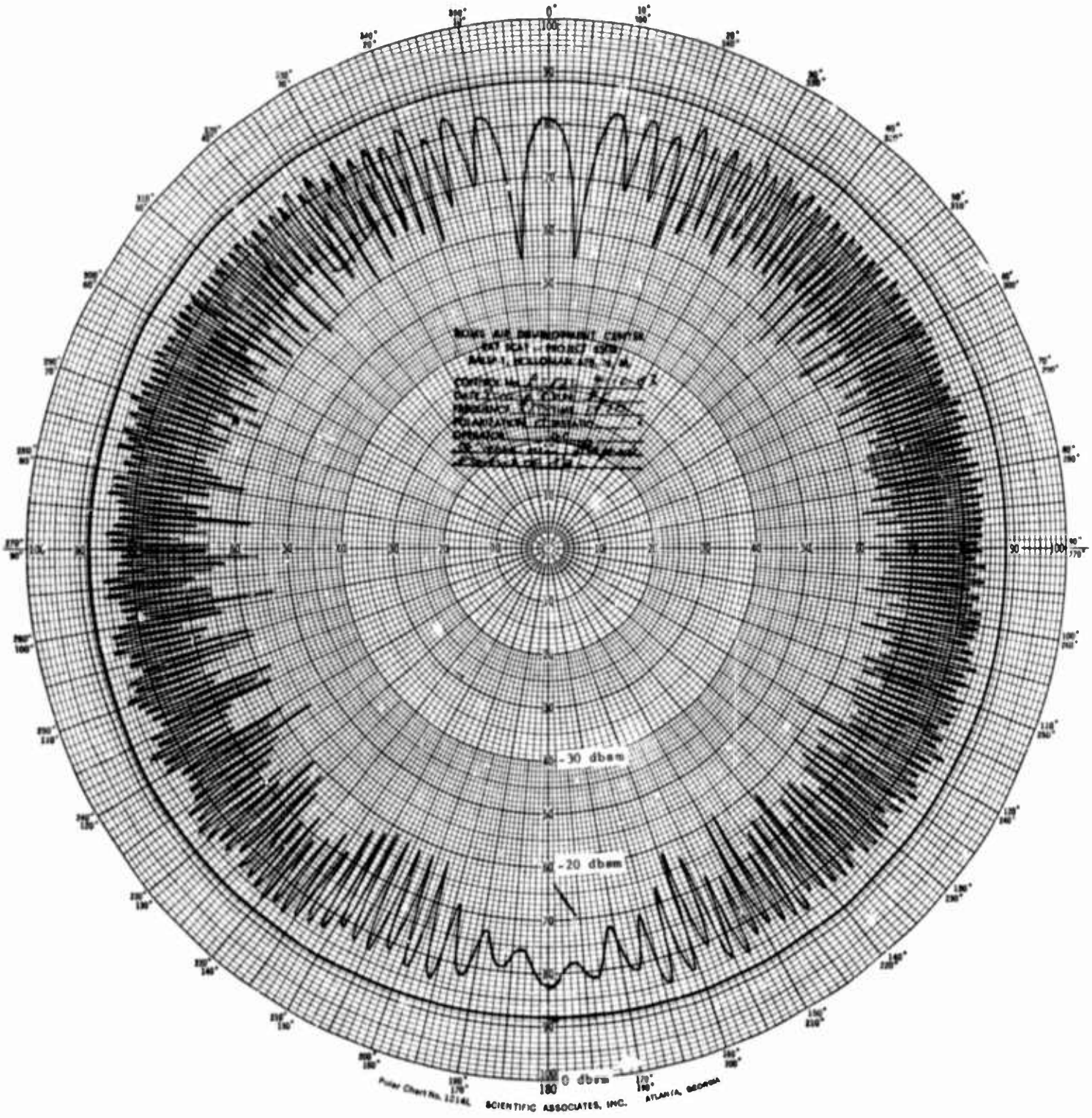

Fig. 5-17 POLAR SCATTERING DIAGRAM
(9300 mc, target C)

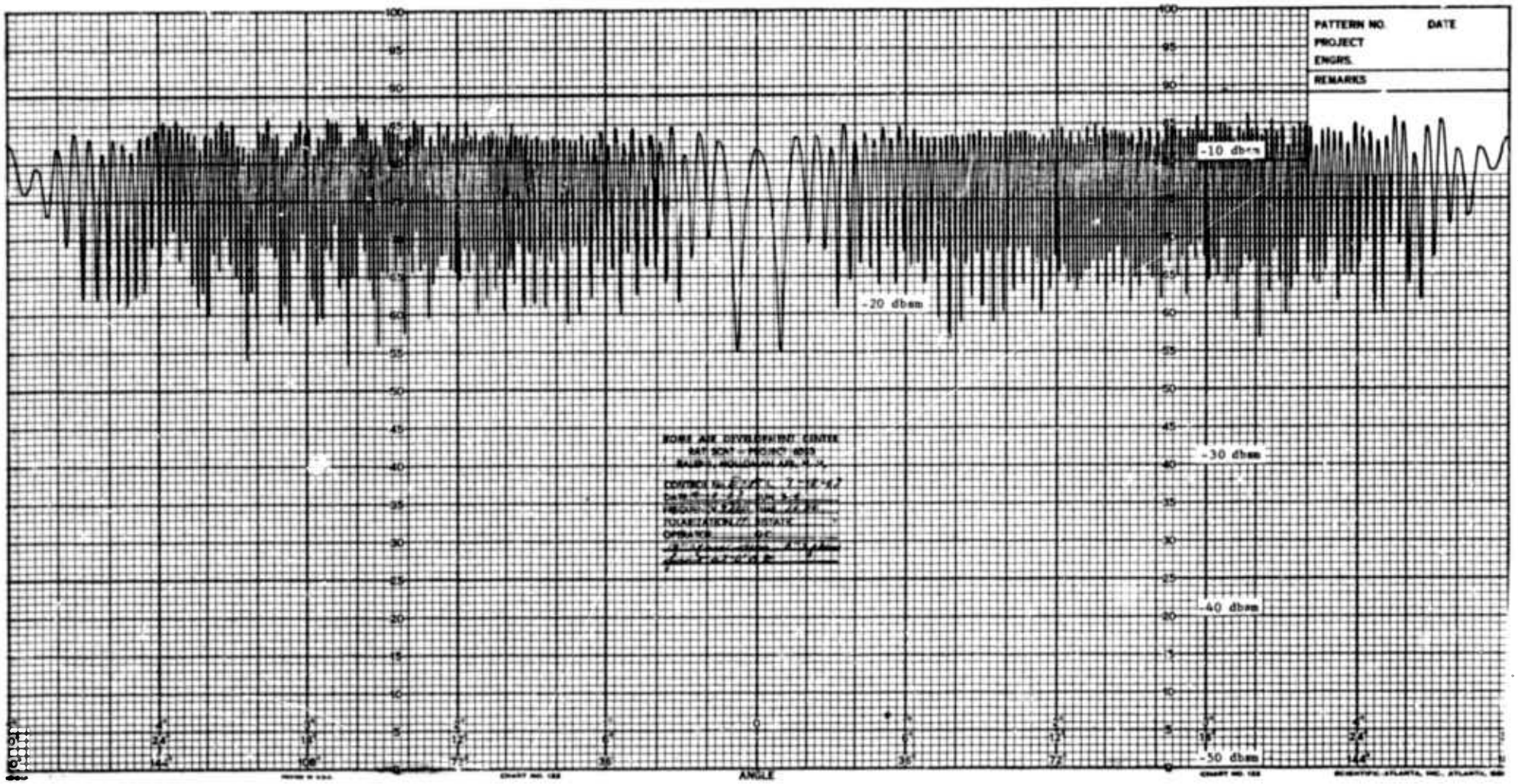

Fig. 5-18 RECTILINEAR SCATTERING DIAGRAM
(9300 mc, target C)

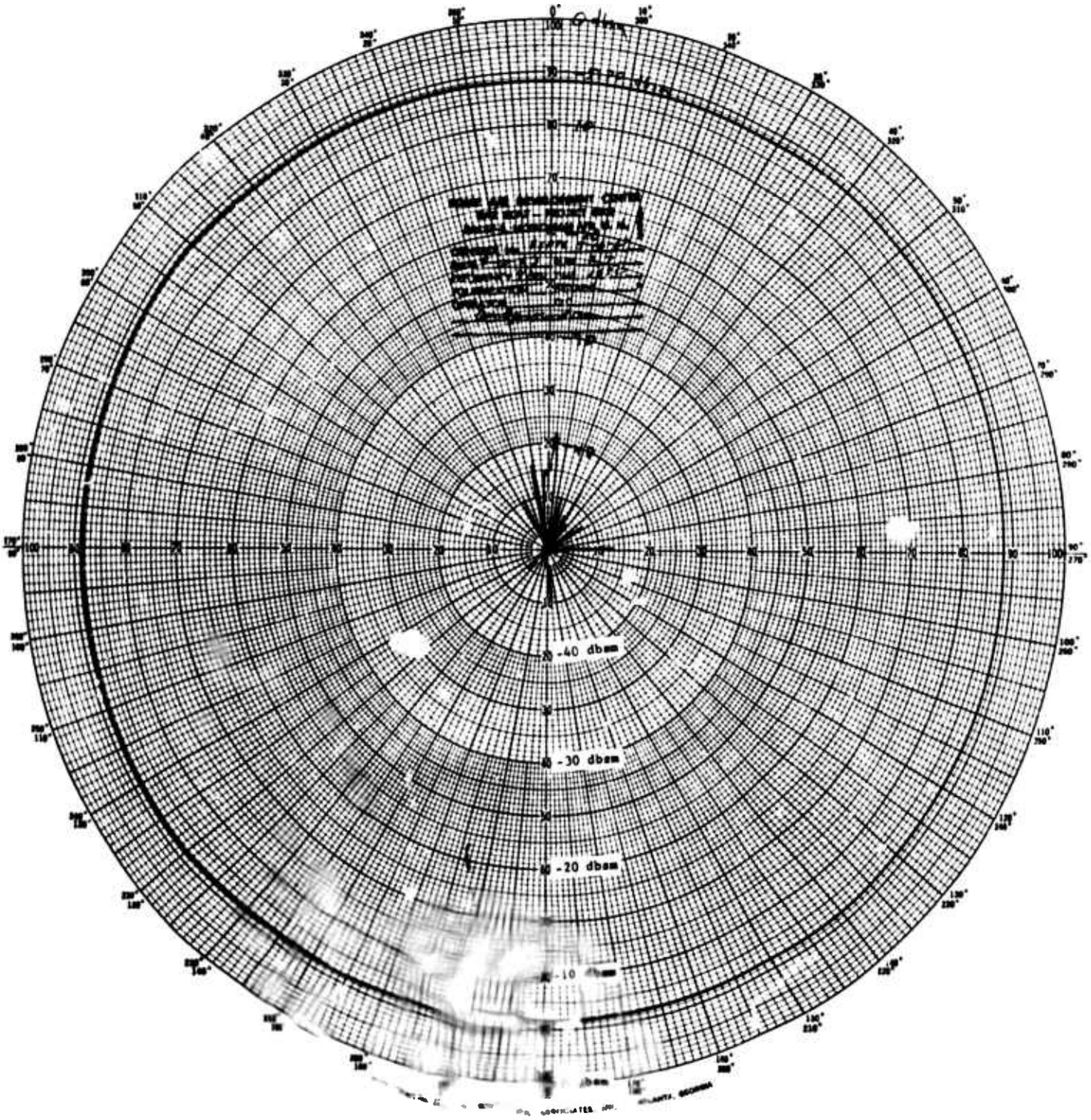

Fig. 5-19 BACKGROUND POLAR SCATTERING DIAGRAM (930 MC)

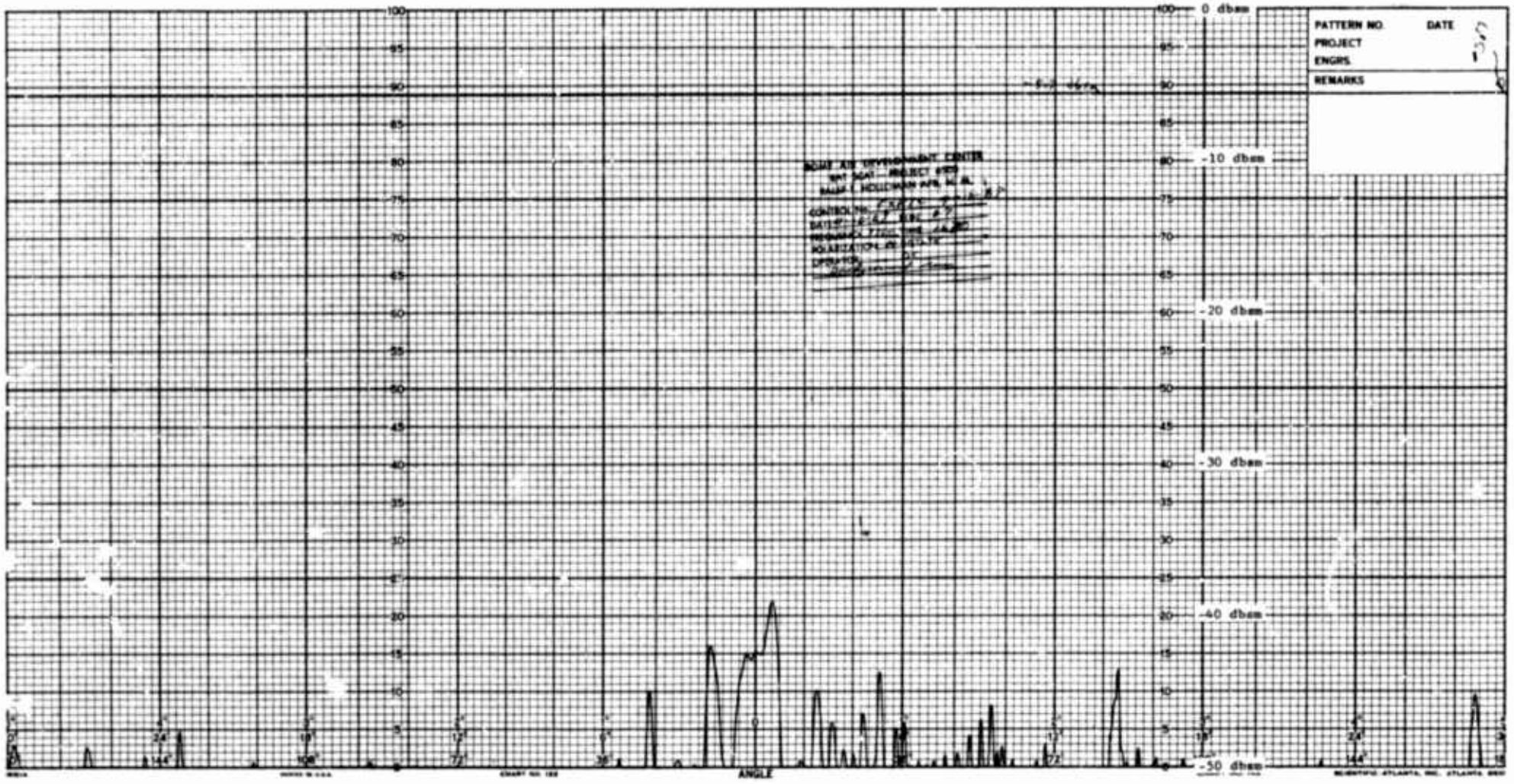

Fig. 5-20 BACKGROUND RECTILINEAR SCATTERING DIAGRAM (9300 mc)

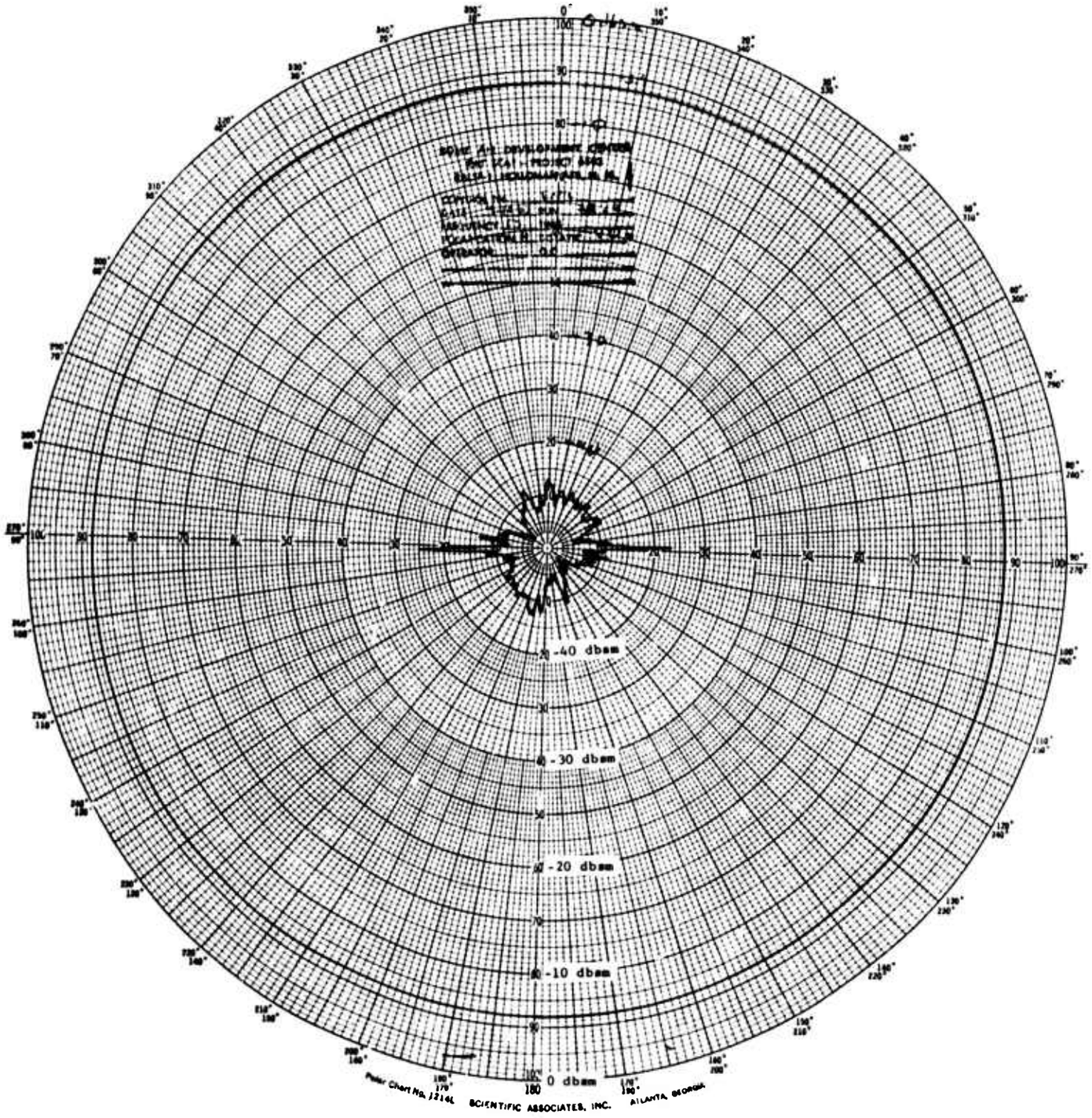

Fig. 5-21 BACKGROUND POLAR SCATTERING DIAGRAM (8800-9800 mc)

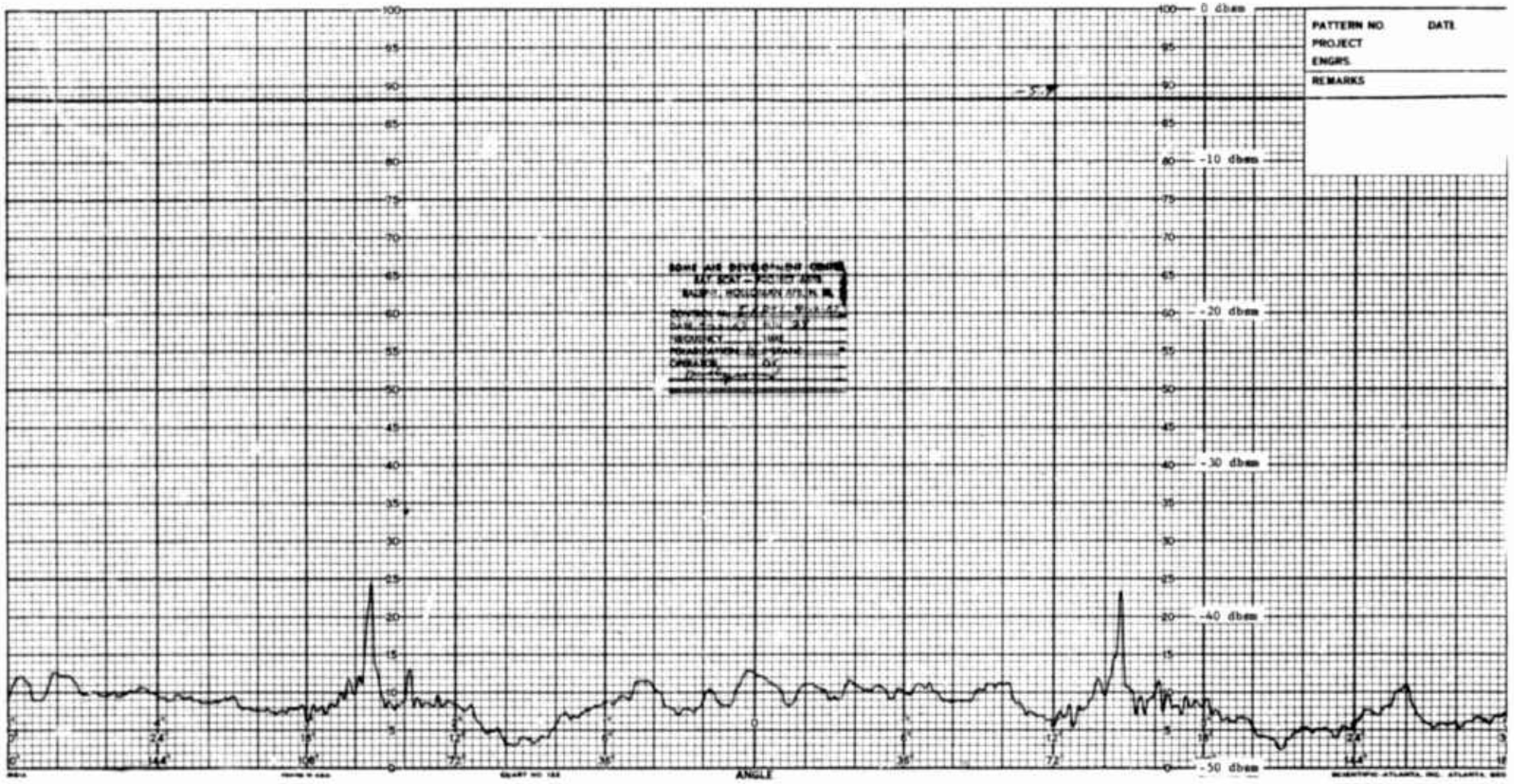

Fig. 5-22 BACKGROUND RECTILINEAR SCATTERING DIAGRAM (8800-9800 mc)

Range Resolution

Final resolution data runs are shown in Figures 5-24 through 5-32. In each figure, the output of the band pass filter is displayed on the upper data strip, and the cart position signals (at 5.0-foot intervals) are displayed on the lower strip. The trace was made from left to right with the cart moving toward the radar on the left side and away from the radar on the right. The video signal appears when the phase center of the corner reflector is at a discrete distance from that of a scatterer. This distance is dependent on monitoring of a particular Doppler-shifted line with the band pass filter. The variable range parameters and target configurations used for each data run are shown in the figures.

The variation in the amplitude of the signals in the forward and backward runs and between runs is attributed primarily to a drift of the band pass filter center frequency about a Doppler-shifted spectral line, although variations in cart velocity had some effect. The sensitivity of the measurement results to the filter setting is qualitatively illustrated in Figure 5-23. These measurements were made with the band pass filter center frequency dial set at the frequencies indicated.

Range resolution measurements were made with the three basic target configurations shown in Figure 5-6. Three corner reflector sizes were used; a 19-inch corner was used in checkout runs because the specified 4-inch corner was not available, and a 4-inch and a 9-inch corner were used in the final data runs. The 9-inch corner appeared to produce the best results. Data runs for (1) Targets A and B (shown in Figure 5-6), (2) different corner sizes and (3) selected azimuth angles are shown. The azimuth angle of 90 degrees corresponds to a broadside aspect angle.

Since the distance between the cart position marks is known and the two data strips were recorded simultaneously, the distance between spheres can be measured for comparison with the theoretical separation. A comparison of the theoretical and measured range differences between the target scatterers is subsequently shown in Table 5-1. The errors are attributed primarily to errors in cart position due to velocity variations and trace distortion introduced by velocity changes and the drift of the band pass filter. Cart velocity changes and band pass filter changes have the effect of distorting the data trace and thereby causing an error when position

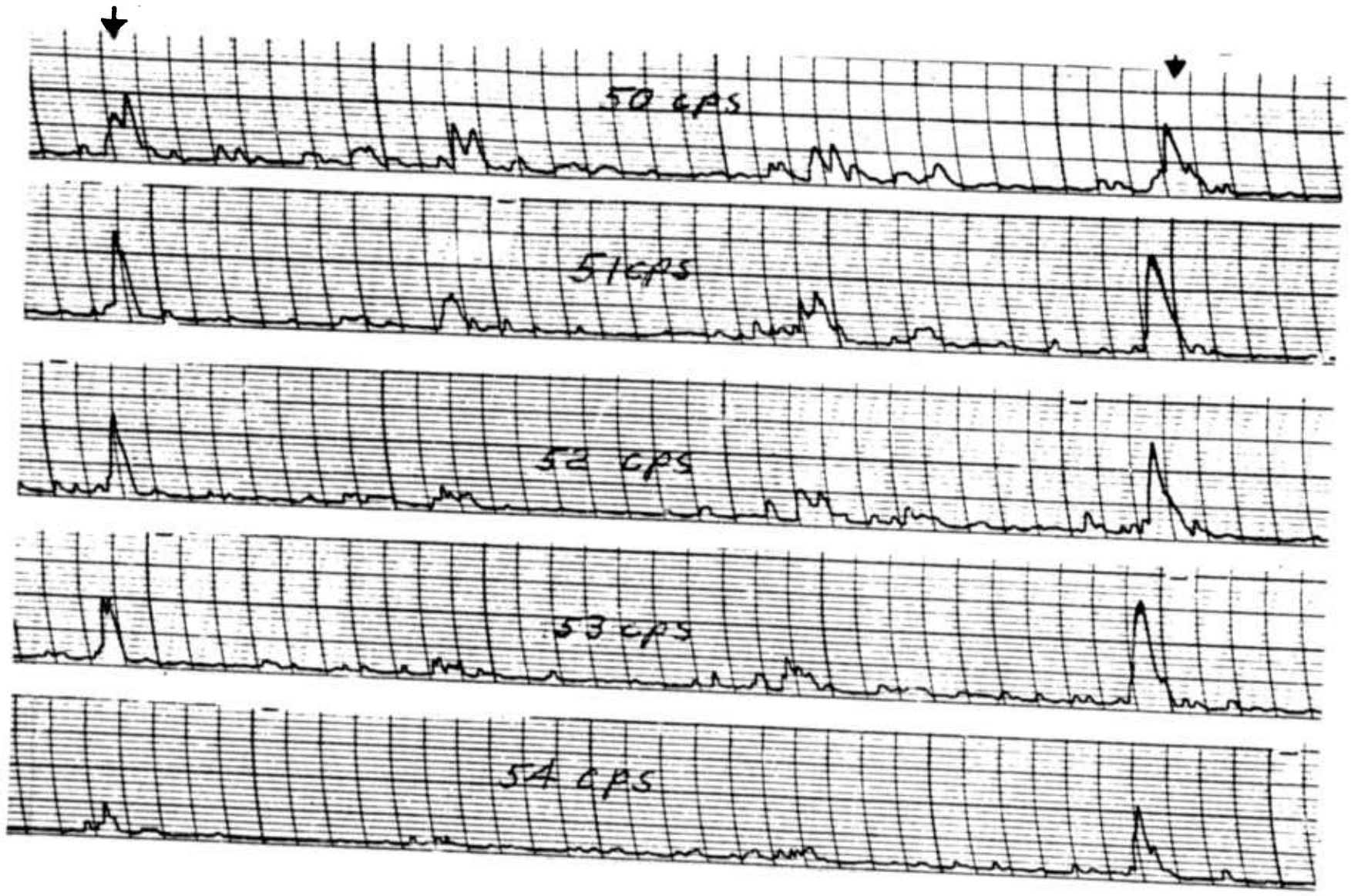

Fig. 5-23 BANDPASS FILTER OUTPUT AS A FUNCTION OF FREQUENCY

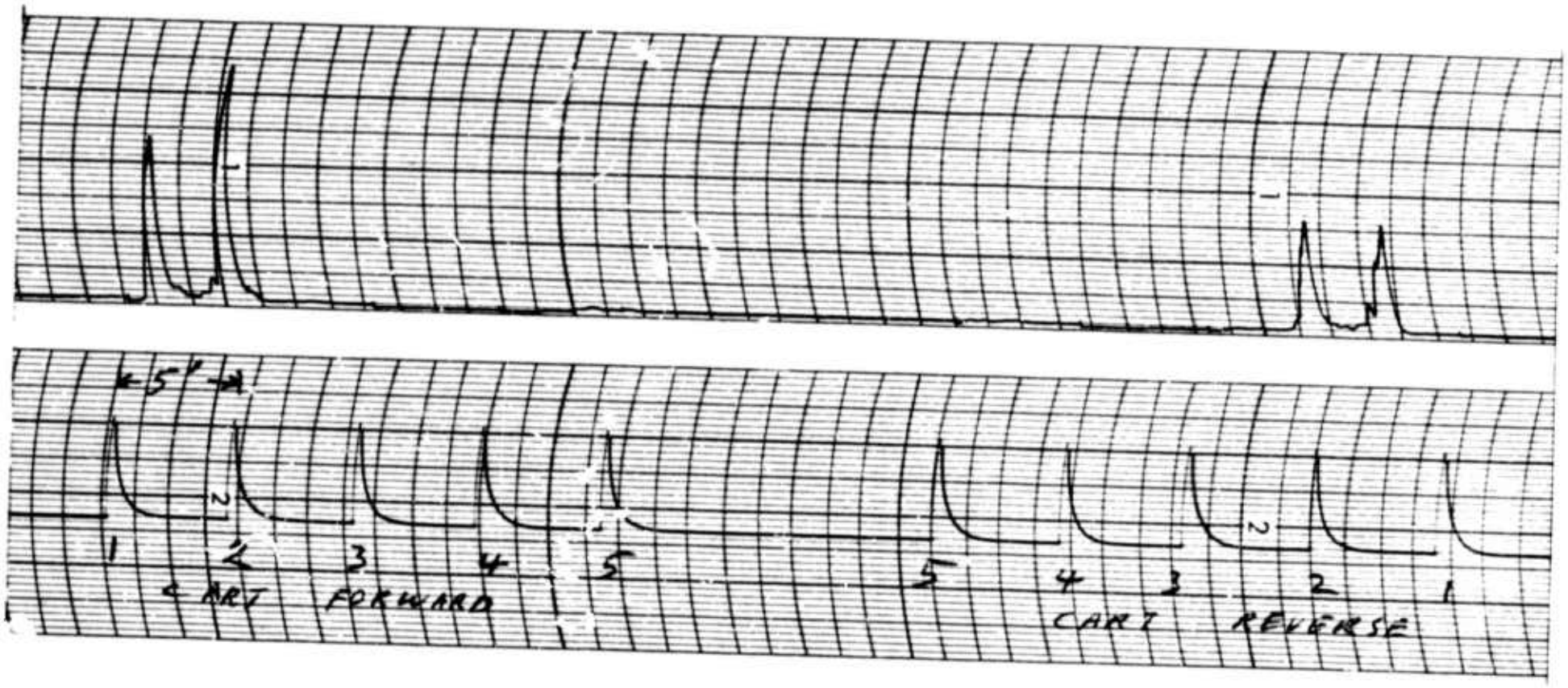

Fig. 5-24 FREQUENCY STEPPING RANGE RESOLUTION DATA
(64 steps, 2560 pps, target B, 0°Az, 4" corner)

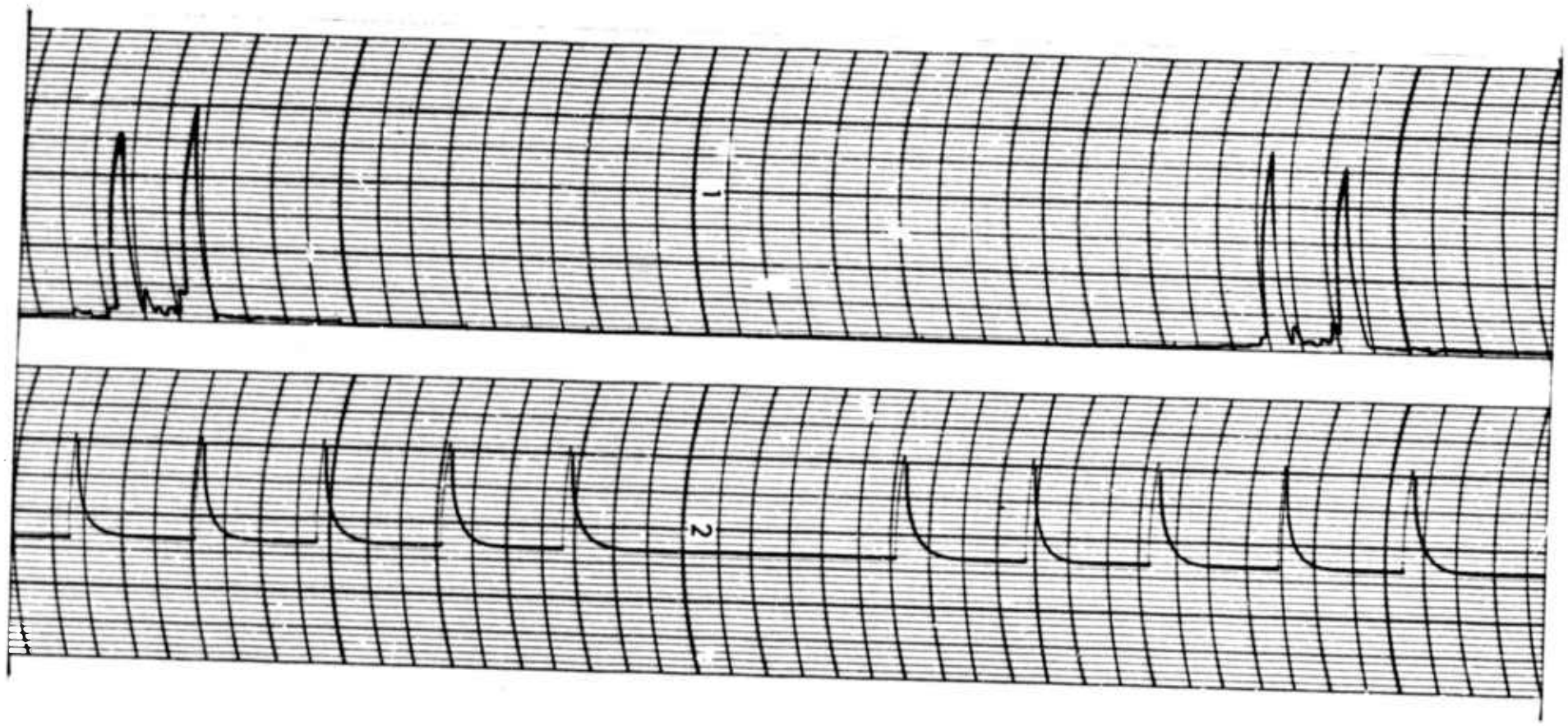

Fig. 5-25 FREQUENCY STEPPING RANGE RESOLUTION DATA
(64 steps, 2560 pps, target B, 00Az, 9" Corner)

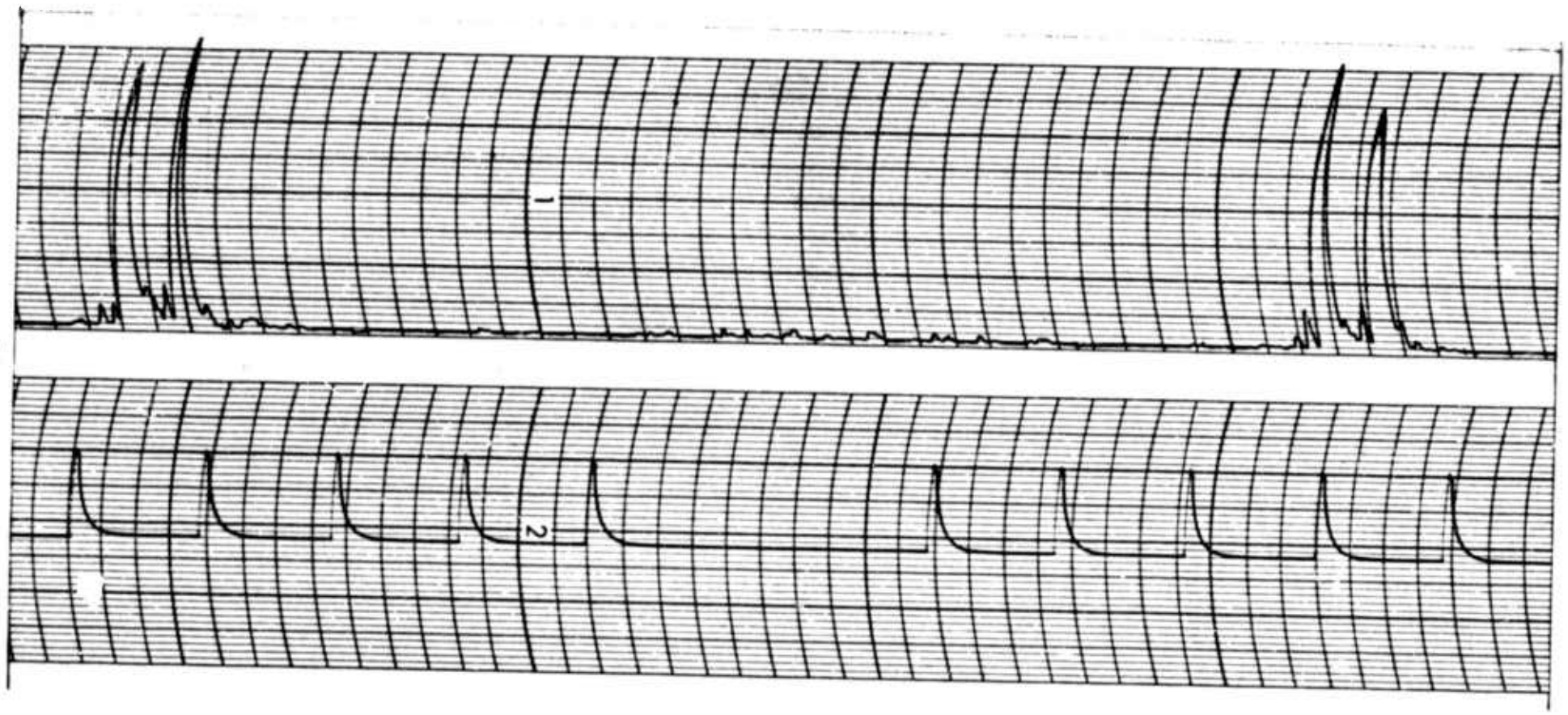

Fig. 5-26 FREQUENCY STEPPING RANGE RESOLUTION DATA
(64 steps, 2560 pps, target A, 45°Az, 9" corner)

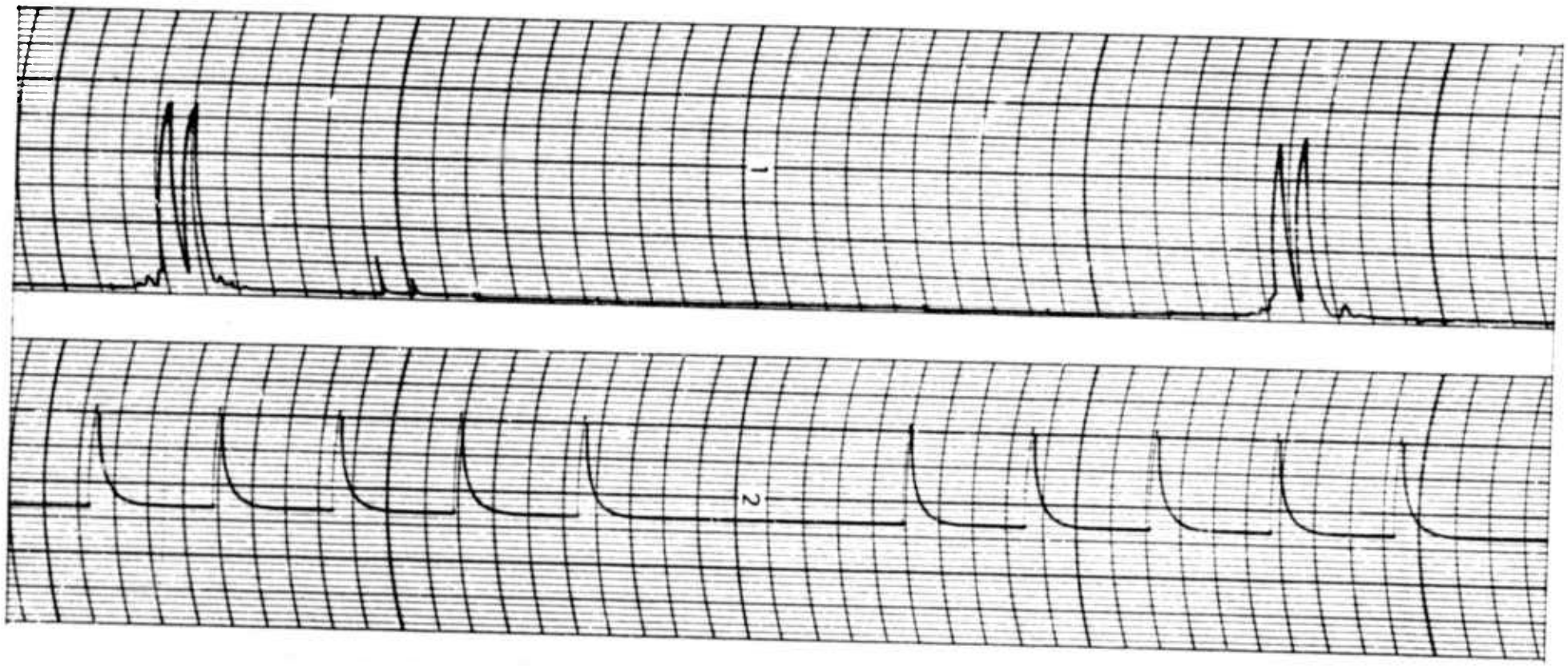

Fig. 5-27 FREQUENCY STEPPING RANGE RESOLUTION DATA
(64 steps, 2560 pus, target B, 70.5°Az, 9" corner)

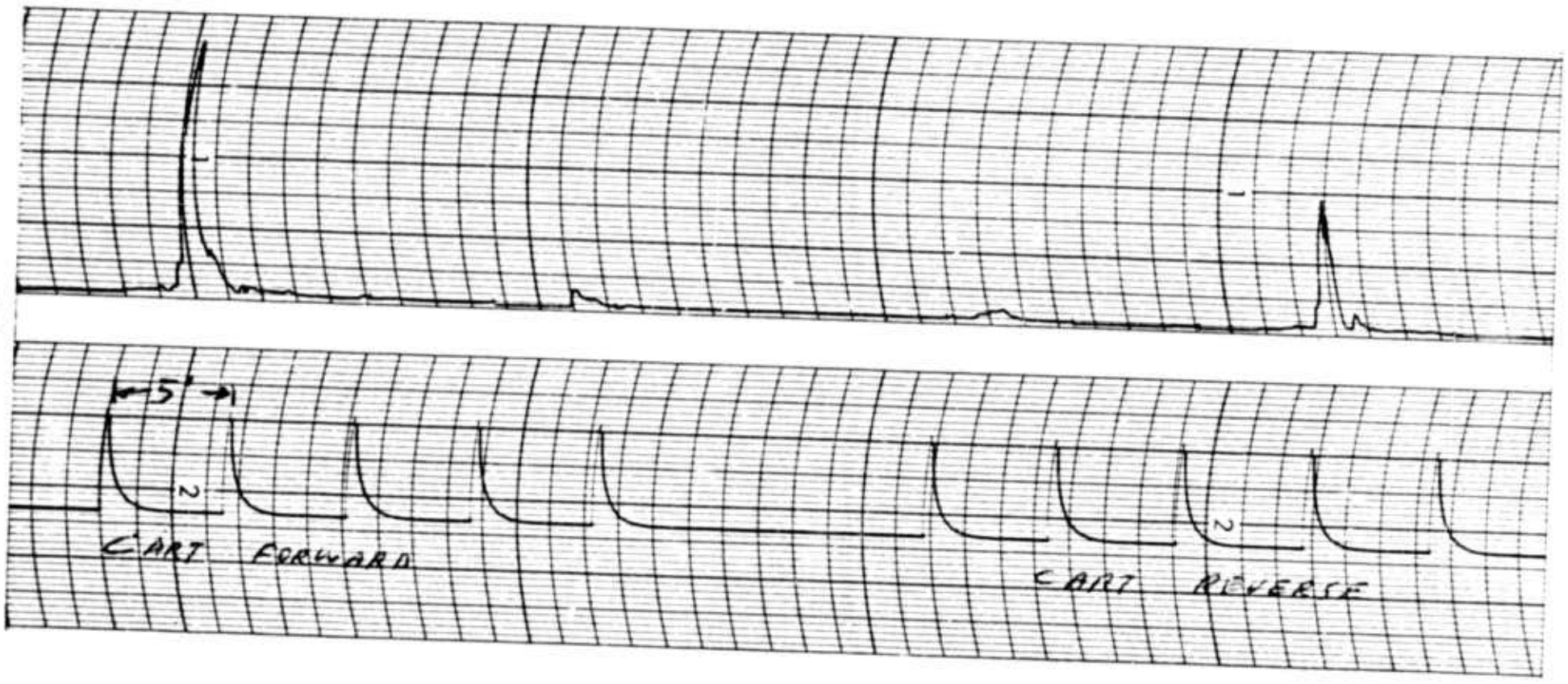

Fig. 5-28 FREQUENCY STEPPING RANGE RESOLUTION DATA
(64 steps, 2560 pps, target B, 90°Az, 4" corner)

measurements are taken from the trace. It can be seen that the larger errors occur when a peak of the trace is distorted.

Consideration of the spectrum derived in Appendix I will reveal that cart velocity changes will not introduce distortion in the data, unless the spectrum shift is out of the band pass filter range. The spectral position of the maxima of $G_1(\omega)$ and $G_2(\omega)$ are influenced by a change in velocity so that the maxima shift in opposite directions for a given change in velocity but in the same direction and the same amount as the Doppler-shifted lines associated with the respective maxima. The direct effect of velocity changes on cart position relative to the target scatterer is the only significant effect of velocity in all practical cases. An examination of the cart velocity data, shown in Table 4-1, suggests that the velocity was reasonably constant although velocity changes of the order indicated could introduce errors of the order shown in Table 5-1 where the average over a 5-foot interval was used to calculate position differences. In any case, cart velocity changes can be readily remedied in an operational model. The velocity changes in this experimental model were generally less that 5 per cent, and it is suggested that this variation was largely due to friction between the wheel flanges and the track and wheel slippage. Data could presumably be taken from the trace more accurately if the scale were expanded, i.e., with higher strip chart speed. In addition, it appears that data reduction would be more accurate if the trace deflection was greater; in this manner, a better reference for measurement between pulses would be provided.

Range resolution data runs were obtained at azimuth angles of 6.5 and 11 degrees in an effort to display relative amplitudes of the return from the spheres for a condition where the one sphere was partially shadowing or influencing the back-scatter pattern of the other sphere. These azimuth angles were chosen through an examination of the single-frequency azimuth pattern shown in Figure 5-33. A definite null and peak appear in the back-scatter pattern at azimuth angles of ≈ 6.5 and ≈ 11.0 degrees (CCW scale), respectively. This finding indicates that the return from the far sphere was relatively small in the first case and larger in the second. This observation is borne out by an examination of the data in Figure 5-29 and 5-30, although the drift of the band pass center frequency may have significantly influenced these results.

Further checks on the shadowing effect was made by using Target C (a 6-inch sphere and a 12-inch diameter sphere). Results of these measurements are shown in Figures 5-31 and 5-32.

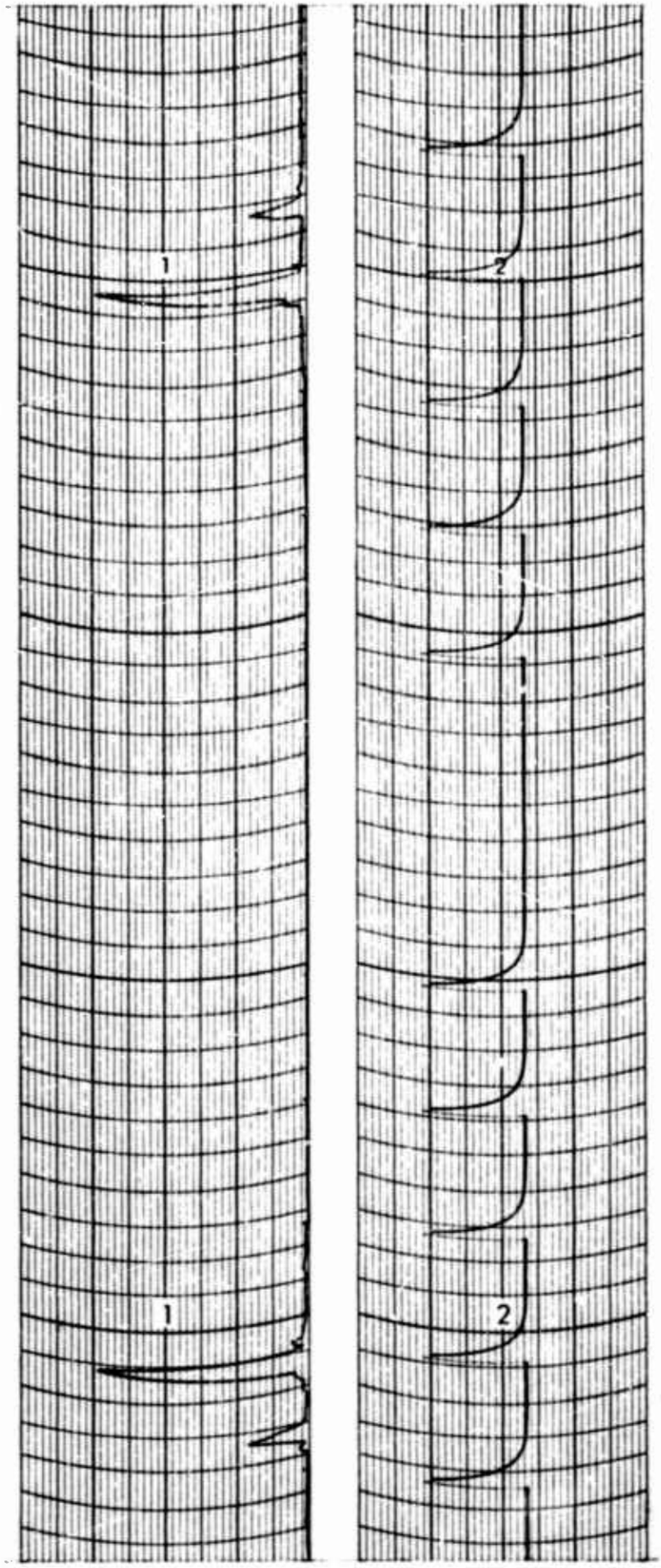

Fig. 5-29 FREQUENCY STEPPING RANGE RESOLUTION DATA
(64 steps, 2560 pps, target B, 6.5°Az, 9" corner)

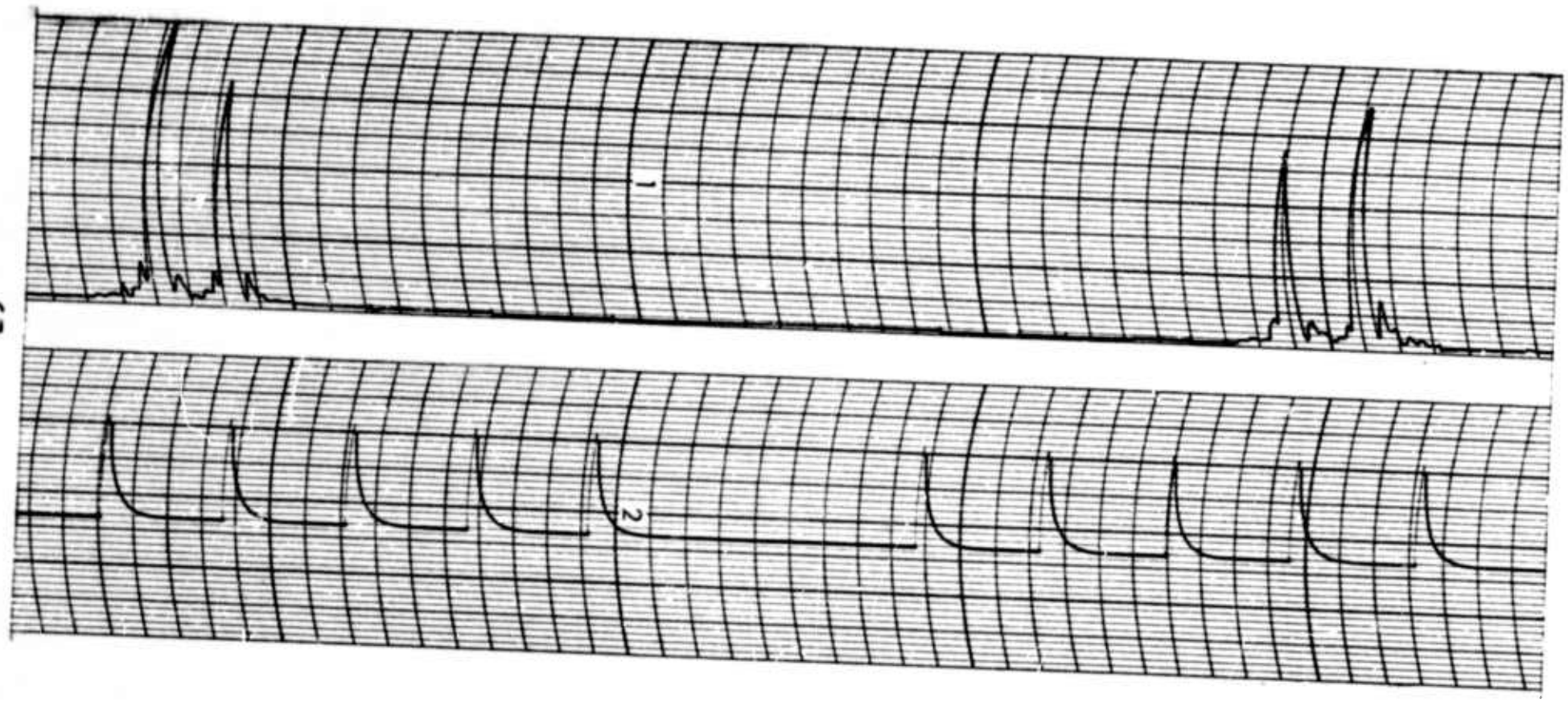

Fig. 5-30 FREQUENCY STEPPING RANGE RESOLUTION DATA
(64 steps, 2560 pps, target B, 11°Az, 9" corner)

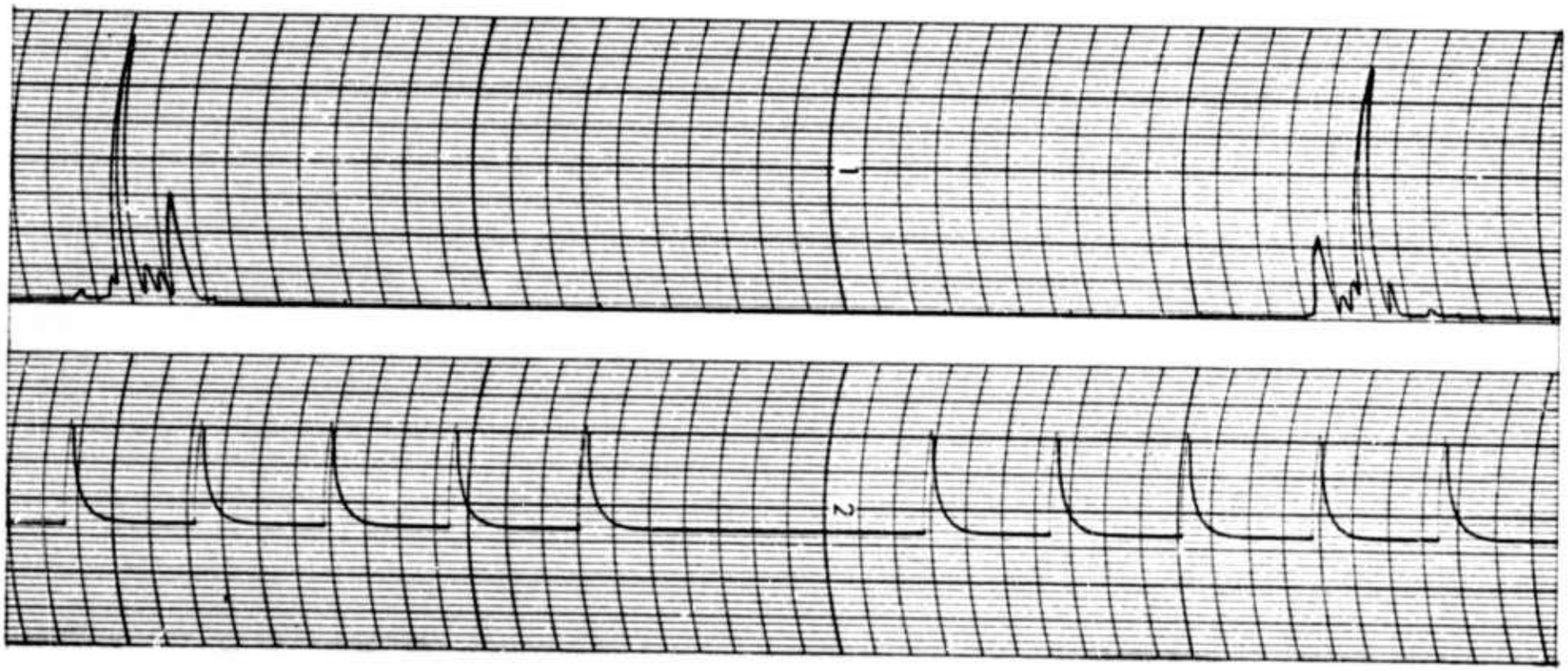

Fig. 5-31 FREQUENCY STEPPING RANGE RESOLUTION DATA
(64 steps, 2560 pps, target C, 45°Az, 9" corner)

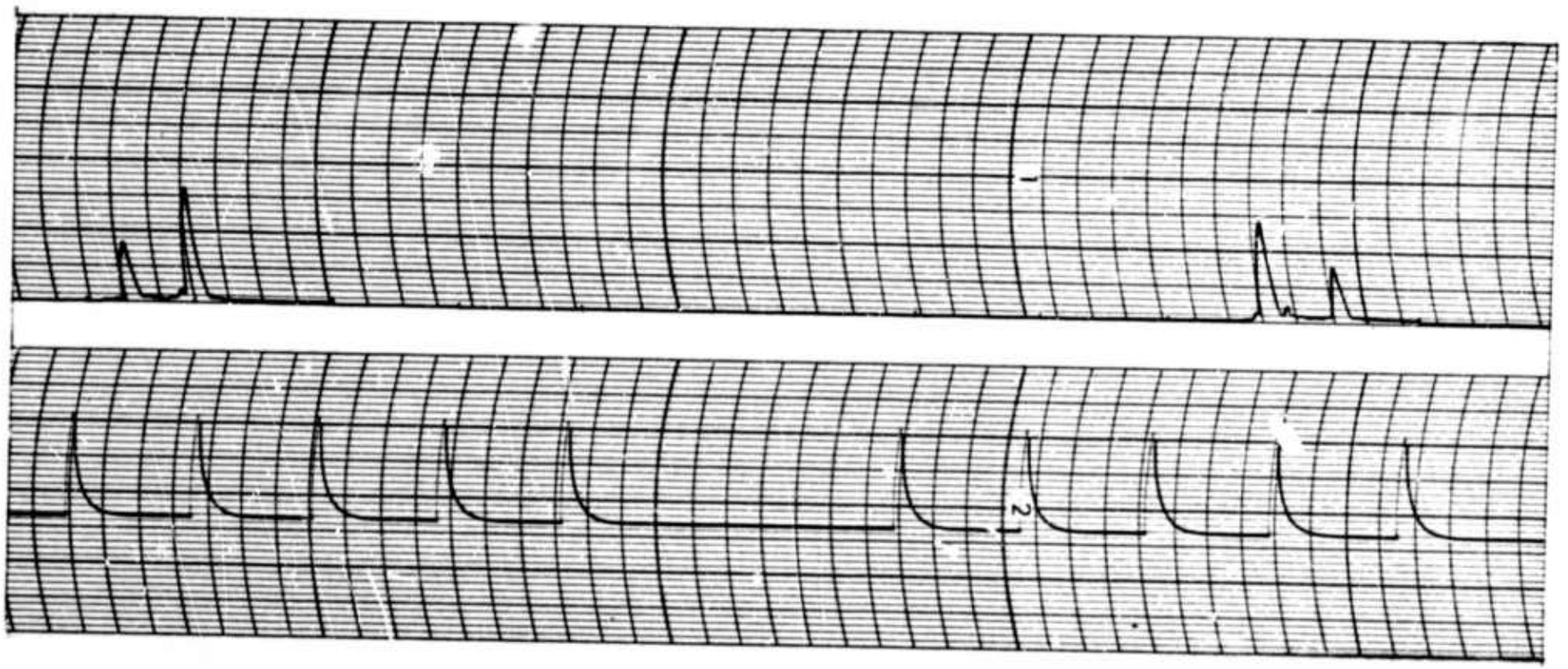

Fig. 5-32 FREQUENCY STEPPING RANGE RESOLUTION DATA
(64 steps, 2560 pps, target C, 0°Az, 9" corner)

In each case, the 6-inch sphere is nearest the radar. The shadowing effect of the 6-inch sphere can be seen in the data in Figure 5-33. The pen displacement was adjusted to keep the trace of the return from the 12-inch sphere on the paper; consequently, the return from the 6-inch spheres appears small relative to previous data runs.

Table 5-1 RANGE RESOLUTION MEASUREMENT RESULTS

Figure Number	Calculated Sphere Separation (feet)	Measured Sphere Separation (feet)	Error (feet)	Error (%)
4-24	3.0	2.81	-0.19	6.33
4-25	3	2.89	-.11	3.66
4-26	2.12	2.10	-0.02	0.944
4-27	1	0.96	-.04	4
4-29*	2.98	2.70	-.28	9.4
4-30	2.94	2.86	-0.08	2.72
4-31*	1.87	2.08	0.21	11.8
4-32*	2.75	2.54	-0.21	7.37

*Note trace distortion.

Additional Observations

The remaining data runs were included to illustrate two interesting phenomena observed during the experiment. An additional "target" appears on the trace of Figures 5-34 and 5-35 although no change was made in the actual target configuration. This effect was caused by the appearance of an ambiguous target return which was removed by doubling the number of steps in the frequency-stepping system. This ambiguous target appears at a range of approximately 16 feet from the center of the pit. The presence of the ambiguous target is not significant in itself, but it does introduce an undesirable data presentation effect. Had the track been only slightly longer than the maximum target dimension, the ambiguous target would not have appeared. This

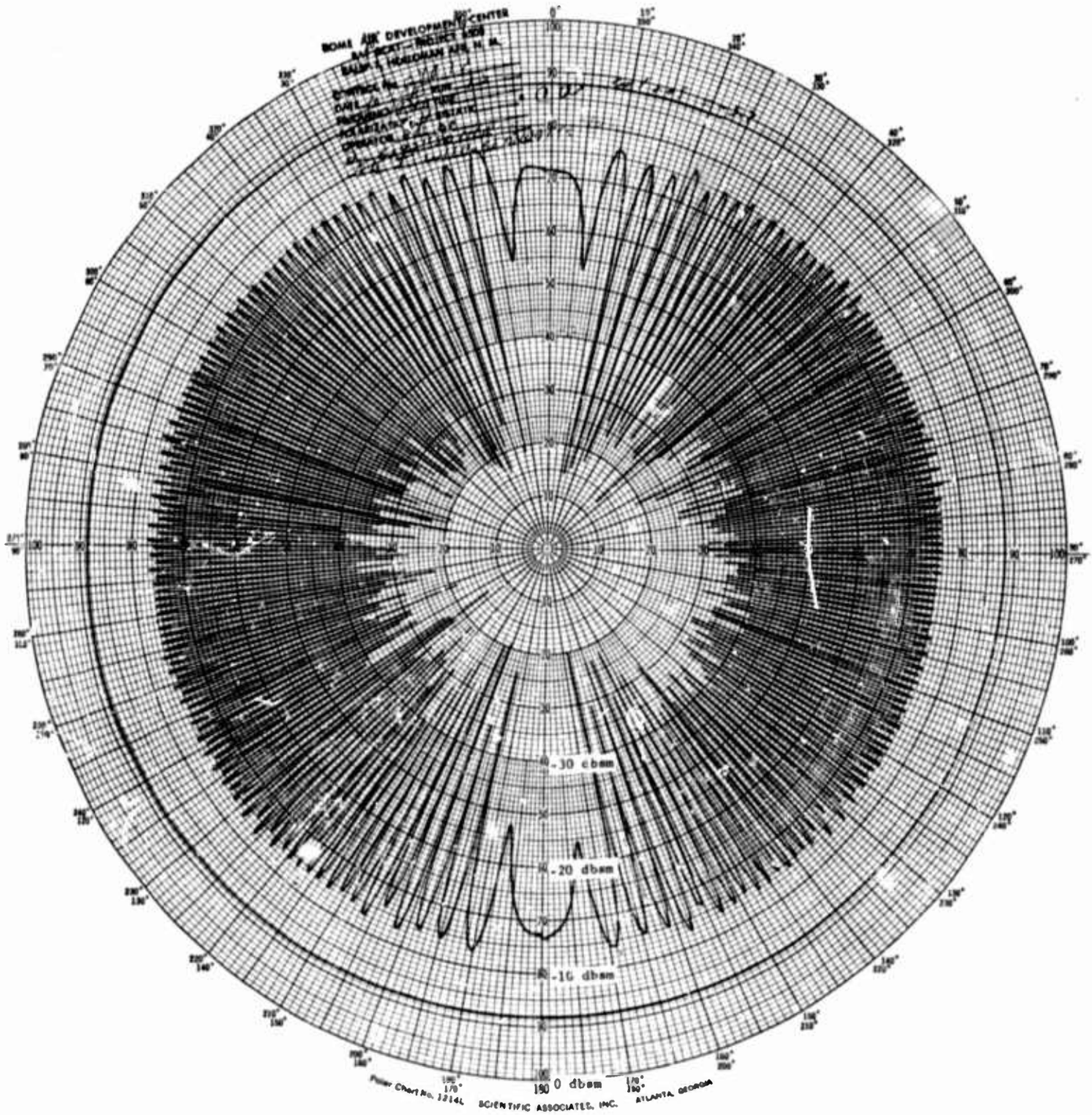

Fig. 5-33 POLAR SCATTERING DIAGRAM
(9300 mc, target B)

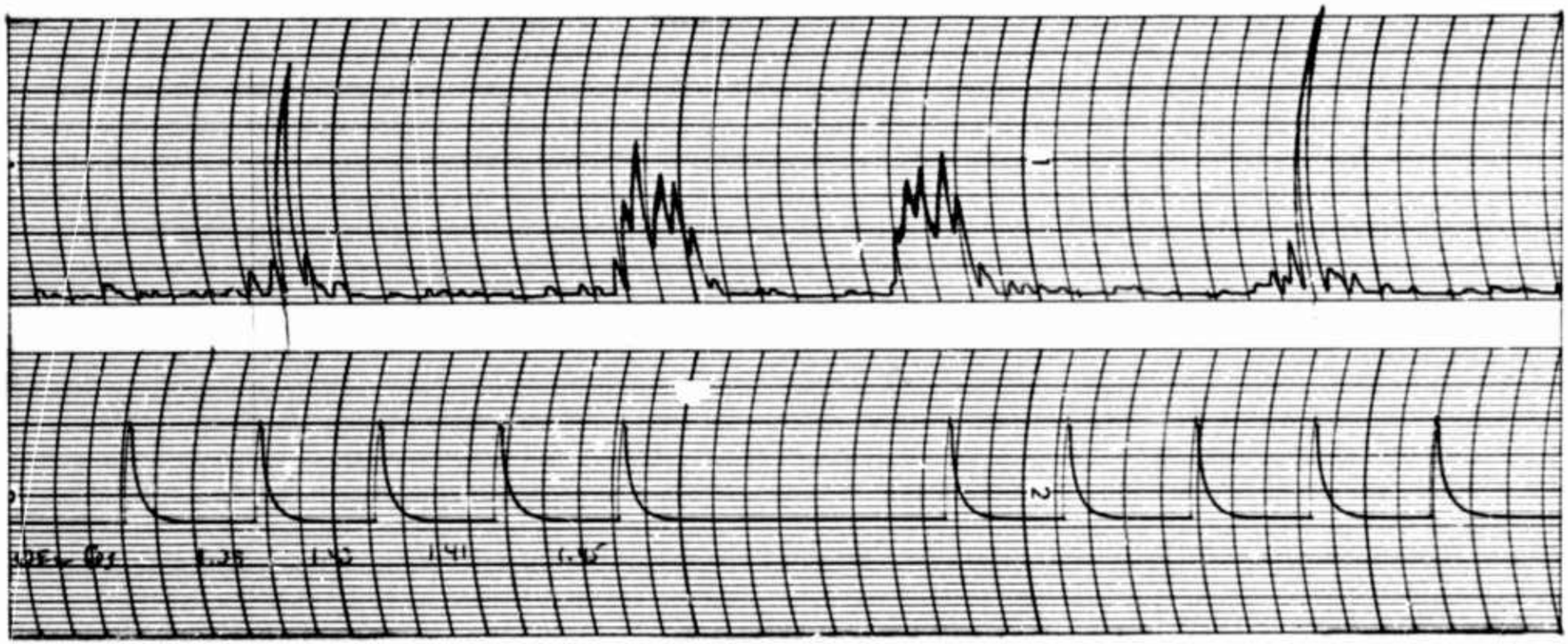

Fig. 5-34 FREQUENCY STEPPING RANGE RESOLUTION DATA
(32 steps, 2560 pps, target A, 90°Az, 4" corner)

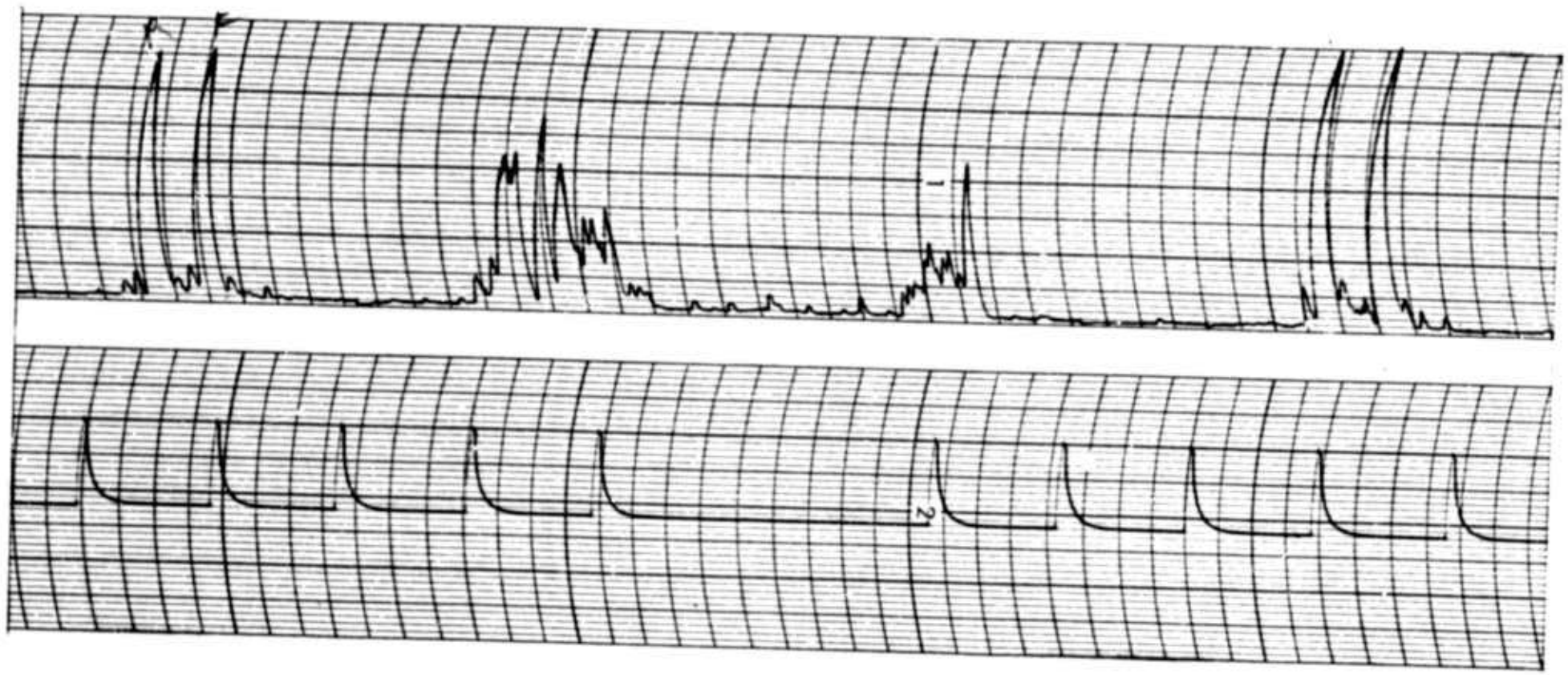

Fig. 5-35 FREQUENCY STEPPING RANGE RESOLUTION DATA
(32 steps, 2560 pps, target A, 45°Az, 4" corner)

phenomenon was treated in Appendix B of the original frequency-stepping document, Reference 1, and that appendix is reproduced in Appendix II of this report. An ambiguous target will appear when the system responds to second order maxima of the auto-correlation function, $C(\theta)$, of the frequency-stepping wave form. As shown in Appendix II, second order maxima will occur when

$$\frac{\Omega\,\theta}{2M} = i\pi \tag{5-10}$$

where Ω = the total angular band width, M = the number of frequency steps, and i is an integer.

The first maxima will occur at

$$\theta_1 = \frac{M}{B} \tag{5-11}$$

which corresponds to a spatial position

$$\Delta d_1 = \frac{Mc}{2B} \tag{5-12}$$

For M = 32 steps and B = 1 kilomegacycle, an ambiguous target will appear when the corner reflector is 15.7 feet from an actual target. Obviously, with 64 steps, this distance is increased to 31.4 feet so that an ambiguous target return will not appear with the cart track length used. A significant feature of the frequency-stepping technique is illustrated by the shape of the ambiguous target return relative to that of the actual target. It can easily be seen that the ambiguous target return is distorted; this effect is the result of system instability and lack of linearity, especially in the frequency ramp, which has the effect of broadening the spectrum. This effect can be seen in Figure 5-35 where the ambiguous returns from two targets have merged together. This effect becomes increasingly severe for maxima further from the zero order so that a system which is dependent on a clean spectrum over a wide band also requires an extremely linear and stable system; such is not the case for the frequency stepping techniques. The results of a linearity measurement are shown in Figure 5-36.

An experimental data run was made by using widely different radar parameters to eliminate the ambiguous target return; the results are shown in Figure 5-37.

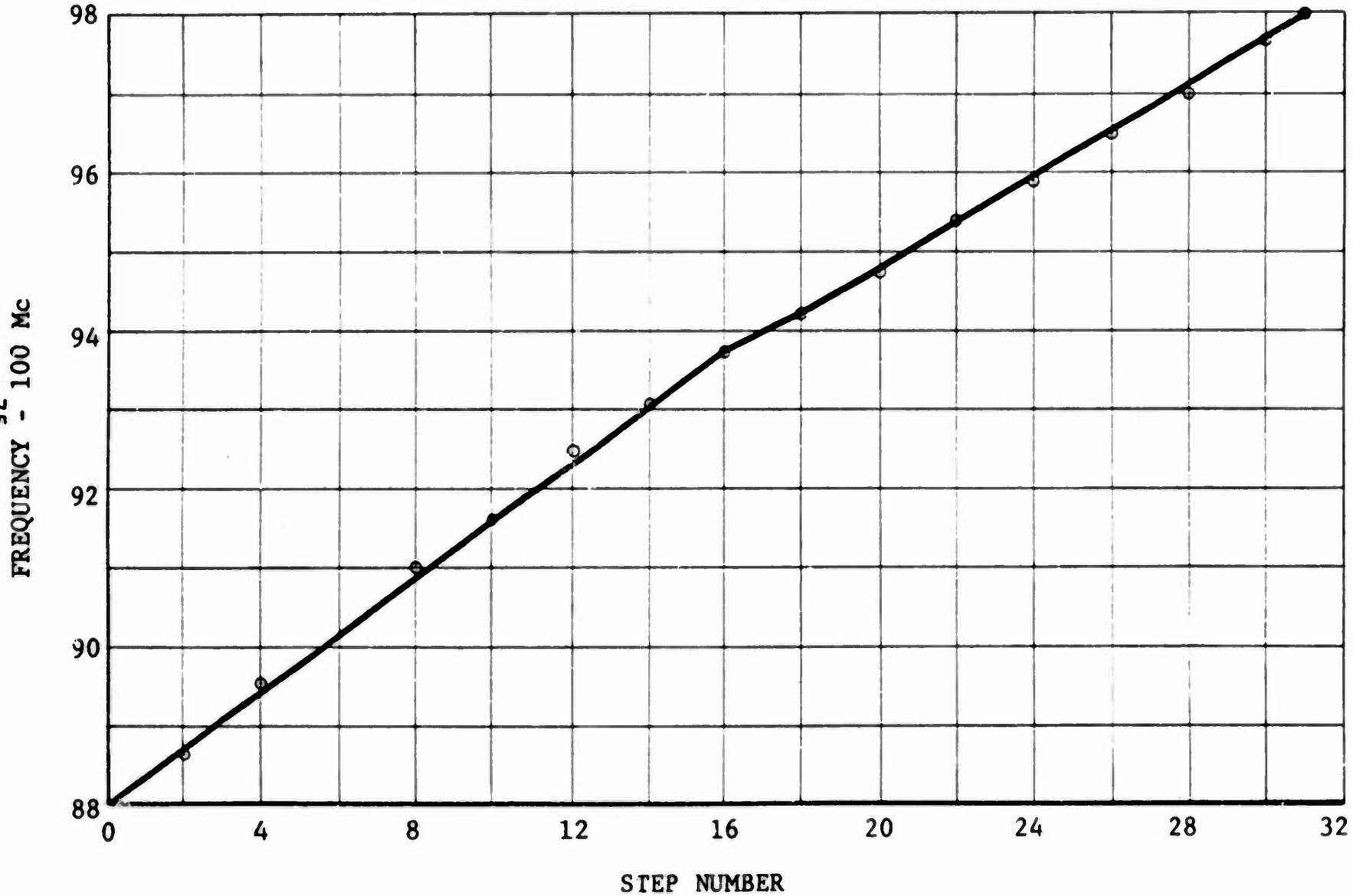

Fig. 5-36 FREQUENCY LINEARITY

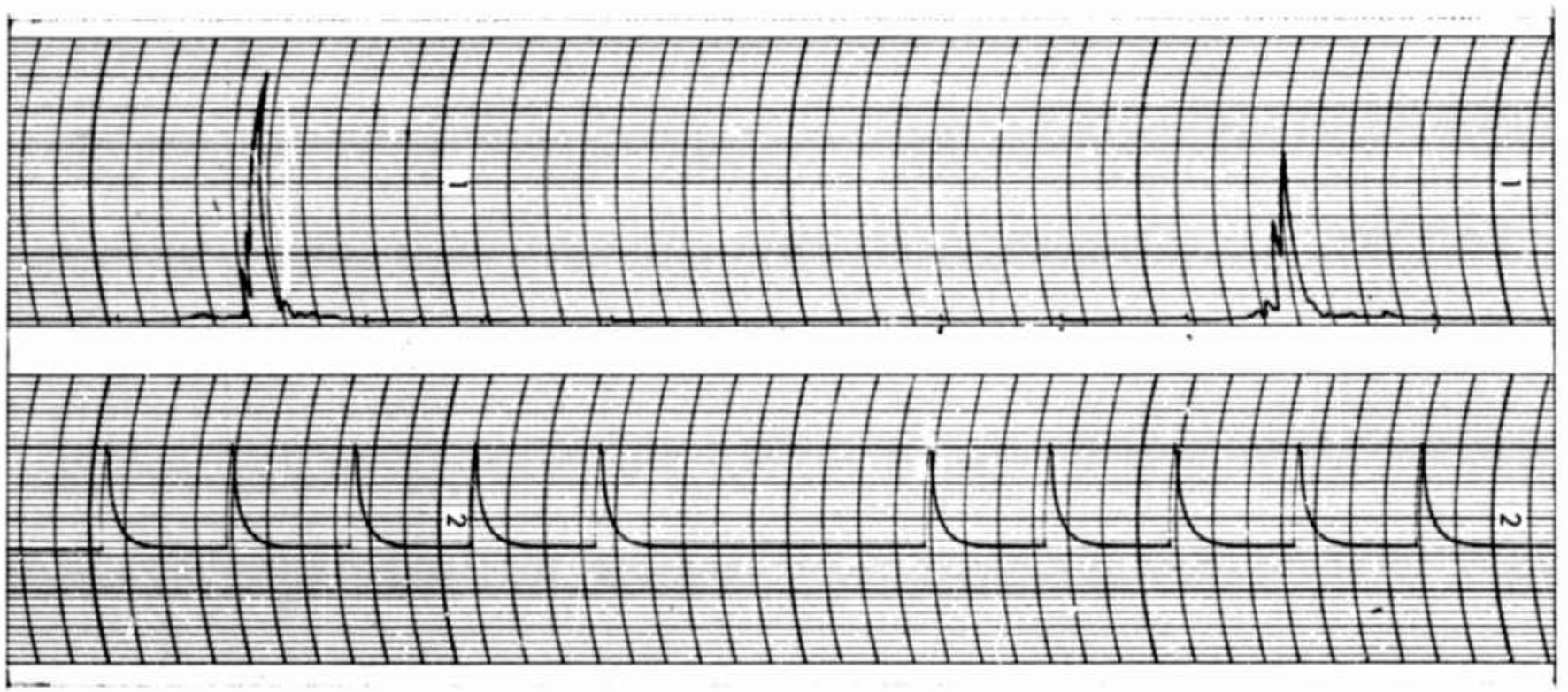

Fig. 5-37 FREQUENCY STEPPING RANGE RESOLUTION DATA
(64 steps, 5500 pps, target A, 90°Az, 4" corner)

The second phenomenon of interest is illustrated in Figure 5-38 where the target (Target A in Figure 5-6) is oriented for a separation of 3 feet between the spheres. It can be seen that the sphere farthest from the radar does not appear. The effect of some type of coupling between the spheres can also be seen on the azimuth patterns near the end-on aspect. This effect was investigated further, first by removing one of the spheres. The results of measurements made with and without frequency stepping are shown in Figures 5-39 through 5-42; the sphere is nearest the radar at 0-degrees azimuth. It is clear from an examination of these data that the Styrofoam support is influencing the back-scatter pattern of the sphere. Also, the effect does not appear to be a resonance phenomenon because it is a broadband effect; i.e., the frequency stepping pattern (1 kilomegacycle bandwidth) is similar to the single-frequency pattern. A possible explanation is that the horizontal portion of the Styrofoam support is ducting the energy as a waveguide. The target configuration was then changed by mounting the single sphere on a 7-inch pedestal. Measurements made on this configuration are shown in Figure 5-43 through 5-46; no significant effect of the Styrofoam appears in these data, and subsequent data runs were made with the spheres on pedestals, as shown in Figure 5-6.

A range resolution data run was made by using Target B in the end-on aspect (see Figures 5-24 and 5-25). Both spheres appear on the trace under these conditions.

Vehicle Target

A limited number of experimental frequency stepping measurements have been considered in a brief analysis of a vehicle configuration which was used as a target. The measurements consisted of single frequency data runs and frequency-stepping averaging and range resolution data runs. The actual data are not included in this report because of security classification. The sketches shown in Figure 5-47 are included to show qualitative results of these measurements. The hypothetical vehicle is also shown in this figure.

An examination of the sketches will reveal the presence of certain theoretically predictable features. The effect of the proximity of scattering centers on averaging can be seen from an examination of the scattering diagram. At the aspect angles where the primary return results from the presence of a number of scattering centers with only a small radial range separation,

the effect of frequency-stepping averaging is small. This effect is illustrated in the vicinity of 90- and 180-degrees of azimuth. At other aspect angles, the primary source of the return consists of scattering centers separated by an appreciable range, and the use of a frequency-stepping system has a pronounced effect on the measurement results.

An examination of the range resolution sketches shown in Figure 5-47 reveals the presence of flare spots in places where flare spots would be expected from an examination of the target configuration.

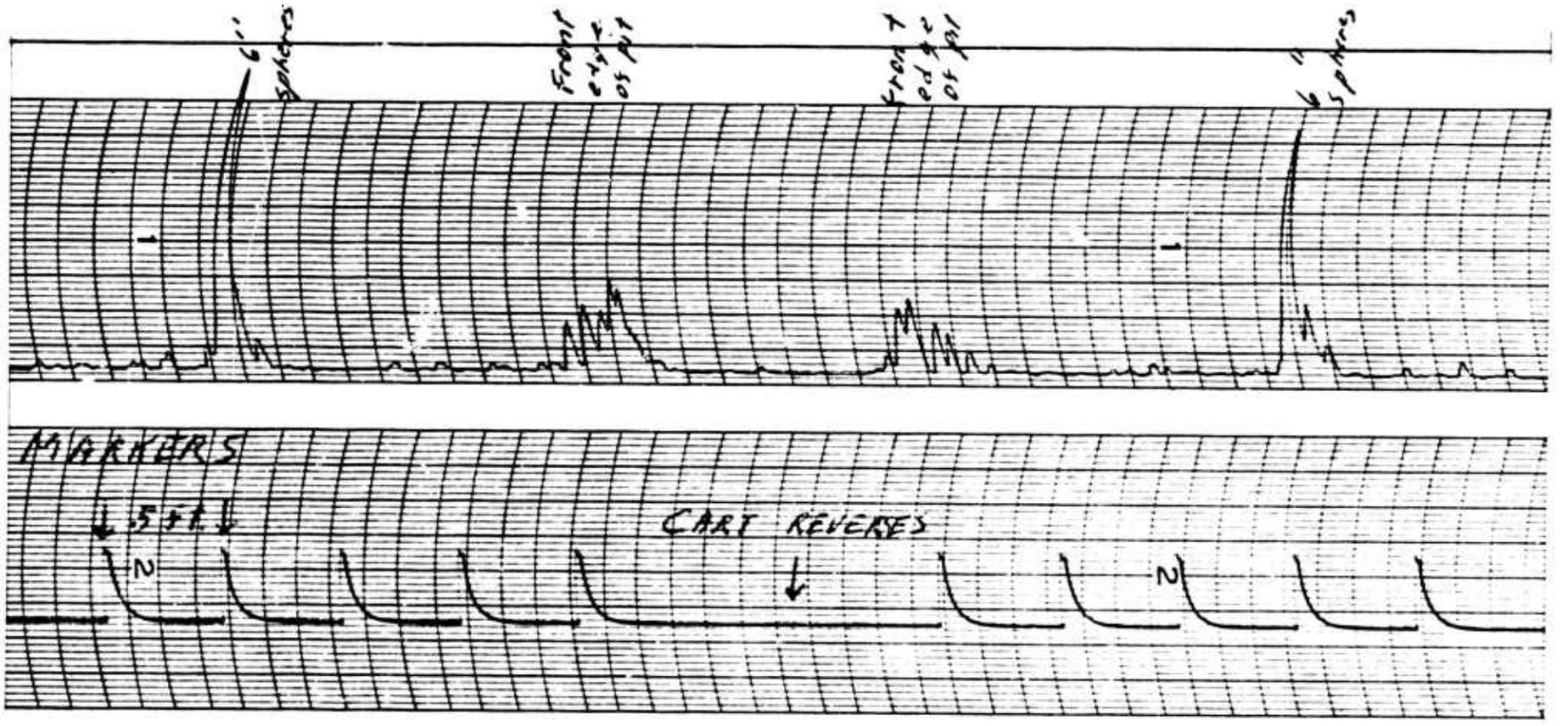

Fig. 5-38 FREQUENCY STEPPING RANGE RESOLUTION DATA
(32 steps, 2560 pps, target A, 0°Az, 19" corner)

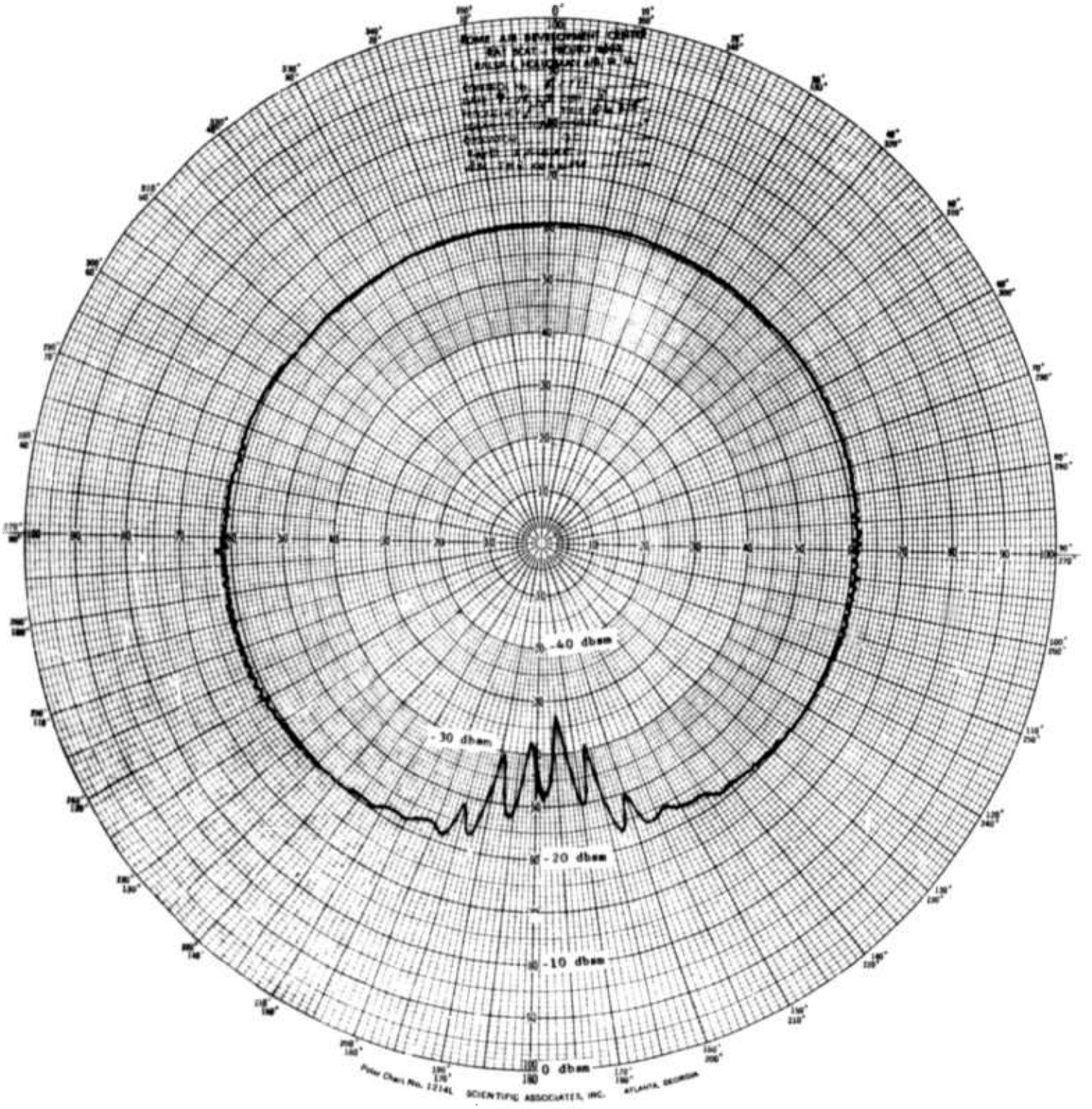

Fig. 5-39 POLAR SCATTERING DIAGRAM
(8800-9800 mc, 32 steps, target A - one sphere)

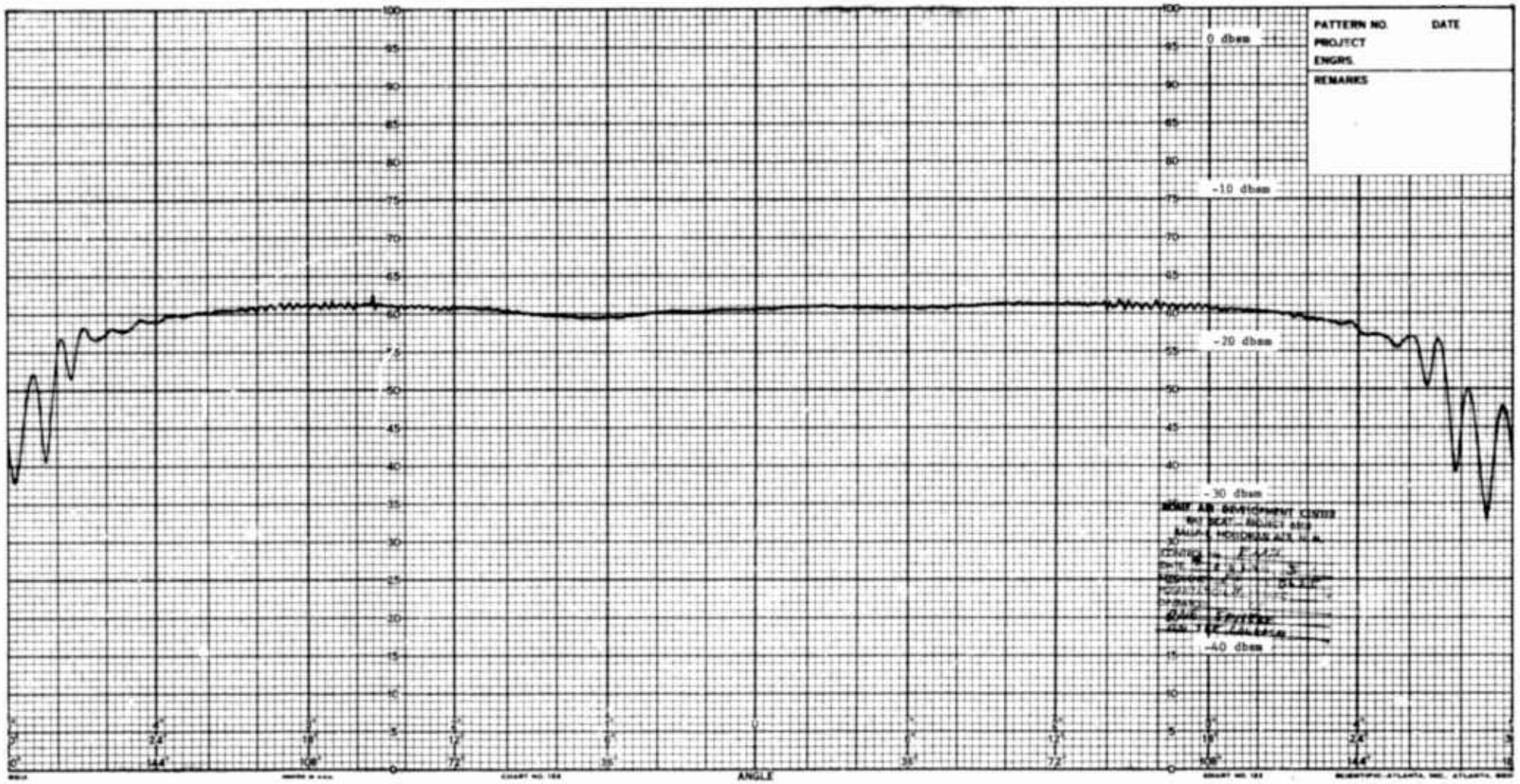

Fig. 5-40 RECTILINEAR SCATTERING DIAGRAM
(8800-9800 mc, 32 steps, target A - one sphere)

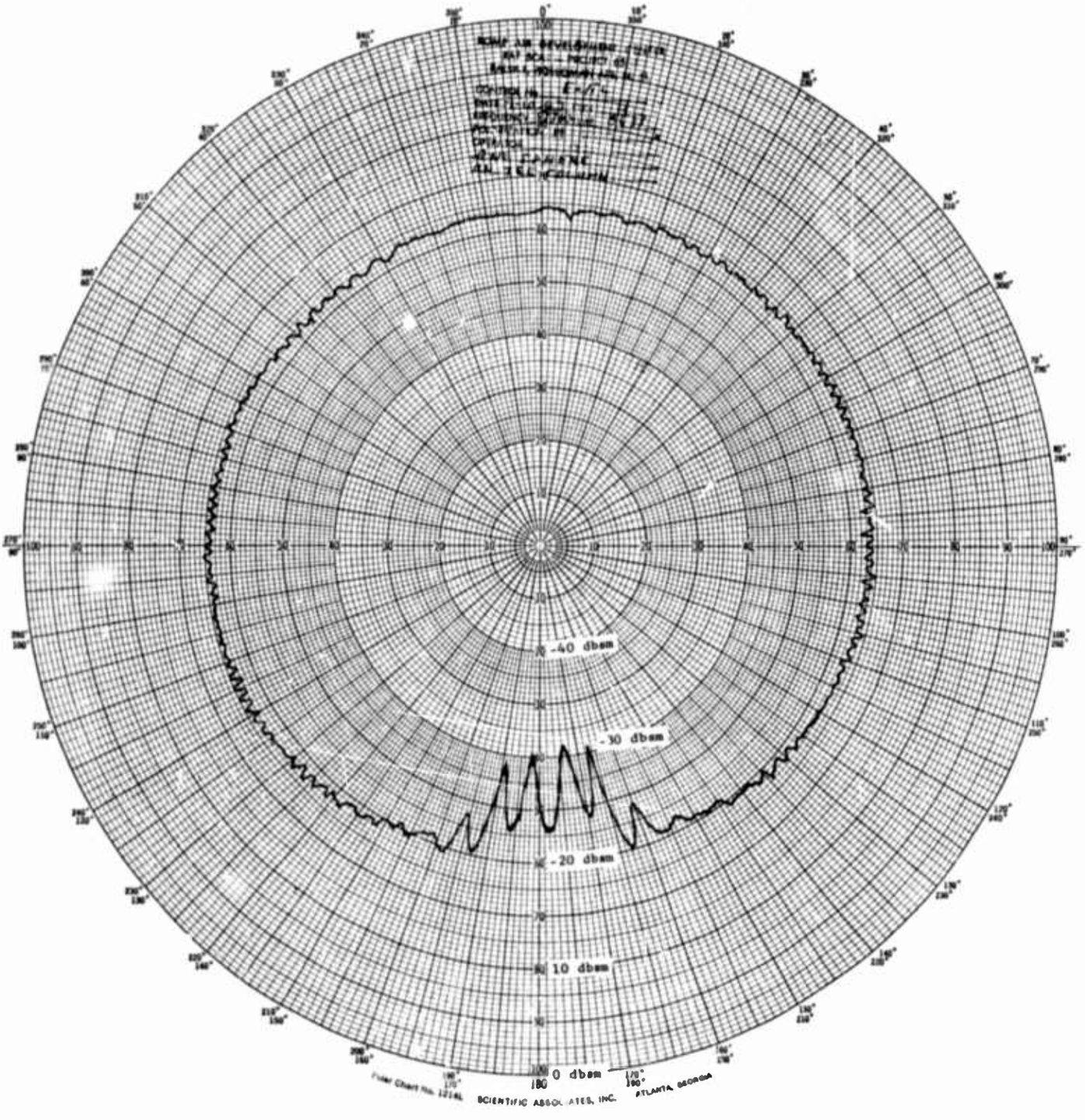

Fig. 5-41 POLAR SCATTERING DIAGRAM
(9300 mc, 32 steps, target A - one sphere)

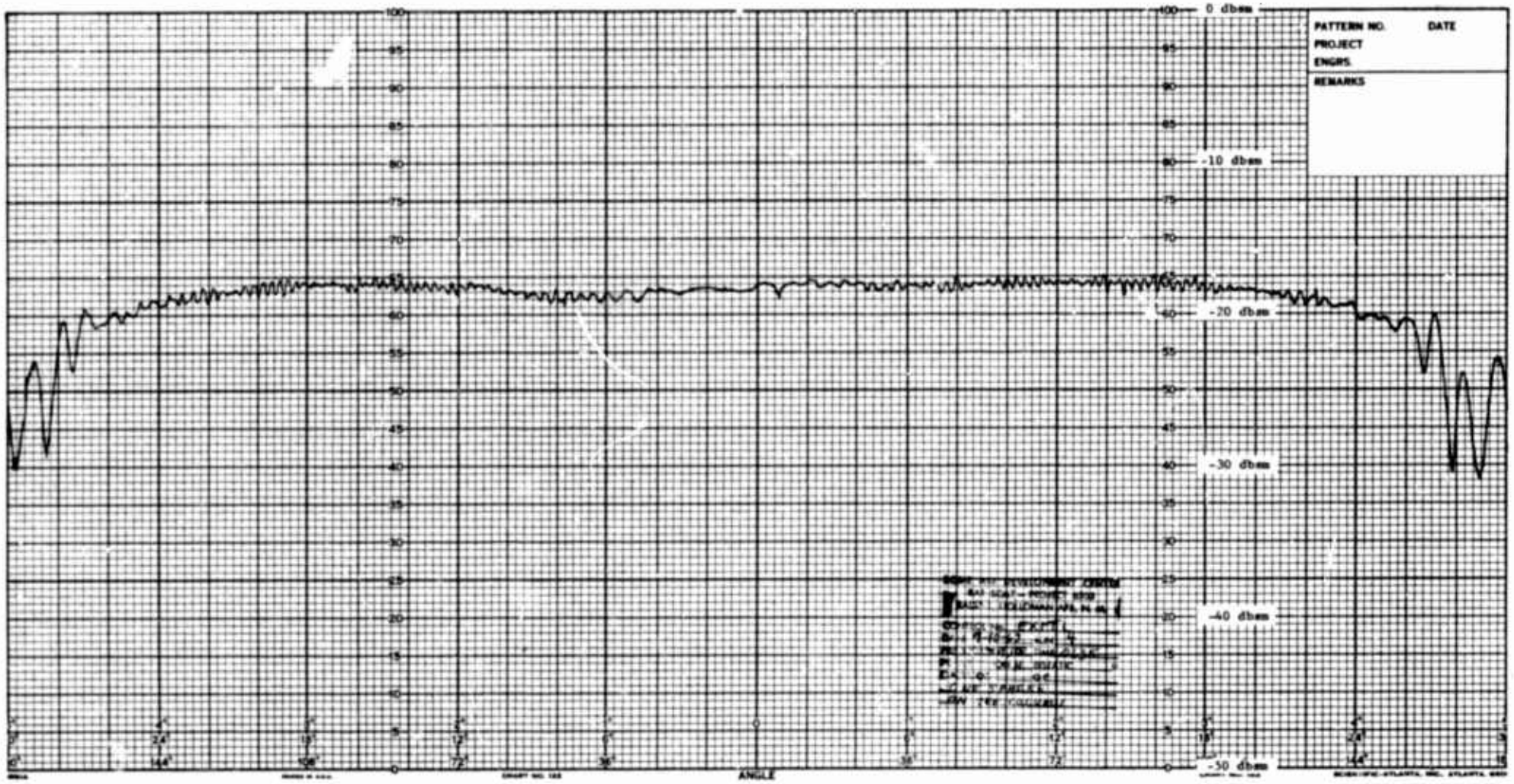

Fig. 5-42 RECTILINEAR SCATTERING DIAGRAM
(9300 mc, 32 steps, target A - one sphere)

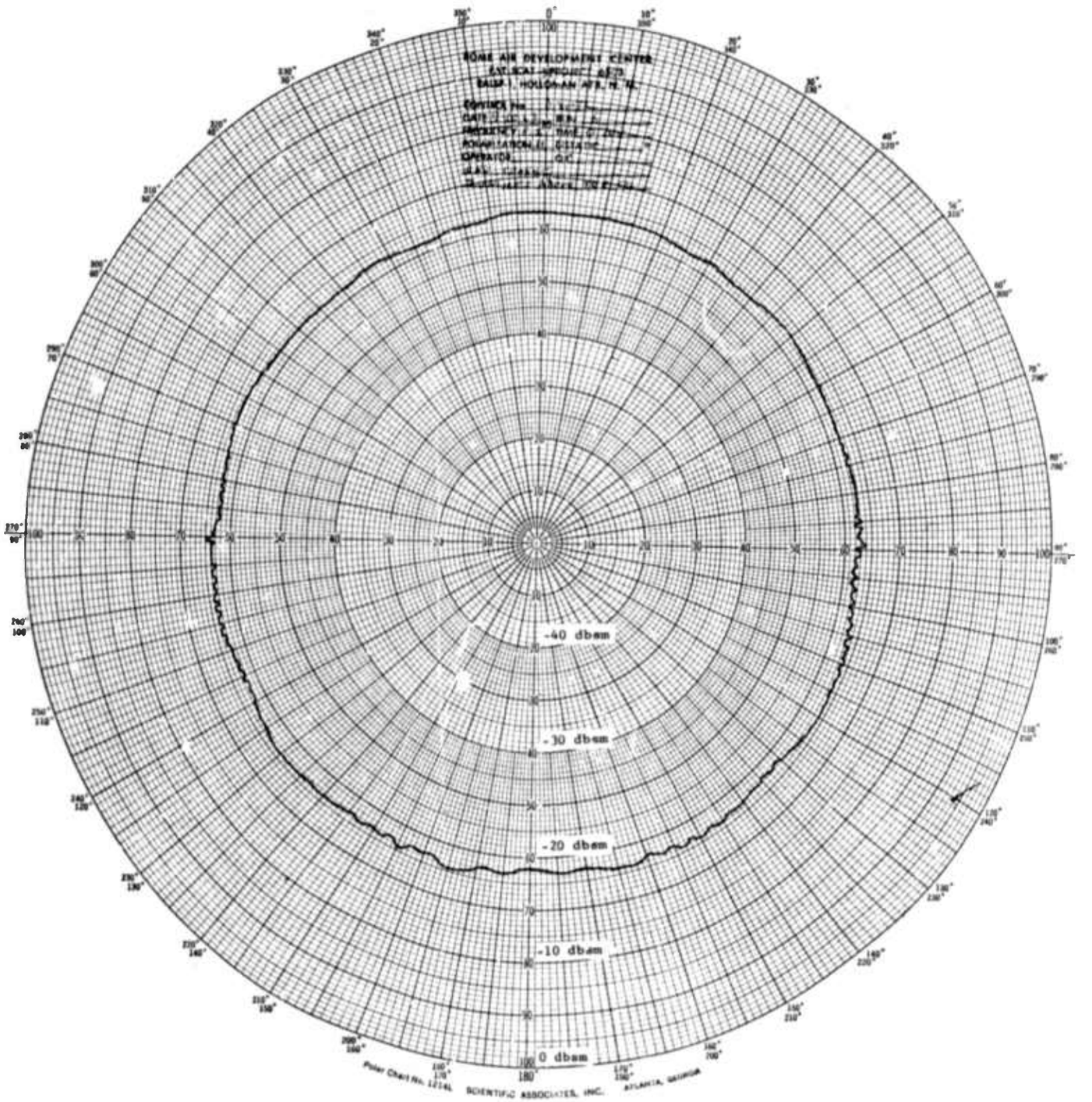

Fig. 5-43 POLAR SCATTERING DIAGRAM
(8800-9800 mc, 32 steps, target B - one sphere)

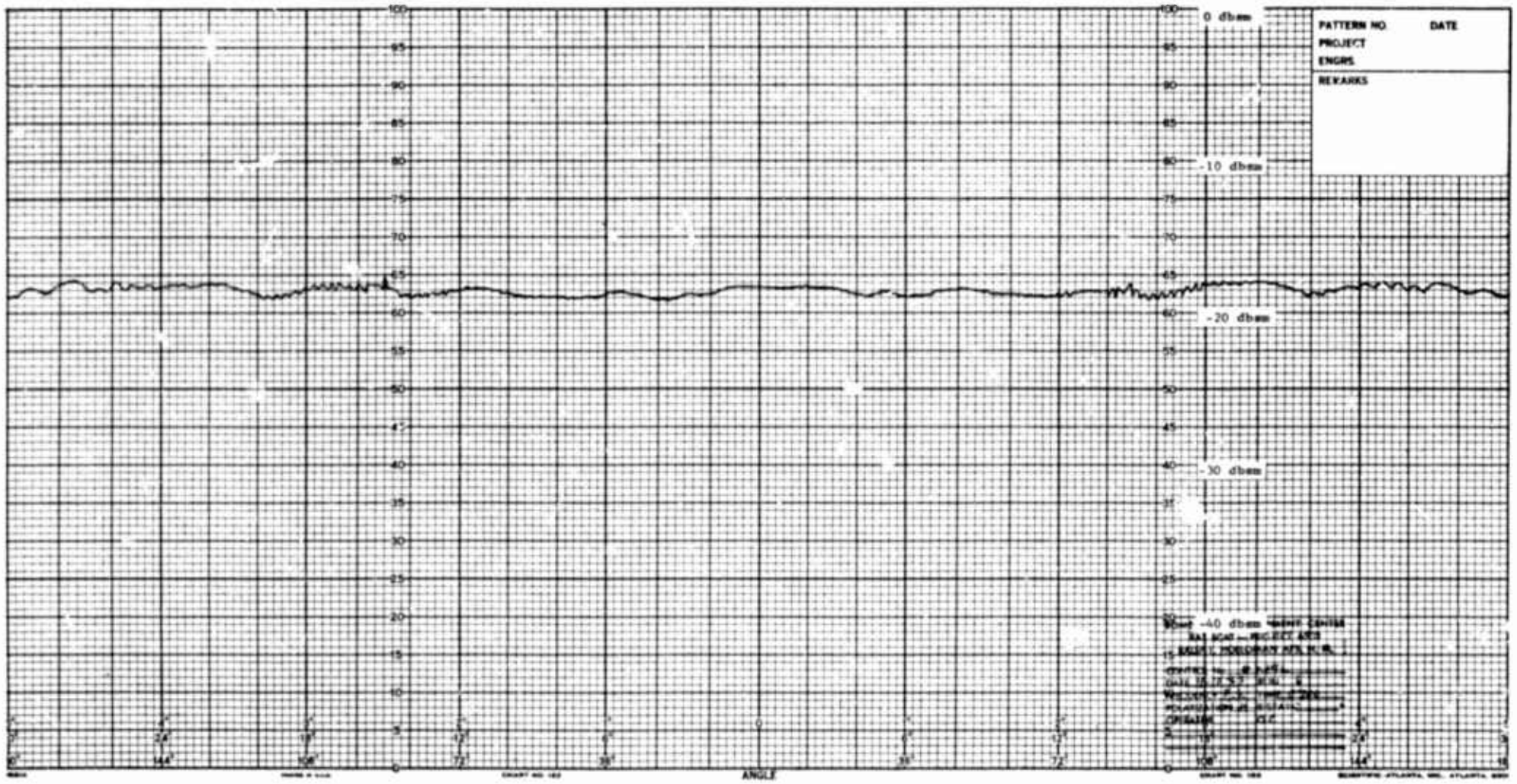

Fig. 5-44 RECTILINEAR SCATTERING DIAGRAM
(8800-9800 mc, 32 steps, target B - one sphere)

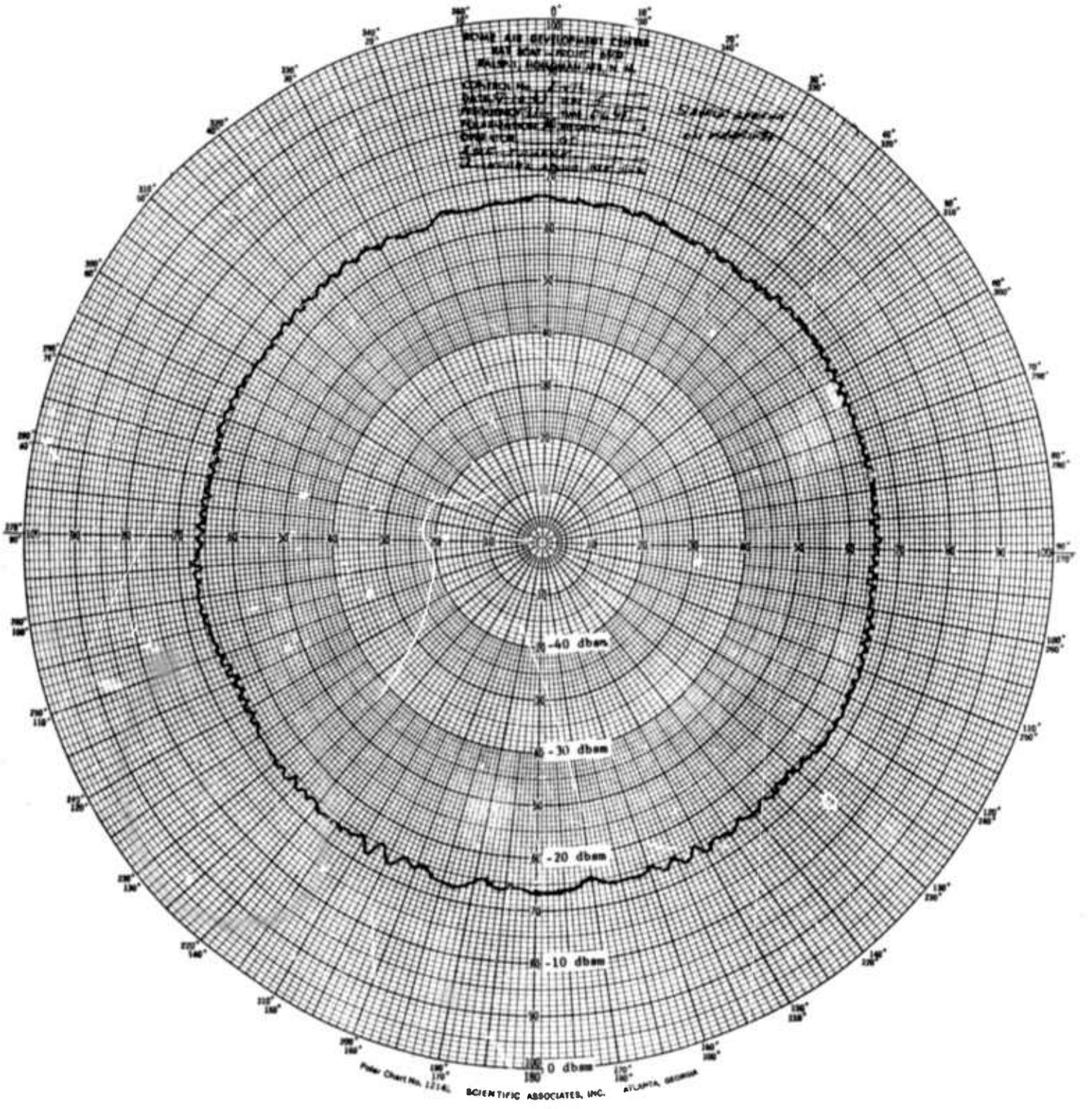

Fig. 5-45 POLAR SCATTERING DIAGRAM
(9300 mc, target B - one sphere)

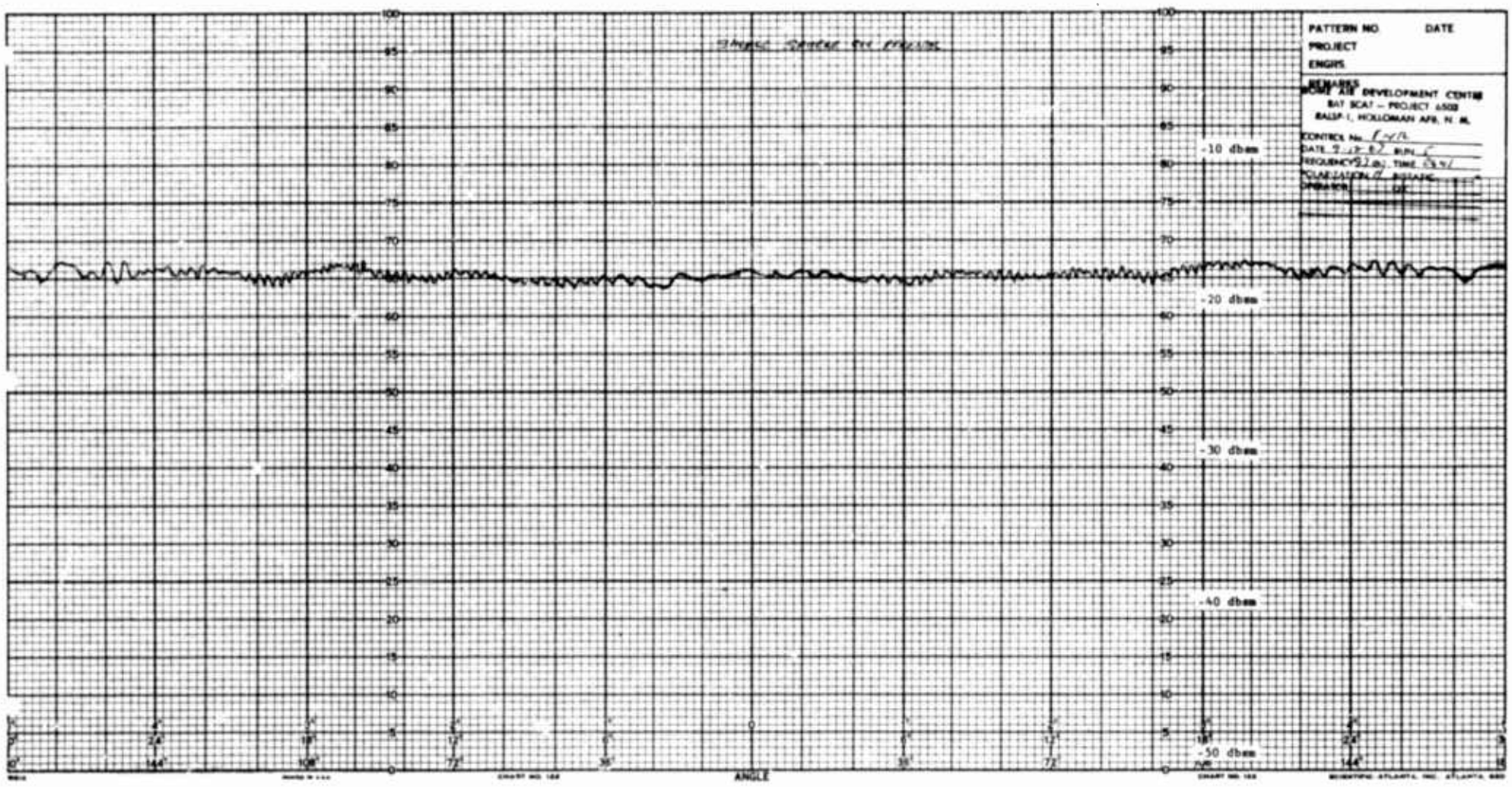

Fig. 5-46 RECTILINEAR SCATTERING DIAGRAM
(9300 mc, target P

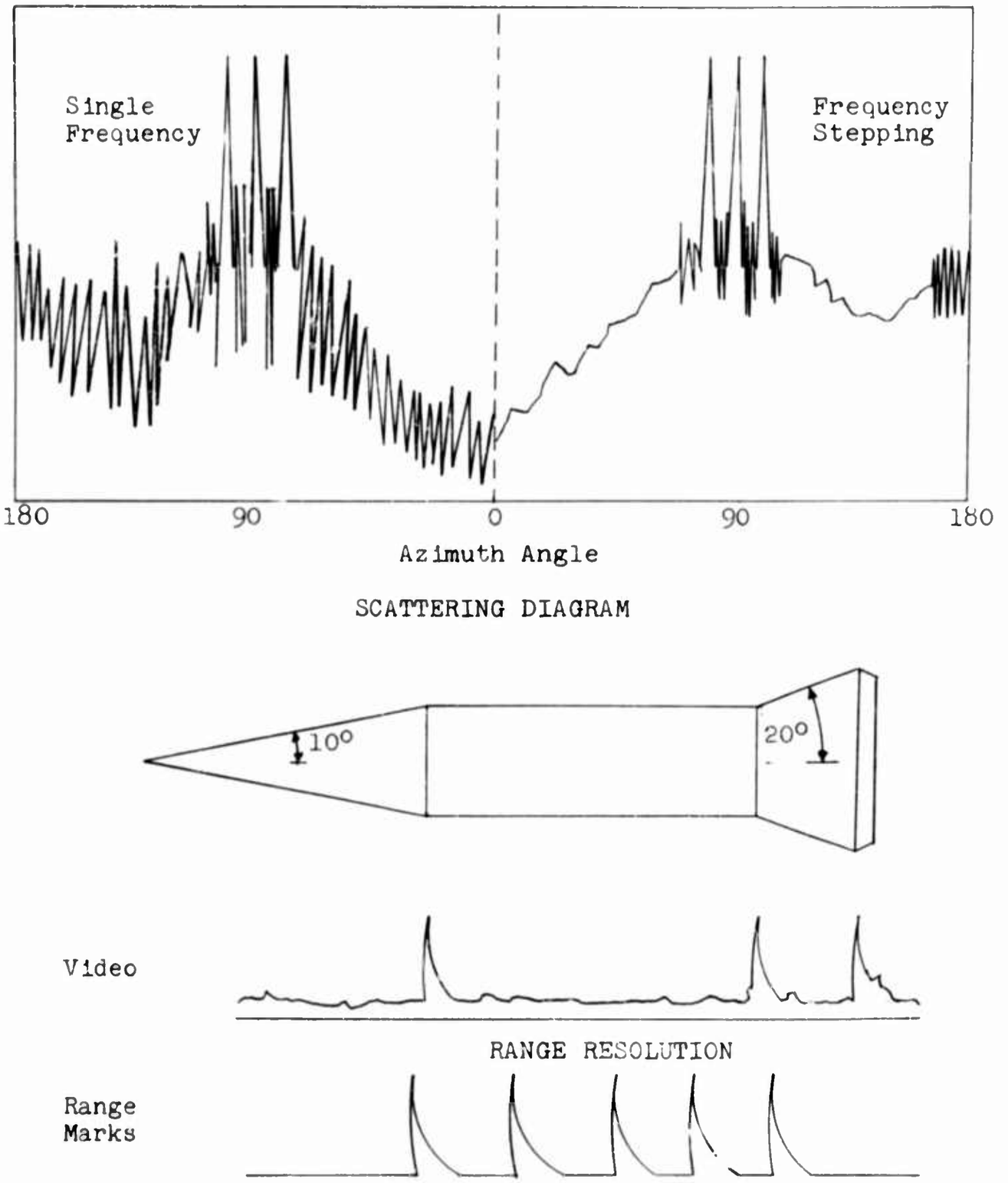

Fig. 5-47 ILLUSTRATION OF FREQUENCY-STEPPING MEASUREMENTS ON A VEHICLE TARGET

SECTION 6

RECOMMENDATIONS

Recommendations for operational procedures and equipment for frequency stepping measurements are presented in this section. In view of the successful frequency stepping measurements previously discussed, no significant changes relative to theoretical considerations or measurement procedure are required.

Procedure

Background level and calibration criteria and procedures for single frequency operation appear to be satisfactory for frequency stepping measurements. Relative background effects were considered briefly in Section 5. Calibration of range resolution measurements, with the system and recorder used, can be accomplished through the use of data runs on a series of spheres of various sizes or by using known attenuation steps to obtain the relation between pen deflection and radar cross section. Alternately, a more elaborate system could be devised to provide radar cross section scales. Unfortunately, this system would have to compensate for the response of the IF amplifiers and the box-car, possibly in a manner similar to the compensation provided by the sigma servo system.

Radar cross section averaging measurements should be made in the same manner as single-frequency measurements. Range resolution measurements should be made in the straightforward manner used for the experiment; the only special setup required is that of adjusting the receiver parameters to provide adequate dynamic range. Measurement results should be independent of the direction of cart travel.

Equipment

The only equipment problems encountered during the experimental runs were associated with the band pass filter and the experimental cart. The band pass filter center frequency drift was excessive. The required stability of the filter is dependent on the filter band width, the cart velocity changes and the degree of measurement accuracy required. For a velocity change of 5 per cent, the Doppler lines will also be shifted 5 per cent in frequency. For the parameters used in the frequency stepping experiment, this shift will be only slightly more than 1 cps. The primary concern is the drift of the filter. In addition,

the skirts of the filter should be suitable steep to preclude a response from the next spectral line. There appears to be no problem involved in constructing such a filter; an active T-filter would be suitable for this application if tuning over a wide frequency range is not required.

Cart velocity requirements are dependent on the position accuracy required and the depth of measurement needed to collect data on the target. The effects of the depth of measurement can be largely eliminated by providing range marker switches at short intervals along the track. A velocity variation of 5 per cent from the average and range markers at 2-foot intervals will be adequate for most practical cases although the cart velocity can be made more constant if desired.

REFERENCES

1. J. W. Tucker, J. W. Jones, and C. H. Fletcher, A Frequency Stepping Method for Radar Scattering Measurement, Contract AF30(602)-2831, GD/FW Report FZE-140, 25 February 1963.

2. Design Report, Band 7 Transmitting Equipment, Contract AF30(602)-2831, GD/FW Report FZE-081, 28 September 1962.

3. Design Report, Band 7 Receiving Systems, Contract AF30(602)-2831, GD/FW Report FZE-082, 28 September 1962.

APPENDIX I

SPECTRAL ANALYSIS FOR RANGE RESOLUTION

The mathematical details of the application of the frequency stepping technique to range discrimination and the analysis of complex scatterers are presented in this appendix. The physical situation that is to be treated may be described as follows:

The radar transmitter provides a sequence of pulses. In each individual pulse the carrier frequency is constant. However this carrier frequency is changed in each succeeding pulse within the sequence. The angular frequency of the m'th pulse is given by

$$\omega = \omega_o + m\alpha T_p$$

where α is the rate of change of frequency and Tp is the interpulse period. The integral index m varies from 0 to M-1 and then the cycle is repeated. There is thus a cycle period $T_c = MT_p$. An observation time T_{obs} is made up of an integral number of cycles N, $T_{obs} = NT_c$. A corner reflector that has a large reflectivity is provided and is moved slowly with constant velocity v toward the radar. In the analysis to be presented herein, consideration is given to the interaction between the reflected wave from the corner reflector and that from one scatterer of a complex target. An extension to the case that involves the several scatterers of the target, as well as the interaction of the reflections from the complex target itself, will be made on the basis of the simplified development.

It has been shown in Section 3 that the output of the radar receiver for a single pulse can be written as

$$P = A + B \cos \frac{2\Delta d}{c} \omega$$

where A and B depend on the cross section of the reflector and the scatterer and

Δd is the distance from the scatterer to the reflector measured positively when the reflector is farther from the radar than the scatterer

ω is the angular frequency of the transmitted radiation

c is the speed of light.

The output from the radar is the sequence of outputs from the pulses that occur during an observation time as shown in Figure 3-3. In the following determination of the spectrum of the radar receiver output, the dc component represented by A will be ignored, and the constant B will be treated as unity. The effect of these simplifications can be allowed for later if desired.

It will be assumed that each receiver output pulse may be treated as an impulse and represented by a δ function. The development is simplified by making this assumption, but the resulting spectrum does not decrease at infinite frequencies. In a complete treatment, the finite width of the pulses would be taken into account so that the spectral denisty would vanish at infinity; however, the frequency range of interest only covers low frequencies and the actual envelope is quite wide for sufficiently short pulses; consequently, any consideration of a vanishing envelope is irrelevant.

The required Fourier transform for the function of time is

$$f(t) = \sum_{T_{obs}} \delta(t-pT_p) \cos\left[\frac{2}{c} d(t)\,\omega(t)\right]$$

It is convenient to count the pulses so that n denotes the cycle in which the pulse occurs and m denotes the location of the pulse within one cycle. Then,

$$f(t) = \sum_{n=0}^{N-1} \sum_{m=0}^{M-1} \delta(t-mT_p-nT_c) \cos\left[\frac{2}{c}\, d(t)\,\omega(t)\right]$$

The Fourier transform is

$$G(\omega) = \int_{-\infty}^{\infty} f(t) e^{-i\omega t} dt$$

which becomes

$$G(\omega) = \int_{-\infty}^{\infty} \sum_{n=o}^{N-1} \sum_{m=o}^{M-1} \delta(t-mT_p - nT_c) \cos\left[\frac{2}{c} d(t)\omega(t)\right] e^{-i\omega t} dt$$

The integration may be carried out to give

$$G(\omega) = \sum_{n=o}^{N-1} \sum_{m=o}^{M-1} \cos\left[\frac{2}{c}\, d(t_{m,n})\omega(t_{m,n})\right] e^{-i\omega t_{m,n}}$$

where $t_{m,n} = mT_p + nT_c$

In this expression, the frequency $\omega(t_{m,n})$ is independent of the value of n because of its periodic nature. Since the reflector is moving with velocity v toward the radar, the distance d may be written $d = d_o - vt$, where d_o is the initial distance from the scatterer to the reflector and distances are measured positively away from the radar. Thus the function $G(\omega)$ may be written in the form

$$G(\omega) = \sum\sum \cos\left[\frac{2}{c}\, d(t_{m,n})\ (\omega_o + m\alpha T_p)\right] \quad e^{-i\omega(mT_p + nT_c)}$$

The argument of the cosine function may be written as

$$\frac{2}{c}\left[d(t_{m,n})(\omega_o + m\alpha T_p)\right] = \frac{2}{c}\left[d(t_{m,n})\omega_o + m\alpha T_p d(t_{m,n})\right]$$

$$= \frac{2}{c}\left[(d_o - vt_{m,n})\,\omega_o + m\alpha T_p d(t_{m,n})\right]$$

$$= \frac{2}{c}\left[(d_o\omega_o - v\omega_o\ (nT_c + mT_p) + m\alpha T_p d\right] .$$

In the latter expression, the time dependence of d in the last term has been suppressed. This approach has been taken because, for small velocities, d is a slowly varying factor and may be considered to be constant over an observation interval. The effects of the time dependence of d will be considered later.

If the cosine term in $G(\omega)$ is replaced by its exponential equivalent, the sums can be evaluated as follows:

$$G(\omega) = \sum_{n=o}^{N-1} \sum_{m=o}^{M-1} \frac{1}{2} e^{-i\omega(nT_c + mT_p)} \left[e^{\frac{2i}{c}(d_o\omega_o - v\omega_o(nT_c + mT_p) + m\alpha T_p d)}\right.$$

$$\left. + e^{\frac{-2i}{c}(d_o\omega_o - v\omega_o(nT_c + mT_p) + m\alpha T_p d)}\right]$$

$$= \frac{1}{2}\left[e^{\frac{2i}{c} d_o\omega_o} \sum_{n=0}^{N-1} e^{-inT_c(\omega + \frac{2v}{c}\omega_o)} \right.$$

$$\cdot \sum_{m=0}^{M-1} e^{-imT_p(\omega + \frac{2v}{c}\omega_o - \frac{2\alpha d}{c})}$$

$$+ e^{\frac{-2id_o\omega_o}{c}} \sum_{n=0}^{N-1} e^{-inT_c(\omega - \frac{2v}{c}\omega_o)}$$

$$\left. \cdot \sum_{m=0}^{M-1} e^{-imT_p(\omega - \frac{2v}{c}\omega_o + \frac{2\alpha d}{c})}\right]$$

In this form the sums are finite, geometric series and may be evaluated to give

$$G(\omega) = \frac{1}{2}\left[e^{\frac{2id_o\omega_o}{c}} \frac{1-e^{-iNT_c(\omega + \frac{2v}{c}\omega_o)}}{1-e^{-iT_c(\omega + \frac{2v}{c}\omega_o)}} \frac{1-e^{-iMT_c(\omega + \frac{2v}{c}\omega_o - \frac{2\alpha d}{c})}}{1-e^{-iT_c(\omega + \frac{2v}{c}\omega_o - \frac{2\alpha d}{c})}}\right.$$

$$\left. + e^{\frac{-2id_o\omega_o}{c}} \frac{1-e^{-iNT_c(\omega - \frac{2v}{c}\omega_o)}}{1-e^{-iT_c(\omega - \frac{2v}{c}\omega_o)}} \frac{1-e^{-iMT_p(\omega - \frac{2v}{c}\omega_o + \frac{2\alpha d}{c})}}{1-e^{-iT_p(\omega - \frac{2v}{c}\omega_o + \frac{2\alpha d}{c})}}\right]$$

This spectrum may be written in a more familiar form as

$$G(\omega) = \frac{1}{2}\left[e^{i\phi_1} \frac{\sin\frac{NT_c}{2}(\omega + \frac{2v}{c}\omega_o)}{\sin\frac{T_c}{2}(\omega + \frac{2v}{c}\omega_o)} \frac{\sin\frac{MT_p}{2}(\omega + \frac{2v}{c}\omega_o - \frac{2\alpha d}{c})}{\sin\frac{T_p}{2}(\omega + \frac{2v}{c}\omega_o - \frac{2\alpha d}{c})}\right.$$

$$\left. + e^{i\phi_2} \frac{\sin\frac{NT_c}{2}(\omega - \frac{2v}{c}\omega_o)}{\sin\frac{T_c}{2}(\omega - \frac{2v}{c}\omega_o)} \frac{\sin\frac{MT_p}{2}(\omega - \frac{2v}{c}\omega_o + \frac{2\alpha d}{c})}{\sin\frac{T_p}{2}(\omega - \frac{2v}{c}\omega_o + \frac{2\alpha d}{c})}\right]$$

where

$$\phi_1 = \frac{2d_o\omega_o}{c} - \frac{NT_c}{2}\left[\omega + \frac{2v}{c}\omega_o\right] - \frac{MT_p}{2}\left[\omega + \frac{2v}{c}\omega_o - \frac{2\alpha d}{c}\right]$$

and

$$\phi_2 = -\frac{2d_o\omega_o}{c} - \frac{NT_c}{2}\left[\omega - \frac{2v}{c}\omega_o\right] - \frac{MT_p}{2}\left[\omega - \frac{2v}{c}\omega_o + \frac{2\alpha d}{c}\right]$$

If $G(\omega) = \frac{1}{2}\left(e^{i\phi_1} G_1 + e^{i\phi_2} G_2\right)$ where G_1 and G_2 are the real functions determined by comparison with the expanded form above, then the function $|G(\omega)|^2$ is given by

$$|G(\omega)|^2 = \frac{1}{4}\left[G_1^2 + G_2^2 + G_1G_2\left(e^{i(\phi_1-\phi_2)} + e^{-i(\phi_1-\phi_2)}\right)\right]$$

$$= \frac{1}{4}\left[G_1^2 + G_2^2 + 2G_1G_2\cos(\phi_1-\phi_2)\right]$$

$$= \frac{1}{4}\left[G_1^2 + G_2^2 + 2G_1G_2\cos\left(\frac{4d_o\omega_o}{c} - NT_c\frac{2v}{c}\omega_o - MT_p\left(\frac{2v}{c}\omega_o - \frac{2\alpha d}{c}\right)\right)\right]$$

The argument of the cosine term does not contain the frequency ω but only the parameters of the system and the separation distance d. In the simple cases, the cosine is one or minus one. If the cosine is one, $|G(\omega)|^2 = \frac{1}{4}(G_1 + G_2)^2$, and if it minus one, $|G(\omega)|^2 = \frac{1}{4}(G_1 - G_2)^2$. In these simple cases it is instructive to consider G_1 and G_2 separately and then take the proper sum and square.

The function G_2 is the product of two well known functions

$$G_2'(\omega) = \frac{\sin\frac{NT_c}{2}\left(\omega - \frac{2v}{c}\omega_o\right)}{\sin\frac{Tc}{2}\left(\omega - \frac{2v}{c}\omega_o\right)}$$

and

$$G_2''(\omega) = \frac{\sin\frac{MT_p}{2}\left(\omega - \frac{2v}{c}\omega_o + \frac{2\alpha d}{c}\right)}{\sin\frac{T_p}{2}\left(\omega - \frac{2v}{c}\omega_o + \frac{2\alpha d}{c}\right)}$$

These functions have the same general form and can be plotted schematically as in Figure I-1.

The influence of the various parameters in G_2' and G_2'' can be described as follows:

1. The locations of the principal maxima are specified by the vanishing of the denominator.

2. The number of minor maxima and minima between consecutive principal maxima is specified by the ratio of the argument in the numerator to that in the denominator.

3. The spacing between successive principal maxima is inversely proportional to the coefficient of ω in the denominator.

Thus G_2' provides a set of closely spaced principal maxima whose spacing is $2\pi/T_c$, and G_2'' provides a set of principal maxima with the larger spacing $2\pi/T_p$. This latter behaves as an envelope of the finer structure. The fine structure maxima are centered on $-2v\omega_0/c + l\pi$ where l is an integer.

If the term which includes d is neglected in $G_2''(\omega)$, the principal maximum at $\omega = 2v_0\omega_0/c$ coincides with a principal maximum of $G_2'(\omega)$, and the nearest zeros of $G_2''(\omega)$ coincide with the nearest principal maxima $G_2'(\omega)$. Thus the spectrum of $G_2(\omega)$ can be represented as shown in Figure I-2. The spectrum of $G_1(\omega)$ is given by reflecting the spectrum of $G_2(\omega)$ in the origin. Since negative frequencies are recorded in physical measurements as if they were positive, as far as physical measurements are concerned the spectrum of G_1 and G_2 coincide. For this reason, it is convenient to discuss only $G_2(\omega)$ to determine the behavior of the system.

The function $G_2(\omega)$ is repeated below as a foundation for the following discussion.

$$G_2(\omega) = G_2' \cdot G_2'' = \frac{\sin \frac{NT_c}{2}\left(\omega - \frac{2v}{c}\omega_o\right)}{\sin \frac{T_c}{2}\left(\omega - \frac{2v}{c}\omega_o\right)} \quad \frac{\sin \frac{MT_p}{2}\left(\omega - \frac{2v}{c}\omega_o + \frac{2\alpha d}{c}\right)}{\sin \frac{T_p}{2}\left(\omega - \frac{2v}{c}\omega_o + \frac{2\alpha d}{c}\right)}$$

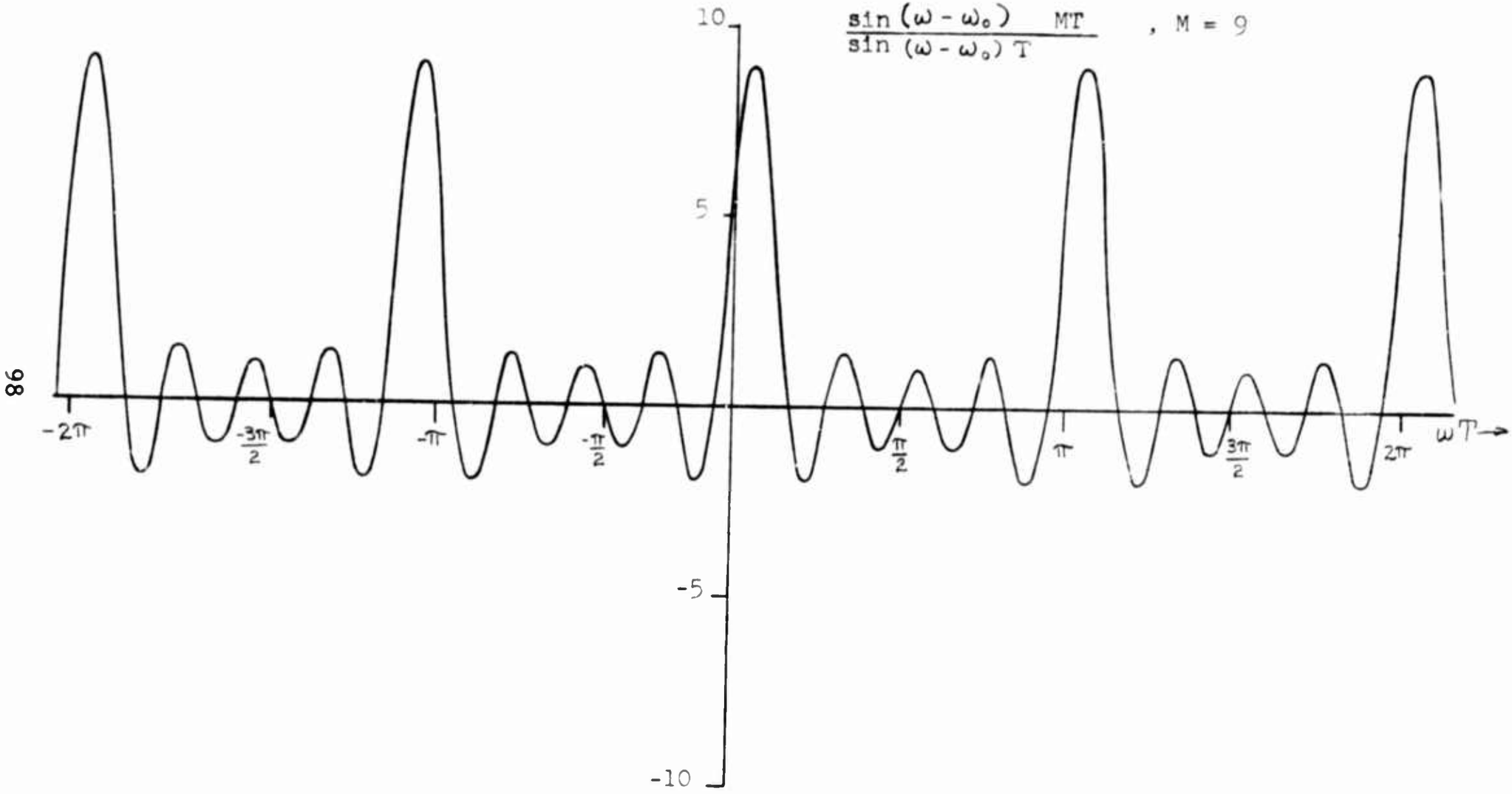

Fig. I-1 GRAPHICAL REPRESENTATION OF $G_2'(w)$ or $G_2''(w)$

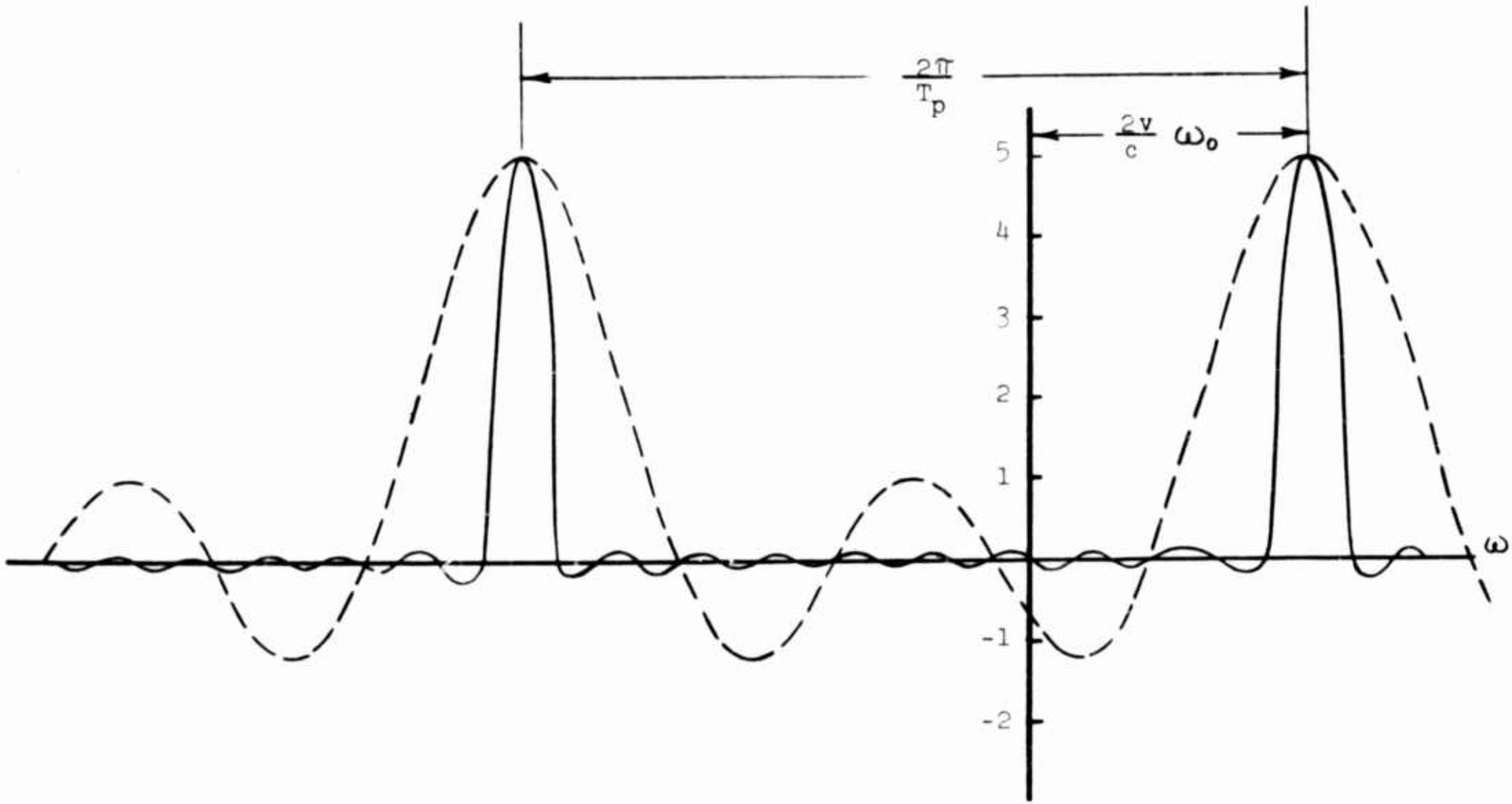

Fig. I-2 SPECTRUM OF $G_2(w)$

For d=0, this spectrum has the form illustrated schematically in Figure I-2. If d has a positive value, the principal maximum of $G_2''(\omega)$ is displaced to the left, and as d decreases in value, this maximum moves towards higher frequencies. As the maximum of $G_2''(\omega)$ moves, it will next coincide with the principal maximum of $G_2'(\omega)$ that is located at $\omega = 2v\omega_b/c + 2\pi/T_c$ and then, in order, with the other principal maxima of $G_2'(\omega)$. An example of the above process can be illustrated by use of the following measurement situation

1. A narrow band filter centered at $2v\omega_b/c$ is used to filter the output of the radar receiver.

2. The target consists of a single scatterer.

3. The reflector starts behind the target and approaches at the low velocity v.

The output of this filter will then increase as d decreases and the maximum of $G_2''(\omega)$ approaches $2v\omega_b/c$. As the reflector passes the target, the output will decrease. If the target is made up of several scatterers, each will furnish its own peak in the output from the filter.

The preceding development can be used as a basis for selecting specific values for the characteristic parameters of a system. The first point to be noted can be established by referring to Figure I-2, if it is kept in mind that amplitudes of negative frequency components are measured as if the frequency were positive. Thus the peak marked A would be observed at $2\pi/T_p - 2v\omega_b/c$. It is somewhat more convenient to change to units of frequency and discuss these quantities in terms of cycles per second, f, where $\omega = 2\pi f$.

If $f_o = \omega_o/2\pi$ is chosen, the offset in the spectrum in Figure I-2 can be adjusted by varying v. The value of this offset has the form of a Doppler shift, $\Delta f = 2vf_o/c$, and it may be conveniently referred to by that name. The cycle frequency $1/T_c$ denotes the spacing between the basic lines given by G_2'. The function G_2'' selects the amplitude associated with each basic line. To avoid superposition of basic lines and the resultant complication of the measurements, the Doppler shift can be chosen in accordance with the following two criteria:

1. The basic lines of the shifted spectrum should not overlap the lines of the spectrum that results from

the interaction of the nonmoving scatterers of the target. These latter lines appear at n/T_c, where n is an integer.

2. The basic lines of the shifted spectrum should not overlap the lines at negative frequencies when these latter are reflected by the measurement (i.e., observed as positive frequencies). The optimum spacing that can be obtained appears when the three sets are equally spaced. This optimum is given by the relation $f = m/(3T_c)$, m = 1, 2, (mod 3)

where Δf is the Doppler shift, T_c is the cycle time, and m is one of the integers 1, 2, 4, 5, 7 ---. The velocity of the corner reflector is thus given by

$$v = \frac{mc}{6f_oT_c}, \quad m = 1, 2 \pmod 3$$

The cycle time is subject to several requirements. First, distance between the three sets of lines discussed above must be sufficiently large to allow their separation by use of a practical filter. If B_f is the bandwidth of the filter, then $1/T_c$ must be greater than $3B_f$. Second, if the cycle frequency is too small, then the observation time becomes too long because the width of the principal maxima of G_2' (i.e., the width of the basic lines) is $2/T_{obs}$ and, for efficiency, the filter should pass most of this band. Third, the width of the moving maxima of G_2'' is given by $2/T_c$, and the ability of the system to resolve individual scatterers in the target depends on the width. The relation involved here is

$$\Delta d = \frac{c}{\alpha_1 T_c}$$

where Δd is the distance the reflector moves to cause the whole of peak B (Figure I-2) to pass the Doppler line. In this relation, $\alpha_1 = \Delta f_o/T_c$ where Δf_o is the available variation in the radar frequencies. Thus $\Delta d = c/\Delta f_o$. Scatterers that are separated by one-half of this distance are usually considered to be resolved. The number of pulses in one cycle determines the intensity of the subsidiary maxima of the dashed curve in Figure I-2.

If a particular radar system incorporates the following properties:

$$f_o = 10^{10} \text{ cycles per second}$$

$$\Delta f_o = 1.5 \times 10^9 \text{ cycles per second}$$

$$B_f = 4 \text{ cycles per second}$$

$$\text{PRF} = \frac{1}{T_p} = 50 \text{ to } 5000 \text{ pulses per second (adjustable)}$$

The resolution available with this system is given by

$$d_r = \frac{c}{2\Delta f_o} = \frac{1}{3} \text{ ft}$$

The parameters should be chosen so that the number of pulses per cycle and the number of cycles per observation time are about the same size. Use of this approach reduces the subsidiary maxima of both curves in Figure I-2.

For convenience, the PRF can be set at 2560 pulses per second and the number of pulses per period, M, at 32; then for a 1/4-second observation time, there are 20 cycles and $t_c = 1/80$ second. By using the relation given above to calculate the velocity, $v = 4m/3$ in feet per second. The useable value of m is unity since the use of m = 2 results in a displacement of twice the expected resolution. With this choice of m, the Doppler frequency becomes $f = 80/3 = 26\ 2/3$ cps. Instrumentation to provide these parameters is within the state-of-the-art and is described in Section 4.

APPENDIX II

AUTOCORRELATION FUNCTION ANALYSIS

FOR RANGE RESOLUTION

The range discrimination feature of a frequency-stepped transmission system is analyzed in this section through the derivation and interpretation of the autocorrelation function of the frequency-stepped wave form.

The frequency-stepped wave form to be considered consists of a sequence 1, 2, ---, M of radio frequency pulses of total bandwidth B, uniform amplitude, duration τ, and spacing $T_p = T_c/M$. The angular frequency of the mth pulse is $\omega_n = \omega_o + m\alpha T_p$, and the duration of one cycle of the sequence is T_c. The total angular bandwidth is $\Omega = \alpha T_c$. Each pulse is described by

$$\cos \omega_m (t - t_m), \quad |t - t_m| \leq \frac{\tau}{2}$$

The autocorrelation function, $C(\theta)$, over the range of θ for which $\theta < \tau$, is given by

$$C(\theta) = \sum_{m=0}^{M-1} \int_{-\tau/2 + \theta}^{\tau/2} \cos \omega_m t \cos \omega_m (t - \theta)\, dt$$

$$= \sum_{m=0}^{M-1} \int_{-\tau/2 + \theta}^{\tau/2} \left[\cos (2\omega_m t - \omega_m \theta) + \cos \omega_m \theta\right] dt$$

which can be written as

$$C(\theta) = \sum_{m=0}^{M-1} \frac{1}{2}\left[\int_{-\frac{\tau}{2} + \theta}^{\frac{\tau}{2}} \cos (2\omega_m t - \omega_m \theta)\, dt + \int_{-\frac{\tau}{2} + \theta}^{\frac{\tau}{2}} \cos \omega_m \theta\, dt\right] .$$

Upon integrating,

$$C(\theta) = \sum_{m=0}^{M-1} \left[\frac{1}{4\omega_m} \sin (2\omega_m t - \omega_m \theta) \Big|_{-\frac{\tau}{2}+\theta}^{\frac{\tau}{2}} + \frac{1}{2}(\cos \omega_m \theta) t \Big|_{-\frac{\tau}{2}+\theta}^{\frac{\tau}{2}} \right]$$

$$= \sum_{m=0}^{M-1} \left[\frac{1}{2\omega_m} \sin (\omega_m \tau - \omega_m \theta) + (\cos \omega_m \theta) \left(\frac{\tau}{2} - \frac{\theta}{2}\right) \right]$$

By factoring out $\tau/2$,

$$C(\theta) = \sum_{m=o}^{M-1} \frac{\tau}{2} \left[\left(1 - \frac{\theta}{\tau}\right) \cos \omega_m \theta + \frac{\sin \omega_m (\tau - \theta)}{\omega_m \tau} \right]$$

Now,

$$\sum_{m=o}^{M-1} \cos \omega_m \theta = \sum_{m=o}^{M-1} \cos \left(\omega_o + \frac{m\Omega}{M}\right) \theta$$

$$= \cos \left[\left(\omega_o + \frac{M-1}{2M} \Omega\right) \theta \right] \frac{\sin \frac{\Omega \theta}{2}}{\sin \frac{\Omega \theta}{2M}}$$

and if $\Omega \ll \omega_o$

$$\sum_{m=o}^{M-1} \frac{\sin \omega_m (\tau - \theta)}{\omega_m \tau} \approx$$

$$\frac{1}{\omega_o \tau} \sin \left[\left(\omega_o - \frac{M-1}{M} \Omega\right) (\tau - \theta) \right] \frac{\sin \frac{1}{2} \Omega (\tau - \theta)}{\sin \frac{1}{2M} \Omega (\tau - \theta)}$$

Therefore,

$$\frac{2}{\tau} C(\theta) \simeq \left(1 - \frac{\theta}{\tau}\right) \cos\left[\left(\omega_o + \frac{M-1}{2M}\Omega\right)\theta\right] \frac{\sin\left(\frac{\Omega\theta}{2}\right)}{\sin\left(\frac{\Omega\theta}{2M}\right)}$$

$$+ \frac{1}{\omega_o \tau} \sin\left[\left(\omega_o - \frac{M-1}{M}\Omega\right)(\tau - \theta)\right] \frac{\sin\frac{1}{2}\Omega(\tau-\theta)}{\sin\frac{1}{2M}\Omega(\tau-\theta)}$$

Typically,

$$\omega_o \geq 2\pi \times 5 \times 10^8$$

$$\tau \geq 1.5 \times 10^{-7}$$

and the second term of the equation makes only a small contribution. By neglecting the fine structure,

$$\frac{2}{\tau} C(\theta) \simeq \left(1 - \frac{\theta}{\tau}\right) \frac{\sin\left(\frac{\Omega\theta}{2}\right)}{\sin\left(\frac{\Omega\theta}{2M}\right)}$$

If the resolution θ_R is taken to be the distance to the first null (analogous to telescopic resolution),

$$\frac{1}{2}\Omega \ \theta_R = \pi$$

or

$$\theta_R = \frac{1}{B}$$

as would be expected. The corresponding spatial resolution is

$$\Delta d = 2\pi \frac{c}{2\alpha T_c}$$

where

$$\propto T_c = \Omega .$$

Δd is found to be equal to

$$\Delta d = \frac{c}{2B}$$

which is the same as equation 3-25.

Second order maxima will occur when

$$\frac{\Omega\theta}{2M} = i\pi$$

where i is an integer. To prevent the occurrence of second order maxima and to cause $C(\theta)$ to exhibit minimum ambiguity, it is desirable that

$$\frac{\Omega\theta}{2M} \leq \frac{\pi}{2}$$

when $0 \leq \theta \leq \tau$, which gives

$$M \geq \frac{2\Omega\tau}{2\pi} = 2B\tau$$

where M is the desired number of pulses. Hence, it is seen that optimum resolution performance will be obtained when the number of steps is equal to or greater than $2B\tau$ where B is the bandwidth and τ is the pulse width. On the other hand, a severe range ambiguity may result if the number of equispaced pulses is less than $B\tau$.

The effects of this ambiguity depend on the nature of the target complex which is being observed. If the target is distributed over a range interval exceeding one-half the pulse width, then the number of pulses per interval must be as shown above to avoid ambiguity. On the other hand, if the extent in range of the target is smaller than $C\tau/2$, then fewer pulses will be required. In particular, for a target of length $D<c\tau/2$, ambiguities must be avoided over an interval of only $0\leq\theta\leq 2D/c$. By using the

value $2D/c$ for θ, it is found that

$$M > \frac{2\Omega 2\ (D/c)}{2\pi} = 2B\tau_{target}$$

where $\tau_{target} = 2D/c$.

Typical values of $M = 2B\tau$ and $M = B\tau$ are shown in Table II-1.

Table II-1 NUMBER OF PULSES REQUIRED FOR OPTIMUM RANGE RESOLUTION PERFORMANCE WHEN PULSE WIDTH = 0.15 MICROSECONDS

APPROXIMATE RESOLUTION (feet)	BANDWIDTH (megacycles)	PER CENT BANDWIDTH AT 1 KMC	PER CENT BANDWIDTH AT 3 KMC	PER CENT BANDWIDTH AT 10 KMC	NO. OF PULSES M= BT	M= 2 BT
5	100	10	3.3	1	15	30
1.7	300	33.3	10	3.3	45	90
0.5	1000	100	33.3	10	150	300